

# **Scheduling of energy storage using probabilistic forecasts and energy-based aggregated models**

Zur Erlangung des akademischen Grades  
**Doktor der Ingenieurwissenschaften**  
von der KIT-Fakultät für Informatik  
des Karlsruher Instituts für Technologie (KIT)

genehmigte  
**Dissertation**

von

M.Sc. Riccardo Remo Appino

Tag der mündlichen Prüfung: 21. November 2019  
Referent: Prof. Dr. Veit Hagenmeyer  
Koreferent: Prof. Dr.-Ing. Timm Faulwasser  
Koreferent: Prof. PhD Mario Paolone



Avevo l'intenzione di fare un segno,  
questo sì, ossia avevo l'intenzione di  
considerare segno una qualsiasi cosa  
che mi venisse fatto di fare, quindi  
avendo io, in quel punto dello spazio  
e non in un altro, fatto qualcosa  
intendendo di fare un segno, risultò  
che ci avevo fatto un segno davvero.

---

*I. Calvino, Le Cosmicomiche*



# Abstract

Scheduling for power systems is frequently performed by means of algorithms based on numerical optimization, where the uncertainty inherent to volatile generation/consumption is handled via sampling-based methods (i.e. scenario optimization). This approach has the advantage of being applicable to general models, but it entails a loss of information about the uncertain parameters—approximated by a finite set of realizations. In contrast to this state-of-the-art approach, the present thesis investigates a method that does not approximate the uncertain parameters, but the description of the physical system and of the scheduling requirements instead.

Taking a holistic perspective and exploiting the interplay between forecasting models and numerical optimization, this thesis proposes a framework for optimization-based scheduling algorithms leveraging probabilistic forecasts and approximated—eventually aggregated—energy-models. This framework shifts part of the computational burden to the forecasting. Specifically, the correlation among uncertain generation/consumption at subsequent time steps, which is difficult both to forecast and to tackle, is indirectly included in predictions in terms of energy. Simulations of several test cases (a household, an industrial campus, and a charging station for electric vehicles) and real-life experiments indicate that the proposed algorithmic framework attains superior performance in comparison to state-of-the-art techniques based on sampling.



# Acknowledgment

The present thesis deals with planning under uncertainty. A topic of great relevance, given that life is so unpredictable. For example, it has never been my plan to get a PhD. But here you are, reading the very beginning of my dissertation. So, what happened? If this document exists, it is because some wise advisers suggested for me to find a mentor, under whose supervision I could have experienced the pain and delight of growing my ideas—and even more, myself. Following that recommendation, I ended up with finding not one, but two supervisors. That started my PhD journey, a path that led to the scientific results that I am about to describe in the next pages. However, before starting, I would like to express my gratitude to all the people that had accompanied me along the road—or at least along a stretch of it—and without which not a line of what follows would have been written.

First of all, I would like to thank my supervisors, Prof Veit Hagenmeyer and Prof Timm Faulwasser. Thank you for having believed in me and having given me the possibility of working with you. I have to admit that it was not always easy to balance between your different personalities, but I am truly glad of having had both of you as mentors. I would have not learned nor accomplished so much without your guidance, your patience, your constructive advice, and the interesting discussions. Veit, thank you for your enthusiasm and for having shown me what it is like to manage a vast group of diverse, brilliant minds. Timm, thank you for the different perspective and for the insight on what science is and what ambition means.

Next, I would like to thank my closer colleagues (in order of appearance): Tillman Mühlpfordt, Jorge Ángel González Ordiano, Alexander En-

gelmann, and Alexander Murray. Till, thank you for having taught me (or at least, for having tried to) the beauty of mathematical rigor and the importance of writing with style. Ángel, thank you for the support and your cheerful mood, it has been truly fundamental more than once; thank you for having listened to my imagination running, and for having advised me on how to bring imagination back to science. Alex E., thank you for having shown me the strength of the quiet ambition, for the imperishable passion of who believes that a better word can and should be built. Alex M., thank you for having been a great office mate, for both the laughs and the discussions, for having gone with me through this growing process—and, yes, also for all the proof reading. I would like to add at the end of this list Dr Niels van Duijkeren, who has somehow been an unofficial member of our working group. Niels, thank you for your wise advice as a “senior” PhD student, much of which manifested in important parts of this thesis.

My gratitude also goes to “my students” (again, in order of appearance): Sébastien Thill, Miguel Muñoz-Ortiz, Giancarlo Noto, Karl Schwenk, and Martin Miller. Supervising you has been the most rewarding part of my job. I hope I was able to transmit to you as much as you gave to me.

I would also like to thank all the professors and scientists that worked with me in the past years. Thanks to Prof Mario Paolone for having reviewed this thesis and for all its precious comments. Thanks to Prof Ralf Mikut, for the support and for all the clever and insightful recommendations. Thanks to all the other doctoral candidates and colleagues at IAI, for the life in the office in the middle of the woods, which goes by among casual discussions waiting for the coffee in a kitchen that is probably too intimate, meetings envisioning plans that are often too ambitious, and Christmas quizzes that are definitely too difficult to answer. Thanks to Prof Pierluigi Mancarella for having hosted me in Melbourne, for his contagious motivation and passion, and the great discussions in Lygon street. Thanks also to Prof Luis (Nando) Ochoa and to all the power system group at The University of Melbourne for the great time down under and for all the ideas fostered by our

discussions. Thanks to Prof Gianfranco Chicco, for the curious attitude and the experienced knowledge. Thanks to the colleagues from the Electrotechnical Institute, Dr James Berry, Dr Bhawna Verma, and Nina Munske, for having believed in my ideas, and for the patient support provided with the experimental equipment; it seemed that it would have never worked, but in the end the results of our efforts become part of this document. I would also acknowledge funding by the German Federal Ministry of Education and Research (BMBF) within the Kopernikus Project ENSURE, “New ENergy grid StructURes for the German Energiewende”, and all the colleagues in this project.

My thanks goes also to all the great people that I have met in Karlsruhe and in Melbourne who, despite not having had any scientific merit in what follows, have been a fundamental support in these PhD years. A special thanks goes to Martina and Silvia, for the brunch discussions on PhD life, on how to get the Nobel prize, and—above all—on how to survive in Germany.

From my understanding, obtaining a PhD means to venture to the farthest border of human knowledge, and proceed a step beyond, planting a flag in unknown territories. Closer to the border you get, less crowded the space becomes. Isolation and lack of purpose can torment the soul of those brave wanderers in the sea of fog. Hence, it is often said that one of the main challenges that doctoral candidates have to face is isolation. I cannot deny it, but the long list of names that I have just unwound demonstrates that it does not have to be that way. While we all grope in a personal chaos, we are also all wanderers. Thank you all once more, for the spark of greatness you emanate in chasing your dreams. Without that light, I would have not gone anywhere.

Last but not least, I would like to thank my family. Thank you for the support, the examples and the education you gave me, without which I could not be here writing this thesis. Thank you for having been always present, even when I was far and distracted. Thank you for having endorsed my decisions, even when you would have preferred me to be closer to you. I

would have probably not embarked on this adventure if I did not know that I can always count on your unconditioned support. I would have not traveled so much if I did not know that there is a place always awaiting for me, a place at the foot of the mountains that I call home.

Karlsruhe, November 2019

*Riccardo Remo Appino*

# Contents

<b>1</b>	<b>Introduction</b>	<b>1</b>
1.1	Motivation	1
1.2	Research Questions	3
1.3	Contributions	7
1.4	Outline	10
<b>2</b>	<b>Scheduling with Stochastic Optimization</b>	<b>13</b>
2.1	Introduction	14
2.1.1	Scheduling	14
2.1.2	Decision-making via Numerical Optimization	16
2.2	Problem Structure and Models	18
2.2.1	Multi-stage Optimization	18
2.3	Computational Tractability	24
2.3.1	Sampling-based Approaches	25
2.3.2	Non-sampling-based Approaches	26
2.4	Data Processing	31
2.5	Summary	33
<b>3</b>	<b>Stochastic Scheduling based on Energy Balance</b>	<b>35</b>
3.1	Models and Requirements	35
3.1.1	System Components	36
3.1.2	Requirements	38
3.1.3	Hierarchical Control	40
3.2	Online Schedule Tracking	41

3.3	Dispatch Schedule Optimization . . . . .	42
3.3.1	Model Modification . . . . .	45
3.3.2	Reformulation of Chance Constraints . . . . .	53
3.3.3	Implementation Aspects . . . . .	56
3.3.4	Computationally Tractable Formulation . . . . .	62
3.4	Online Rescheduling . . . . .	63
3.5	Summary . . . . .	65
<b>4</b>	<b>Aggregated Scheduling of EC-DERs . . . . .</b>	<b>67</b>
4.1	Models and Requirements . . . . .	68
4.1.1	Hierarchical Control . . . . .	69
4.2	Scheduling with Aggregated Models . . . . .	71
4.3	Bounds for the Aggregated Model . . . . .	75
4.4	Ensuring Schedule Feasibility . . . . .	83
4.5	Existence and Computation of Consistent Dispersions . . . . .	86
4.5.1	Proofs of Theorem 1 & 2 . . . . .	89
4.5.2	Discussion . . . . .	94
4.6	Aggregation and Conversion Losses . . . . .	95
4.7	Aggregation and Uncertainty . . . . .	98
4.8	Time-Varying Connections . . . . .	101
4.8.1	Aggregated Model with Time-Varying Connections . . . . .	101
4.8.2	Additional Sources of Uncertainty . . . . .	105
4.9	Summary . . . . .	107
<b>5</b>	<b>Case Studies on a single EC-DER . . . . .</b>	<b>111</b>
5.1	Case Study 1: Simulation of a Household . . . . .	112
5.1.1	Description of the Case study . . . . .	112
5.1.2	Simulation Setup . . . . .	113
5.1.3	Forecasts . . . . .	114
5.1.4	Benchmarks . . . . .	116
5.1.5	Results . . . . .	120

---

5.1.6	Summary . . . . .	125
5.2	Case Study 2: Simulation of an Industrial Campus . . . . .	127
5.2.1	Description of the Case Study . . . . .	127
5.2.2	Simulation Setup . . . . .	129
5.2.3	Forecasts . . . . .	130
5.2.4	Results . . . . .	131
5.2.5	Summary . . . . .	134
5.3	Case Study 3: Experimental Dispatch of Solar Generation . . . . .	138
5.3.1	Description of the Case Study . . . . .	138
5.3.2	Implementation Aspects . . . . .	140
5.3.3	Simulation and Experimental Setup . . . . .	142
5.3.4	Results . . . . .	143
5.3.5	Summary . . . . .	149
5.4	Summary . . . . .	150
<b>6</b>	<b>Case Study on a Population of EC-DERs . . . . .</b>	<b>151</b>
6.1	General Modeling of a Dispatchable Charging Station . . . . .	151
6.1.1	Device Models . . . . .	151
6.1.2	Requirements . . . . .	153
6.2	Three-stage Scheduling and Operation . . . . .	154
6.3	Simulation . . . . .	158
6.3.1	Description of the Case Study . . . . .	159
6.3.2	Forecasts . . . . .	162
6.3.3	Benchmark Scheduling Method . . . . .	162
6.3.4	Simulation Setup . . . . .	164
6.3.5	Results . . . . .	164
6.4	Summary . . . . .	170
<b>7</b>	<b>Conclusions and Outlook . . . . .</b>	<b>171</b>
7.1	Conclusions . . . . .	171
7.2	Suggestions for Future Work . . . . .	174



# Nomenclature

## Acronyms

Acronym	Full name
AC	Alternate Current
BESS	Battery Energy Storage System
CDF	Cumulative Distribution Function
DC	Direct Current
DCS	Dispatchable Charging Station
DER	Distributed Energy Resource
DFS	Deterministic Forecast Scheduling
DS	Dispatch Schedule
EC-DER	Energy Constrained Distributed Energy Resource
MPC	Model Predictive Control
PDF	Probability Density Function
PEV	Plug-in Electric Vehicle
PFS	Probabilistic Forecast Scheduling
PV	PhotoVoltaic
SFS	Scenario Forecast Scheduling
SOC	State Of Charge

## General Notation

Notation	Description
$x$	Lower case letters denoting real or integer values
$X$	Serif, upper case letters denoting random variables
$\mathbf{x}, \mathbf{X}$	Bold letters denoting vectors (both for real/integer values and for random variables)
$[x_1 \dots x_N]$	Vector with elements $x_1, \dots, x_N$
$\mathcal{X}$	Calligraphic, upper case letters denoting sets
$[a, b] \subset \mathbb{R}$	Real interval with endpoints $a$ and $b$
$x(k)$	Value of $x$ at time step $k$
$\mathbb{E}[X]$	Expected value of random variable $X$
$\hat{x} = \mathbb{E}[X]$	Alternative shorthand notation to denote the expected value of a random variable
$X$	Roman, upper case letters denoting events
$\mathbb{P}(X)$	Probability of event $X$
$F_X(x)$	Cumulative density function of random variable $X$
$q_X(y)$	$y$ -th quantile of random variable $X$
$\{\cdot\}_{\mathcal{K}}$	Sequence of $\cdot$ over $\mathcal{K}$
$\#\{\cdot\}$	Cardinality of set $\{\cdot\}$
$\oplus$	Operator denoting the Minkowski sum
$\mathbf{1}$	Column vector of ones
$\times_{j \in \mathcal{N}} \mathcal{A}_j$	Cartesian product of all the sets $\mathcal{A}_j$ indexed in $\mathcal{N}$

## Specific Symbols

Symbol	Description
$k \in \mathbb{N}$	Discrete time index
$k^0 \in \mathbb{N}$	Time at which the schedule is computed
$\mathcal{K} \subset \mathbb{N}$	Scheduling horizon

Symbol	Description
$K \in \mathbb{N}$	Cardinality of $\mathcal{K}$ , $K = \#\{\mathcal{K}\}$
$\mathcal{K}^+ \subset \mathbb{N}$	Scheduling horizon shifted of one time step in the future
$k^b \in \mathbb{N}$	Beginning of the scheduling horizon
$k^e \in \mathbb{N}$	End of the scheduling horizon
$\delta \in \mathbb{R}$	Sampling period
$\mathcal{K}^s \subset \mathbb{N}$	Extended scheduling horizon
$k^s \in \mathbb{N}$	End of the extended scheduling horizon
$\mathcal{K}^0 \subset \mathbb{N}$	Offset between the computation and the execution of the schedule
$\mathcal{M} \subset \mathbb{N}$	Online rescheduling horizon
$\mathcal{S} \subset \mathbb{N}^\Omega$	Set of outcomes of an experiment
$\omega \in \mathcal{S}$	Outcome of an experiment
$\mathcal{S}' \subset \mathcal{S}$	Set of enumerated scenarios
$\omega' \in \mathcal{S}'$	Index of a scenario
$\pi^{\omega'} \in [0, 1]$	Probability of scenario $\omega'$
$\mathcal{N} \subset \mathbb{N}$	Index set denoting the EC-DERs within an aggregation
$N \in \mathbb{N}$	Cardinality of $\mathcal{N}$
$\mathcal{N}_1 \subset \mathbb{N}$	Index set denoting the uncertain inflexible prosumption within an aggregation
$N_1 \in \mathbb{N}$	Cardinality of $\mathcal{N}_1$
$(1 - \varepsilon) \in [0, 1]$	Security level
$l \in \mathbb{R}$	Uncertain inflexible prosumption
$p \in \mathbb{R}$	Active power output of an EC-DER
$g \in \mathbb{R}$	Active power exchange with the outer grid
$\tilde{g} \in \mathbb{R}$	DS
$\Delta g \in \mathbb{R}$	Deviation from the DS (imbalance)

Symbol	Description
$\mathcal{P} = [\underline{p}, \bar{p}]$	Set of feasible power outputs of an EC-DER
$e \in \mathbb{R}$	Energy state of an EC-DER
$\mu \in [0, 1]$	Conversion efficiency of an EC-DER
$\mathcal{E} = [\underline{e}, \bar{e}]$	Set of feasible energy states of an EC-DER
$c^{\text{DS}}(\tilde{g}(k), k)$	Cost function for the DS
$C^{\text{DS}} \in \mathbb{R}$	Cost of the DS
$c^i(\Delta g(k))$	Cost function for the imbalances
$C^i \in \mathbb{R}$	Expected cost of imbalances
$\epsilon \in \mathbb{R}$	Coefficient for softening of the energy constraint
$\rho \in \mathbb{R}$	Coefficient for relaxation of the energy constraint at the beginning of the DS
$s(\cdot)$	Aggregating function
$\mathcal{R} \subset \mathbb{R}$	Set of feasible and reachable energy states of an EC-DER
$\mathcal{N}_{\mathcal{K}}$	Index set denoting the EC-DERs within an aggregation connected for at least one time step in $\mathcal{K}$
$\mathcal{N}_{\mathcal{K}}(k)$	Index set denoting the EC-DERs within an aggregation connected at $k$
$e_v^{\min}$	Minimum energy state of the $v$ -th EC-DER upon disconnection
$k_v^{\text{a}}$	Connection time of the $v$ -th EC-DER
$k_v^{\text{d}}$	Disconnection time of the $v$ -th EC-DER

# 1 Introduction

## 1.1 Motivation

The fast advancements in information and communication technologies, the availability of cheap and efficient means to store and convert electric energy, and the rising concerns for environmental issues are reshaping the way in which electric power systems are structured and operated. Diverse scenarios are under discussion, depending on the interplay of political, economical, and environmental factors [ENTSO, 2018]. Despite their differences, all discussed scenarios involve an increase in the number of Distributed Energy Resources (DERs).

The exploitation of the technical and economical potential of DERs will largely depend on their integration within energy markets. Several market structures have been suggested in the literature to address this requirement, and the debate continues until today [Parag and Sovacool, 2016]. A well investigated option for the integration of DERs is to allow aggregations of DERs and loads—such as microgrids, virtual power plants and energy communities—to participate in existing energy markets [Koirala *et al.*, 2016]. The idea is that aggregated resources/loads commit to a given value of active power exchange with the external system, via regulated market auctions or bilateral agreements, cf. [Wang *et al.*, 2015]. The DERs within the aggregation are then coordinated such that the total active power output of the aggregation is dispatched in accordance with the pre-determined commitment. The rationale behind this concept is that coordinated operation of

DERs allows scalable services, bringing value to the entire system [Burger *et al.*, 2017].

However, coordinating DERs to dispatch power in accordance with a pre-computed schedule is not easy. The power output of some loads and DERs within the aggregation, such as PhotoVoltaic (PV) generation, may be inflexible, volatile, and uncertain; in short: not dispatchable. If this is the case, DERs with a flexible (directly controllable) power output (e.g.: storage systems, demand response) should balance this volatility, such that the total power exchange of the aggregation complies with the pre-determined commitment. However, directly controllable power outputs are often limited by the constraints of their respective device. The flexible DERs can modify their power output in response to deviations of the inflexible power outputs from their expected value only if they are not expected to operate at their capacity or capability limits. Thus, some power and energy reserves are required.

A challenging decision problem arises: how much power and energy reserves should be allocated? Unused reserves do not bring any profit to the aggregation of DERs. On the contrary, they represent a cost, because they could have been used to enhance the market revenues (for example, by actuating energy arbitrage). At the same time, a deficiency of reserves results in unplanned deviations from the committed dispatch, namely *imbalances*. Imbalances are costly, because they are penalized a-posteriori by the market regulator [Morales *et al.*, 2013]. In other words, the monetary revenues (or costs) of the aggregation of DERs highly depend on the chosen trade off between i) using the flexible resources for energy arbitrage, and ii) using the flexible resources to compensate for the uncertainty surrounding the production/consumption of the inflexible DERs and loads. Balancing these two aspects is non-trivial, and becomes particularly challenging when the market commitments involve a relatively long time period (e.g.: day-ahead market). Furthermore, additional constraint may arise whenever the flexible DERs perform additional functions besides storing energy, e.g. Plug-in

Electric Vehicle (PEV) necessitating a specified level of charge by a given time. All these aspects motivate the design of cost-effective scheduling algorithms, combining the latest advancements in forecasting, stochastic optimization, and numerical solvers.

## 1.2 Research Questions

This thesis focus on the problem of scheduling and operating an aggregation of flexible DERs and inflexible DERs/loads. In particular, we consider the context of an energy market that requires an a-priori commitment to a given dispatch level over a certain period of time, e.g. day-ahead market. The main challenge is represented by the uncertainty surrounding key data, such as the future power output of the inflexible DERs, that requires planning appropriate reserves together with the schedule. This problem is well studied in the literature, with several works distinguishing by the considered pricing policies, type of devices, and forecasting method. For example, Beltran *et al.* [2013], Perez *et al.* [2013], and Saez-de Ibarra *et al.* [2016] propose to schedule the generation of a “PV power plant” starting from deterministic predictions of the solar irradiation and energy prices. Similarly, Korpaas *et al.* [2003] and Lampropoulos *et al.* [2015] utilize deterministic predictions in scheduling; the first investigate wind generation coupled to storage, and the second analyze a setting including uncertain load and PV generation. Kou *et al.* [2015a] examine a similar case, but they employ parametric probabilistic forecasts of the uncertain generation. Sossan *et al.* [2016] and Namor *et al.* [2018] tackle planning the dispatch of a distribution feeder, where the uncertainty affecting the forecasts of the inflexible elements is compensated by a storage system. Therein, worst case scenarios for the power and energy prosumption are used in computing the schedule.<sup>1</sup> Fabietti *et al.* [2018] address a similar problem, by adding the option of using office buildings as thermal storage. In this case, scheduling is based

---

<sup>1</sup> Prosumption denotes coupled production and consumption.

on scenario forecasts. Zwartscholten *et al.* [2018] extend this setting to multiple “dispatchable systems”, introducing a hierarchy among them. Finally, Saint-Pierre and Mancarella [2016] and Stai *et al.* [2018] include grid constraints in the problem, moving as well from scenario forecasts. Further examples can be found in the literature, see the review [Nosratabadi *et al.*, 2017]. Despite differences in the considered aspects, all the mentioned works propose a similar approach to the problem itself. In particular, there is a tendency to address scheduling and operation in subsequent hierarchical steps: i) a day-ahead dispatch schedule is computed via deterministic or stochastic optimization; ii) intra-day rescheduling is performed by means of receding horizon optimization in order to minimize unavoidable imbalances and to re-allocate resources accordingly; iii) a feedback controller is implemented to regulate the dispatched power to the desired level.

The first step (scheduling) includes (more or less indirectly) the challenging problem of pre-allocating power and energy reserves, as previously discussed. With respect to this problem, the majority of the cited works that consider uncertainty in the scheduling process tackle computational tractability by means of sampling-based techniques—i.e. the uncertain parameters are replaced by a finite number of potential realizations.<sup>2</sup> A reason behind this choice is that sampling-based methods are always applicable, regardless of the model of the physical system and of the type of uncertainty [Shapiro *et al.*, 2009]. Another reason is connected to the fact that computing samples for the uncertain parameters is generally easier and more accurate than using other descriptions of the uncertain parameter, e.g. parametric description based on standard distributions. For example, consider non-parametric probabilistic forecasting models trained by means of machine learning, which have shown promising results when predicting the evolution of inflexible loads and renewable generation [Hong *et al.*, 2016].

---

<sup>2</sup> An exception is the work of Kou *et al.* [2015a], where computational tractability of chance constraint is achieved by means of a wrapping function obtained by using a sparse online warped Gaussian process to create the probabilistic forecasts.

Their output is a set of density forecasts or quantile forecasts that describe the distribution of uncertain parameters. Density/quantile forecasts cannot enter as-is into an optimization problem; however, they can be used to sample profiles (scenarios) of the forecasted parameters [Pinson *et al.*, 2009; González Ordiano, 2019].

Unfortunately, there are some pitfalls involved with sampling-based approaches, causing a loss of information on the uncertainty itself. Information is lost because the potentially infinite realizations of the uncertainty are approximated by a finite set [Nemirovski and Shapiro, 2006], and information is lost in generating the samples [González Ordiano, 2019].<sup>3</sup> These downsides motivate investigation of different approaches to the scheduling problem, which can cope with non-parametric probabilistic forecasts while avoiding sampling. In particular, it is unclear whether methods that make use of the full information provided by non-parametric probabilistic forecasts—at the cost of assumptions/approximations on the mathematical description of the physical system and of its control requirements—would outperform state-of-the-art scheduling based on sampling and scenario forecasts—where some of the available information is anyway lost in approximating the uncertainty.

Regardless of the extensive amount of schemes proposed in the literature, a number of open questions still need to be addressed in the design of a scheduling algorithm that can make use of non-parametric probabilistic forecasts. We divide these questions into three groups, to be tackled sequentially.

---

<sup>3</sup> Studies presented in [González Ordiano, 2019] highlight that samples generated from non-parametric probabilistic forecasts are less accurate in describing the tails of the actual distribution than the forecasts from which they originate.

## **Investigation and Classification of Existing Methods**

Existing approaches should be investigated with respect to their compatibility with non-parametric probabilistic forecasts. In particular, it is of interest to understand:

- Which existing approaches to stochastic programming allow for use of the entire information provided by non-parametric probabilistic forecasts?
- Are these approaches applicable to scheduling for an aggregation of several loads, generators and storage systems?
- What are the advantages and disadvantages of these methods?

## **Extension of Existing Methods in a Novel Algorithmic Framework**

Moving from the suggestions proposed in the literature, the next step is to design a novel algorithmic framework with improved performance in comparison to existing ones. This requires the following:

- Can approximations of the mathematical model of the physical system and of its control requirements improve the use of non-parametric probabilistic forecasts in scheduling?
- If so, are these approximations justified in practical cases?
- Which additional aspects should be considered in implementation?
- Is aggregated scheduling theoretically justified?
- Can aggregated models ease scheduling when some devices in the aggregation have uncertain power outputs?
- In this framework, is aggregated scheduling with stochastic programming viable for populations of devices that can connect and disconnect over the scheduling horizon?

### **Test of the Proposed Framework**

Finally, the performance of the proposed framework should be tested. To this end, the following questions shall be answered:

- Does the designed algorithm realize the desired outcomes in simulation?
- How does it perform in comparison to state-of-the-art methods?
- Is it applicable regardless of the size of the considered system?
- Does the scheduling algorithm realize the desired outcomes also in a real-life experiment?

## **1.3 Contributions**

The present thesis addresses the questions outlined in the previous section, aiming at the design of a scheduling approach for the dispatch of an aggregated energy system—comprising both flexible and uncertain power outputs—that combine non-parametric probabilistic forecasting and numerical computing without resorting to sampling and scenario forecasts. The core idea of this thesis is that such a scheduling algorithm can be constructed around a stochastic program where no constraints involve more than one uncertain parameter. The formulation of such a stochastic program builds upon an approximated energy-based model, where a single state lumps together the energy states of all flexible DERs. In this framework, the uncertain parameters entering the stochastic program do not necessarily represent a physical quantity, but they can be values incorporating information on the system (e.g. virtual energy states). Thus, the proposed algorithm is itself a bridge between model-based optimization and machine learning: some of the physical and statistical relations among system quantities are explicitly modeled in the stochastic program (model-based optimization), while others

are indirectly accounted for into the forecasting models of the uncertain parameters (built using machine learning techniques). In this perspective, this thesis locates itself in the emerging field of Energy Informatics because it deals with interdisciplinary research questions and methods at the interface of Electrical Engineering, Computer Science and Control Engineering.

## **Chapter 2: Scheduling with Stochastic Optimization**

We introduce a comprehensive classification of the various elements composing scheduling algorithms based on stochastic programming. We discuss not only the subsequent steps required to obtain a schedule, but also the dimensions to consider in formulating a tractable stochastic program when some parameters are uncertain. Starting from this classification—that to the best of the author’s knowledge has not been outlined in this way before—we discuss the potential to improve the performance of the overall scheduling algorithm by harmonizing the interaction of the various elements rather than by improving the capabilities of the single elements considered as separate entities.

## **Chapter 3: Stochastic Scheduling based on Energy Balance**

We propose a novel optimization-based algorithm to schedule the dispatch of an aggregation of DERs and loads entailing inflexible DERs/loads and a single flexible Energy Constrained Distributed Energy Resource (EC-DER). Unlike state-of-the-art schemes based on sampling methods and scenario forecasts, the proposed algorithm links non-parametric probabilistic forecasts with non-sampling based approaches to computational tractability. The core novelty of the proposed algorithm is the formulation of a stochastic program where each constraint does not involve more than a single random parameter. This way, the constraints can be formulated as chance constraints, and rendered computationally tractable with the sole knowledge of the Cumulative Distribution Function (CDF) of the involved random param-

eter. This CDF can be obtained from a non-parametric probabilistic forecast via fitting. We also discuss aspects of practical implementation of the algorithm, such as distinction among power flow directions, uncertain energy state at the beginning of the schedule and length of the optimization interval.

The ideas presented in this chapter have already been published in [Appino *et al.*, 2018a,b].

#### **Chapter 4: Aggregated Scheduling of Energy-constrained Distributed Energy Resources**

We derive sufficient conditions that an aggregated model can be used for scheduling without comprising feasibility of the individual constraints, hence reinforcing the theoretical reasons on which existing works on aggregated models are based. Furthermore, we propose a new methodology to ensure consistent online tracking of the aggregated schedule. This methodology is based on an appropriate “dispersion” (that we call *consistent dispersion*), computed via an optimization problem that can be solved point-wise in time. Moving from our findings, we discuss the case of a dynamic aggregation of EC-DERs considering multiple sources of uncertainty (e.g. forecast errors and unknown state of charge of PEVs upon arrival).

Most of the ideas presented in this chapter have already been published in [Appino *et al.*, 2019b, 2018c].

#### **Chapter 5: Case Studies on a single EC-DER**

We run simulations of the proposed scheduling and operation scheme on realistic settings involving a households and an industrial campus, investigating the performance of the proposed scheduling algorithm against state-of-the-art methods based on deterministic and scenario forecasts. Both schedule tracking and cost efficiency are considered as evaluating criteria. Furthermore, we examine whether the proposed scheduling algorithm is scalable to an industrial setting, with consideration of realistic energy prices

for the dispatched power. Last, we evaluate the results by applying it to an experimental setting.

Most of the results presented in this chapter have already been published in [Appino *et al.*, 2018a,b, 2019a].

## **Chapter 6: Case Study on a Population of EC-DER**

We run simulations of the proposed scheduling and operation scheme for a population of EC-DERs on a realistic setting involving a charging station for PEVs located in the parking area of an office building and provided with PV generation. We investigate the performance of the proposed scheduling algorithm against state-of-the-art methods based on scenario forecasts.

The results presented in this chapter have already been published in [Appino *et al.*, 2018c].

## **1.4 Outline**

The main part of this thesis is divided in five chapters: Chapter 2 reviews and classifies existing methods, Chapter 3 and Chapter 4 describe the proposed algorithmic framework and its theoretical justifications, and Chapter 5 and Chapter 6 report simulation and experimental result obtained from the application of the proposed framework to realistic cases. In detail, the chapters are structured as follows.

### **Chapter 2**

The first part of the chapter deals with the elements of automated scheduling with numerical optimization. Next, we introduce uncertain parameters in terms of random processes. Uncertainty mainly impacts three elements of the decision scheme: problem structure and model, computational tractability, and data processing. We analyze these elements separately and report state-of-the-art methods to deal with uncertainty in each case.

### **Chapter 3**

In the first part of the chapter, we present the models and requirements of the considered system. Then, we introduce a hierarchical scheme for its scheduling and operation. Next, we proceed by describing each level of the hierarchical scheme, with particular attention to the scheduling algorithm. An innovative optimization-based scheduling algorithm is introduced, based on a novel formulation of the stochastic program at its core. Finally, we discuss aspects entailing a practical implementation of the method.

### **Chapter 4**

In this chapter, we first present and discuss state-of-the-art aggregated scheduling for a population of EC-DERs. Next, we examine some deficiencies of such methods. Moving from those considerations, we derive sufficient conditions that an aggregated “time-varying battery” model for a population of EC-DERs can be used for scheduling without comprising feasibility of the individual constraints of the EC-DERs. Then, we propose a methodology to ensure consistent online tracking of the aggregated Dispatch Schedule (DS). This methodology is based on an appropriate “dispersion” (that we call *consistent dispersion*), computed via an optimization problem that can be solved point-wise in time. Finally, we comment on conversion losses, uncertainty, and aggregations of EC-DERs with time-varying connections.

### **Chapter 5 and Chapter 6**

In the first part of Chapter 5, we present and discuss simulation results concerning a household case. Then, we proceed with reporting and commenting upon simulation results concerning an industrial campus case. Last, we compare simulation results with measurements taken from real-life experiments. In Chapter 6, we presents and discusses simulation results over a

Dispatchable Charging Station (DCS), aggregating uncertain PV generation and a charging station for PEVs.

## 2 Scheduling with Stochastic Optimization

I don't think that mankind ever was meant to apprehend randomness and probabilities.

---

*J. Hoffmann-Jørgensen*

Optimization-based scheduling for systems comprising uncertain parameters is a research topic of interest in many scientific areas, ranging from mathematics to computer science, from production management to energy systems. The joint—but often uncoordinated—effort of diverse communities has a twofold outcome: on the one hand, there exists a vast body of literature on the topic; on the other hand, there is a lack of a coherent notion and terminology. Since the present thesis builds upon concepts from different scientific domains, it is pivotal to introduce a terminology that can be unambiguously used throughout the thesis. The present chapters deal with this crucial task. In particular, we first identify the different steps composing an optimization-based scheduling algorithm and the elements considered in engineering the optimization problem at its core. Then, we analyze the impact of uncertain parameters on some of those steps and elements, reporting briefly on some techniques to deal with each of those points, using examples taken mostly (but not exclusively) from the energy sector. To the best of the author's knowledge, such a classification is unprecedented. However, we remark that this chapter does not constitute a comprehensive report on the

topic. Such a level of detail is beyond scope here; we redirect the curious reader to the listed references.

## 2.1 Introduction

### 2.1.1 Scheduling

Throughout the thesis, *scheduling* refers to a method to compute a *schedule*, which is an ordered sequence of values assigned to a quantity of interest over a given time horizon. In particular, we focus on scheduling problems with the following characteristics:

- the schedule covers a discrete time horizon going from  $k^b$  to  $k^e$ ,

$$\mathcal{K} := \{k^b, k^b + 1, \dots, k^e\} \subset \mathbb{N},$$

with cardinality  $K$ , time index  $k \in \mathcal{K}$ , and sampling period  $\delta$ ;

- scheduling takes place before the scheduling horizon, at

$$k^0 := k^b - O \cdot \delta < k^b$$

with  $O \in \mathbb{N}$ ;

- the schedule is a decision that cannot be adjusted in operation and it is entirely applied once computed
- subsequent schedules are computed—covering non-overlapping time intervals<sup>1</sup>

Examples of scheduling problem presenting the listed properties are the day-ahead commitment required by the regulation of most energy markets, cf.

---

<sup>1</sup> This scheduling problem represents a decision process following a rolling horizon scheme. This is different from a receding horizon scheme, where subsequent schedules cover overlapping time intervals and only the first part of the schedule is applied before a new schedule is computed to overtake the previous one.

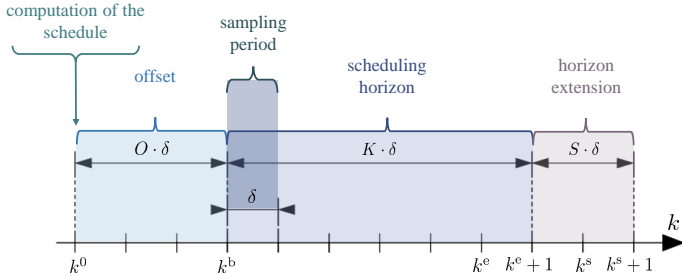


Figure 2.1: Discrete-time scheduling horizon, including the offset elapsed between computation and execution and an extension in the subsequent scheduling horizon.

[EPEX SPOT, 2018; Swissgrid, 2016], and the unit commitment problem in planning the operation of power plants, cf. [Padhy, 2004].

Note that, even if subsequent schedules are computed one at a time, the scheduling process should target an efficient operation over a time period covered by multiple schedules (potentially infinite). To this end, scheduling should pay particular attention to the system state at  $k^b$ , which couples subsequent schedules. Different strategies are proposed in the literature, as described in [Grüne *et al.*, 2010]. These strategies can be sorted into two main groups: i) methods aiming to steer the system towards an advantageous starting conditions for the following schedule, and ii) methods entailing an extension of the scheduling horizon such that the requirements of the following schedule are already explicitly considered in the current one.<sup>2</sup> While both options have been deeply investigated, none can claim to be better than the other in any case. Deciding upon an appropriate terminal condition can be as hard as determining a suitable extension of the horizon. Preference of a method over the other should be decided upon the specific case.

The scheme in Figure 2.1 summarizes the notation for the schedule, including an extension of the scheduling horizon of  $S$  steps until  $k^s$ .

<sup>2</sup> This way, the rolling horizon structure becomes a receding horizon one, because of the partial overlap of subsequent schedules.

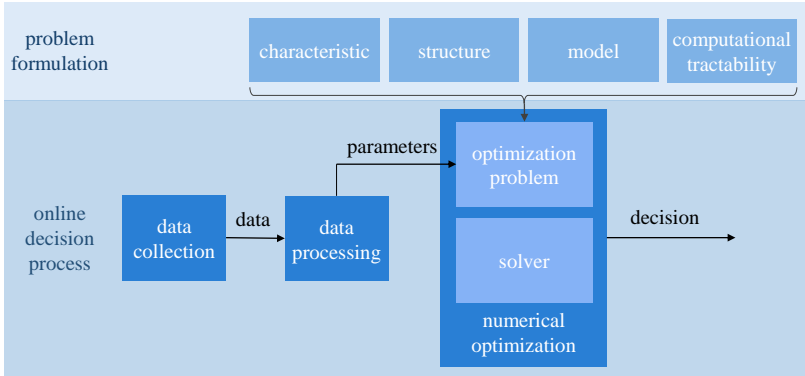


Figure 2.2: Phases of an automated decision process and aspects of problem formulation

### 2.1.2 Decision-making via Numerical Optimization

Scheduling is a challenging task that is often addressed by means of numerical optimization. This procedure hinges on an optimization problem, engineered to comply with the requirements and the constraints of the system. Formulating an appropriate optimization problem requires consideration of different items. In absence of coherent notation, we divide these elements in four main categories (see Figure 2.2): characteristics, structure, model and computational tractability. The characteristics are the properties and the requirements that are relevant in scheduling; for example, the requirement of operating a system with the minimum cost or the limitations on the power output of a device. The structure is the organization of the decision process; for example, taking all decision at once rather than in subsequent moments. The model is the mathematical abstraction of the characteristics and of the structure, which might involve approximations to a certain degree. Finally, computational tractability concern the possibility to tackle the optimization with state-of-the-art numerical solvers.

Once an optimization problem is formulated, an online decision process can be set up around it. The online decision process requires three steps to achieve a schedule:

- Data Collection: collect the data needed for data processing
- Data Processing: deduce the parameters required in the optimization problem starting from available data<sup>3</sup>
- Numerical Optimization: solve numerically the optimization problem

This is a well established decision process with a plethora of methods available to undertake each step; see for an example [Engell and Harjunoski, 2012; Yang *et al.*, 2015; Nosratabadi *et al.*, 2017] and references therein. Nevertheless, it should be considered that scheduling involves planning for the future and some or all of the parameters may be unknown. While accurate forecasting techniques are available for a large range of applications, predictions may often differ from reality. If this is the case, the uncertainty surrounding the forecasts should be directly considered both in the formulation of the optimization problem and in the online decision process. In particular, uncertainty plays a role in:

- problem structure and model,
- computational tractability,
- data processing.

In the following, we will examine each of these points and report state-of-the-art tools to deal with uncertainty in each case.

---

<sup>3</sup> The term *parameter* has different meanings in different contexts [Parameter, 2019]. In this thesis, we employ the term *parameter* similarly to how it is used in computer science. Specifically, we consider optimization problems as maps receiving parameters in input and returning optimal decision variables in output. In this context, we call parameter also what in control theory is generally regarded as a *disturbance* [Aström and Murray, 2010] or as an *exogenous signal* [Francis and Wonham, 1976].

## 2.2 Problem Structure and Models

### 2.2.1 Multi-stage Optimization

In scheduling with uncertainty, problem structure and models play a crucial role. Despite the large amount of literature on the topic, a general set of always applicable rules is missing. Nevertheless, there exists some recommendations to follow when engineering the optimization problem [King and Wallace, 2012].

To start with, consider the following (deterministic) parametric optimization problem

$$\begin{aligned}
 & \min_{\{\mathbf{x}\}_{\mathcal{K}}} \sum_{k \in \mathcal{K}} c(\mathbf{x}(k), \mathbf{w}(k)) \\
 & \text{s.t.} \\
 & \quad g(\{\mathbf{x}, \mathbf{w}\}_{\mathcal{K}}) \leq \mathbf{0}, \\
 & \quad h(\{\mathbf{x}, \mathbf{w}\}_{\mathcal{K}}) = \mathbf{0},
 \end{aligned} \tag{2.1}$$

with  $c : \mathbb{R}^{(X+W) \cdot \mathcal{K}} \rightarrow \mathbb{R}$ ,  $g : \mathbb{R}^{(X+W) \cdot \mathcal{K}} \rightarrow \mathbb{R}^G$ ,  $h : \mathbb{R}^{(X+W) \cdot \mathcal{K}} \rightarrow \mathbb{R}^H$ , vector  $\mathbf{x}(k) \in \mathbb{R}^X$  collecting the decision variables at step  $k$ ,  $\mathbf{w}(k) \in \mathbb{R}^W$  collecting the parameters at step  $k$ , and  $\mathbf{0}$  being a vector of zeros of appropriate dimension. We introduce the notation  $\{\cdot\}_{\mathcal{K}}$  to indicate the sequence of a time-dependent quantity (or quantities) over  $\mathcal{K}$ . For example

$$\{\mathbf{x}\}_{\mathcal{K}} := \{\mathbf{x}(k^b), \dots, \mathbf{x}(k^e)\}.$$

This notation is used also with functions, for example

$$g(\{\mathbf{x}\}_{\mathcal{K}}) := g(\mathbf{x}(k^b), \dots, \mathbf{x}(k^e)).$$

We assume that the constraints of (2.1) define a nonempty and compact set, and that  $c(\mathbf{x}(k), \mathbf{w}(k))$  is continuous on this set for whatever choice of

$\boldsymbol{w}(k) \in \mathbb{R}^W$ . Thus, in view of the extreme values theorem, it always exists a minimizing solution to (2.1).

Introducing uncertainty in the optimization problem implies describing some (or all) of the parameters and/or the decision variables as a discrete-time multivariate random (stochastic) process. A discrete-time random process  $\{Y(\omega)\}_{\mathcal{K}}$  associates each element  $\omega$  of the set  $\mathcal{S}$  of outcomes of an experiment to a time-dependent sequence  $\{y\}_{\mathcal{K}}$  [Carlton *et al.*, 2014].<sup>4</sup> A sequence  $\{y\}_{\mathcal{K}}$  is called a *realization* of  $\{Y(\omega)\}_{\mathcal{K}}$ , and  $\mathcal{S}$  can also be referred to as *sample set*.

The first step in introducing uncertainty in (2.1) is to establish *what* is uncertain. We refer to this choice as *problem structure*. First, parameters can be uncertain. Thus, we subdivide the parameters into a group that we model using random variables,  $\mathbf{W}^{\text{rv}}(k, \omega)$ , and into a group that we model using deterministic variables,  $\boldsymbol{w}^{\text{dv}}(k)$ . In the following, we refer to the elements of the first group as *random parameters* and to the elements of the second group as *deterministic parameters*. The meaning of a random parameter in an optimization problem within a scheduling process is quite intuitive: it is a parameter that cannot be described with certainty at the moment in which scheduling takes place because its value stems from the result of a (subsequent) random experiment. The future profile of uncontrollable loads is an example of a random parameter in the power system sector.

Similarly, we partition also the decision variables in a group that we model using random variables,  $\mathbf{X}^{\text{rv}}(k, \omega)$ , and into a group that we model using deterministic variables,  $\boldsymbol{x}^{\text{dv}}(k)$ . As for the parameters, we use the term *random decision variables* to indicate the elements of the first group, and the term *deterministic decision variables* to indicate the elements of the second group. Contrary to the case of random parameters, not only the role of

---

<sup>4</sup> Here and for the rest of the chapter, we employ the word *experiment* in the statistical sense, i.e. an action or activity whose outcome is subject to uncertainty [Carlton *et al.*, 2014]. Furthermore, note that we distinguish random variables from their realization using capitalization together with a different font.

a random decision variable is not self-evident, but even the term “random decision variable” sounds an oxymoron itself. We clarify this point in the following, introducing the concept of a *stage*. A stage defines a moment in which a decision is taken [King and Wallace, 2012]. The introduction of stages implies a subdivision of the decision variables  $\{\mathbf{x}\}_{\mathcal{K}}$  in subgroups, each corresponding to a stage. For example, a single-stage structure models taking all the decisions required over the horizon at the same time; these choices are then applied regardless of the realizations of the uncertainty. In this case, the decision variables are not divided in groups, because there is only one decision stage. All the decision variables are deterministic, i.e.  $\{\mathbf{x}\}_{\mathcal{K}} \equiv \mathbf{x}^{\text{dv}}(k)$ . On the contrary, a two-stage decision structure allows some decisions to be postponed to a second stage, once the outcome of the experiment  $\omega \in \mathcal{S}$  is known [Morales *et al.*, 2013]. In this case, the decision variables are divided in two groups: i) the first-stage decision variables  $\mathbf{x}^{\text{dv}}(k)$ , which are deterministic; and ii) the second-stage decision variables (postponed decisions)  $\mathbf{X}^{\text{tv}}(k, \omega)$ , which are random variables—because their value depends on the (unknown) outcome of the experiment. Observe that both random parameters and random decision variables map the outcome of an experiment to a value, with the difference that the mapping is *given* in the case of random parameters and it is instead a *choice* in the case of random decision variables [Charnes and Cooper, 1959].<sup>5</sup> In short, with the term “random” decision variable we do not refer to a decision that is taken casually, but a decision that is actually *not-taken* together with  $\mathbf{x}^{\text{dv}}(k)$ . Introducing random decision variables might be the only mathematically viable choice to cope with equality constraints when some parameters are random, as detailed later. However, if the decision problem that is tackled by means of numerical optimization permits to postpone some decisions, a two-stage scheme should still be preferred over a single-stage one. In fact,

---

<sup>5</sup> Note that this mapping does not need to have an explicit form.

a two-stage scheme includes the so-called value of options, which improves (statistically) the quality of the solution [Kall *et al.*, 1994].

Despite being commonly used, a two-stage structure can be a misleading representation of reality, because the realization of the random parameter  $\{\mathbf{w}^{\text{rv}}\}_{\mathcal{K}}$ , which is directly accessible, is not the outcome of the experiment  $\omega$ . In order to map back  $\{\mathbf{w}^{\text{rv}}\}_{\mathcal{K}}$  to its corresponding  $\omega$ , the entire sequence of  $\mathbf{w}^{\text{rv}}(k)$  over  $\mathcal{K}$  is needed. However, a decision  $\mathbf{x}^{\text{rv}}(k)$  may be required before knowing the entire sequence  $\{\mathbf{w}^{\text{rv}}\}_{\mathcal{K}}$ , which means before knowing the outcome  $\omega$  [Fabietti *et al.*, 2016]. This observation pushed the development of multi-stage structures, where the correlation between  $\mathbf{X}^{\text{rv}}(k, \omega)$  and  $\{\mathbf{W}^{\text{rv}}(\omega)\}_{\mathcal{K}'}$ , with  $\mathcal{K}' = \{k^{\text{b}}, \dots, k\}$ , is explicitly described and used to define the mapping  $\mathbf{X}^{\text{rv}}(k, \omega)$ , i.e.

$$\mathbf{x}^{\text{rv}}(k) := f(\{\mathbf{w}^{\text{rv}}\}_{\mathcal{K}'}). \quad (2.2)$$

This mapping enters the problem as an additional constraint, and the decision to be taken shifts from  $\mathbf{X}^{\text{rv}}(k, \omega)$  to function  $f$ . Examples of works investigating this structure for different applications are [Bitlislioglu *et al.*, 2017; Warrington *et al.*, 2013].

Summing up, introducing multivariate stochastic processes in (2.1) leads to the subsequent conceptual problem formulation

$$\begin{aligned} & \underset{\substack{\{\mathbf{x}^{\text{dv}}\}_{\mathcal{K}}, \\ \{\mathbf{X}^{\text{rv}}(\omega)\}_{\mathcal{K}}}}{\text{min}} \sum_{k \in \mathcal{K}} c(\mathbf{x}^{\text{dv}}(k), \mathbf{X}^{\text{rv}}(k, \omega), \mathbf{w}^{\text{dv}}(k), \mathbf{W}^{\text{rv}}(k, \omega)) \\ & \text{s.t.} \\ & g(\{\mathbf{x}^{\text{dv}}, \mathbf{X}^{\text{rv}}(\omega), \mathbf{w}^{\text{dv}}, \mathbf{W}^{\text{rv}}(\omega)\}_{\mathcal{K}}) \leq \mathbf{0} \\ & h(\{\mathbf{x}^{\text{dv}}, \mathbf{X}^{\text{rv}}(\omega), \mathbf{w}^{\text{dv}}, \mathbf{W}^{\text{rv}}(\omega)\}_{\mathcal{K}}) = \mathbf{0}, \end{aligned} \quad (2.3)$$

where, following [Kall *et al.*, 1994], the notation “min” indicates that (2.3) is not a well-defined decision problem. Note that, for the sake of notation simplicity, we consider here a two-stage structure.

Interpretation of Problem (2.3) raises several questions. What does it mean to minimize a function of random variables? What is an equality constraint with random variables? How to interpret an inequality constraint with random variables? In the following, we examine these points one at a time. Note that we only discuss the *interpretation* of Problem (2.3) in this section, leaving the review of methods to address computational tractability to Section 2.3.

### **Function with Random Variable**

A function of random variables is a random variable itself. Therefore, minimizing a function of random variables is not straightforward, because it requires to introduce an order among random variables. To this end, a common practice is to use moments. For example, the cost function of a stochastic program such as (2.3) is commonly interpreted as the minimization of the expected value of the cost function, cf. [Shapiro *et al.*, 2009]. This means that, given two random variables  $X(\omega)$  and  $Y(\omega)$ ,  $X(\omega) < Y(\omega)$  holds if  $\mathbb{E}[X(\omega)] < \mathbb{E}[Y(\omega)]$ , where notation  $\mathbb{E}[X(\omega)]$  denotes the expected value of  $X(\omega)$ . However, ordering of random variables is not standard, thus the interpretation of a cost function with random variables is an engineering decision. Other options than using the expected value are indeed proposed: see [Nagy and Braatz, 2003] for an example including the variance.

### Equality Constraints

An equality constraint involving random variables introduces a correlation among them. The equality must hold for each outcome  $\omega$  of the sampling set  $\mathcal{S}$ , i.e.

$$h(\{\mathbf{x}^{\text{dv}}, \mathbf{X}^{\text{rv}}(\omega), \mathbf{w}^{\text{dv}}, \mathbf{W}^{\text{rv}}(\omega)\}_{\mathcal{K}}) = \mathbf{0} \quad \forall \omega \in \mathcal{S}.$$

### Inequality Constraints

Inequality constraints leave room to different interpretations. An option, often going under the name of *robust optimization* [Bertsimas *et al.*, 2011], is to impose the satisfaction of the inequality constraint for all possible realizations, i.e.

$$g(\{\mathbf{x}^{\text{dv}}, \mathbf{X}^{\text{rv}}(\omega), \mathbf{w}^{\text{dv}}, \mathbf{W}^{\text{rv}}(\omega)\}_{\mathcal{K}}) \leq \mathbf{0} \quad \forall \omega \in \mathcal{S}.$$

However, this method can be conservative and it is not applicable whenever the uncertainty cannot be described with a finite set of outcomes, i.e. in case of random variables with infinite support. Thus, a common interpretation of inequality constraints involving random variables is in terms of chance constraints [Charnes *et al.*, 1958]. In this case, the satisfaction of the inequality constraints is required only with at least a given probability  $(1 - \varepsilon)$ , i.e.

$$\mathbb{P}(\{\omega : g(\{\mathbf{x}^{\text{dv}}, \mathbf{X}^{\text{rv}}(\omega), \mathbf{w}^{\text{dv}}, \mathbf{W}^{\text{rv}}(\omega)\}_{\mathcal{K}}) \leq \mathbf{0}\}) \geq (1 - \varepsilon). \quad (2.4)$$

The value  $(1 - \varepsilon)$  is often called security level. Note that if  $G > 1$  (i.e. the constraints set includes more than one inequality) the chance constraints can be formulated either as separate chance constraints or as a joint chance constraint. In the first case, each individual inequality has to be satisfied with its own security level  $(1 - \varepsilon)$ ; in the latter, as in (2.4),  $(1 - \varepsilon)$  is the lowest probability of all the inequalities to hold at the same time. Note

that, as for the cost function, the interpretation of inequalities with random variables is not standard and is the result of an engineering decision.

In view of these considerations, we rewrite (2.3) in the following (meaningful) form

$$\begin{aligned}
 & \min_{\substack{\{\mathbf{x}^{\text{dv}}\}_{\mathcal{K}}, \\ \{\mathbf{x}^{\text{rv}}(\omega)\}_{\mathcal{K}}}} \mathbb{E} \left[ \sum_{k \in \mathcal{K}} c(\mathbf{x}^{\text{dv}}(k), \mathbf{X}^{\text{rv}}(k, \omega), \mathbf{w}^{\text{dv}}(k), \mathbf{W}^{\text{rv}}(k, \omega)) \right] \\
 & \text{s.t.} \tag{2.5} \\
 & \mathbb{P}(\{\omega : g(\{\mathbf{x}^{\text{dv}}, \mathbf{X}^{\text{rv}}(\omega), \mathbf{w}^{\text{dv}}, \mathbf{W}^{\text{rv}}(\omega)\}_{\mathcal{K}}) \leq \mathbf{0}\}) \geq (1 - \varepsilon), \\
 & h(\{\mathbf{x}^{\text{dv}}, \mathbf{X}^{\text{rv}}(\omega), \mathbf{w}^{\text{dv}}, \mathbf{W}^{\text{rv}}(\omega)\}_{\mathcal{K}}) = \mathbf{0} \quad \forall s \in \mathcal{S}.
 \end{aligned}$$

## 2.3 Computational Tractability

Design of appropriate decision structures and models leads to a meaningful stochastic program. The next step is to solve the stochastic program. This is not an easy task: an optimization problem with random variables is potentially infinite dimensional and cannot be solved directly by well established numerical solvers. Thus, the problem has to be first rendered computationally tractable [Nemirovski and Shapiro, 2006]. In the literature, there are many methods to handle this task, as discussed in the following. Despite their differences, these methods can be sorted on a high level into two complementary categories:

- sampling-based approaches
- non-sampling-based approaches

Note that each category requires a specific representation of the uncertainty. In the next sections, we recall the main aspects of each type, as well as their advantages and disadvantages.

### 2.3.1 Sampling-based Approaches

Sampling-based approaches to stochastic programming are well investigated [Shapiro *et al.*, 2009]. Scenario-based optimization is a popular sampling-based approach, especially when a multivariate stochastic processes is involved [Campi *et al.*, 2009; Conejo *et al.*, 2010]. Despite differences, the basic idea is to augment the dimension of the problem, replicating equality and inequality constraints for a subset of the outcome set,  $\mathcal{S}' \subset \mathcal{S}$  with cardinality  $\Omega'$ . All the constraints are considered for each *scenario*  $\omega' \in \mathcal{S}'$ , by substituting the stochastic processes with their realization under  $\omega'$  for both random parameters (whose realizations are given) and random decision variables (whose realization have to be determined, either directly or as functions of the realization of random parameters). Furthermore, a probability  $\pi^{\omega'} \in \mathbb{R}$  is assigned to each  $\omega' \in \mathcal{S}'$  such that

$$\sum_{\omega' \in \mathcal{S}'} \pi^{\omega'} = 1.$$

This probability is employed in computing the expected cost of  $c$ . In particular, the expected cost of  $c$  is the average of the realizations of  $c$  under all  $\omega' \in \mathcal{S}'$  weighted with  $\pi^{\omega'}$ . Applying a scenario-based approach to (2.1) results into

$$\begin{aligned} & \min_{\substack{\{\mathbf{x}\}_{\mathcal{K}}, \\ \{\mathbf{x}^{\omega'}\}_{\mathcal{K}}}} \sum_{k \in \mathcal{K}} \sum_{\omega' \in \mathcal{S}'} \pi^{\omega'} \cdot c(\mathbf{x}(k), \mathbf{x}^{\omega'}(k), \mathbf{w}(k), \mathbf{w}^{\omega'}(k)) \\ & \text{s.t.} \\ & g(\{\mathbf{x}, \mathbf{x}^{\omega'}, \mathbf{w}, \mathbf{w}^{\omega'}\}_{\mathcal{K}}) \leq 0 \quad \forall \omega' \in \mathcal{S}', \\ & h(\{\mathbf{x}, \mathbf{x}^{\omega'}, \mathbf{w}, \mathbf{w}^{\omega'}\}_{\mathcal{K}}) = 0 \quad \forall \omega' \in \mathcal{S}'. \end{aligned} \tag{2.6}$$

where  $\mathbf{w}^{\omega'}$  and  $\mathbf{x}^{\omega'}$  denote the realization under scenario  $\omega'$  of the random parameters and of the random decision variables, respectively. By compar-

ing the inequalities in (2.6) to the original chance constraint (2.4), it can be seen that set  $\mathcal{S}'$  should be chosen such that

$$\mathbb{P}(\{\omega : \omega \in \mathcal{S}'\}) \geq (1 - \varepsilon). \quad (2.7)$$

Indication on how to construct such a set can be found in [Campi *et al.*, 2009].

### **Advantages and Disadvantages**

Sampling-based methods are intuitive and can be applied to any problem in the form (2.5). Therefore, they are largely used, also in the energy sector. Examples can be found in [Garcia-Gonzalez *et al.*, 2008; Ding *et al.*, 2012; Su *et al.*, 2013; Stai *et al.*, 2018; Good and Mancarella, 2017]. However, sampling-based methods present drawbacks which stem from the fact that the approximation of the original problem obtained using scenarios is itself random. In fact, the theoretical number of scenarios required to satisfy (2.7) may lead to conservative solutions in practice [Shapiro *et al.*, 2009]. Furthermore, augmenting the problem in terms of constraints and decision variables raises the computational burden. Scenario-reduction techniques are proposed to partially alleviate these issues. An exemplary algorithm for scenario reduction can be found in [Conejo *et al.*, 2010]. Alternatively, Margellos *et al.* [2014] propose to compute bounds that envelope the set of scenarios with a given probability, and then to use these bounds to ensure the satisfaction of the constraints under all the scenarios.

### **2.3.2 Non-sampling-based Approaches**

Contrary to scenario-based approaches, where the starting point is a set of realizations of the random parameters, non-sampling based methods build upon the moments or upon an analytic description of the Probability Density Function (PDF) and/or of the CDF of the multivariate stochastic process.

The general idea of non-sampling based approaches is to achieve computational tractability of (2.5) by exploiting some properties of the problem or of the random variables describing the uncertainties. In particular, two main aspects have to be addressed: i) how do the equalities translates in relations among moments, PDF, CDF, or quantiles?, and ii) how to reformulate chance constraints in terms of moments, PDF, CDF, or quantiles?

### **Equality Constraints with Non-sampling-based Approaches**

For the sake of completeness, we report in the following two non-sampling based approaches to tackle (non trivial) equalities among random variables.

The first one is Polynomial Chaos Expansion (PCE). PCE is a spectral method that can be used to expand scalar random variables into a weighted sum of orthogonal polynomial of independent scalar random variables [Xiu, 2010; Kim *et al.*, 2013]. This way, the original random variable can be uniquely represented by a set of PCE coefficients—i.e. the weights of the polynomial series. The advantage of PCE lays in the possibility to describe each of the random variables of interest as a function of some independent random variables (namely, the *stochastic germ*) in a way that preserves the correlation imposed by the equality constraints. In fact, appropriate projection techniques can translate the relations among random variables expressed by the equality constraints into equalities among PCE coefficients, thus enabling their computational tractability. The major limitation of applying PCE to stochastic scheduling is the requirement of known PCE coefficients for the random parameters. These coefficients should consider the correlation among random parameters and are not always easy to compute.

A second method to deal with equality constraints with random variables is moment closure. The idea is to move from an (infinite dimensional) equation involving random variables to a finite system of equations, each containing only the moments of a given order of the random variables appearing in the original equation. This method is particularly useful in analyzing

the dynamics of systems involving a large number of random states. By applying moment closure, the intractable infinite-dimensional dynamics describing the system behavior can be substituted with a number of (tractable) equations describing each the evolution of the moments of a given order, e.g. [Hespanha and Singh, 2005; Lee *et al.*, 2009]. The major limitation of this method is that an accurate description of the original dynamics may require a large number of single-moment equations. Therefore, approximations may be required to express the original dynamics only in terms of a limited number of “lower-order moments”.

### Chance Constraints With Non-sampling-based Approaches

The main idea of tackling computational tractability of chance constraints with a non-sampling-based approach is to enforce the satisfaction of the constraints for realizations of the uncertainty within an interval around the expected value [Calafiore and El Ghaoui, 2006]. To this end, several methods have been proposed in the literature, distinguishing by the way of computing this interval. The most general methods do not require any specific knowledge on the distribution of the uncertainty, relying, for example, either on the moments of the distribution [Van Parys *et al.*, 2016] or on an empirical iterative algorithm [Roald, 2016].

More general approaches can be applied whenever additional information on the uncertainty are available. For example, chance constraints can be reformulated exactly in case of log-concave and symmetric distributions [Lagoa *et al.*, 2001]. In the following, we analyze closely the case of a joint chance constraint in the form of

$$\mathbb{P}(\{\omega : g_{\mathbf{x}}(Z(\omega)) \in \mathcal{Y}\}) \geq (1 - \varepsilon), \quad (2.8)$$

where  $g_{\mathbf{x}}$  is a continuous invertible function  $g_{\mathbf{x}} : \mathbb{R} \rightarrow \mathbb{R}$  with parameters  $\mathbf{x} \in \mathbb{R}^X$ ,<sup>6</sup>  $Z(\omega)$  is a random variable and  $\mathcal{Y}$  is a continuous real in-

---

<sup>6</sup> Note that this requirements excludes the presence of quadratic terms in  $g_{\mathbf{x}}$ .

terval. Furthermore, we assume a known CDF for  $Z(\omega)$ , which we denote as  $F_Z(z)$ .<sup>7</sup> Constraint (2.8) with known  $F_Z(z)$  is of particular interest for the scheduling problem discussed in the following chapters. Note that we consider a general shape for  $F_Z(z)$ . Therefore, techniques that require restrictive assumptions on the distribution of the random variables, as the one presented in [Lagoa *et al.*, 2001], do not apply.

We present two methods to deal with (2.8) in its equivalent form

$$\mathbb{P}(\{\omega : Z(\omega) \in g_x^{-1}(\mathcal{Y})\}) \geq (1 - \varepsilon). \quad (2.9)$$

The first method makes use of the quantiles of  $Z(\omega)$ , the second one of an analytic description of  $F_Z(z)$ .

First, we analyze the quantile-based approach [Vrakopoulou *et al.*, 2013]. In the following,  $q_Z(j)$  denotes the  $j$ -th quantile of  $Z(\omega)$ , which is the quantity for for which  $\mathbb{P}(\{\omega : Z(\omega) < q_Z(j)\}) = j$  [Murphy, 2012]. The main idea of quantile-based approaches is to use the quantiles of the random variable  $Z(\omega)$  to compute the interval

$$\mathcal{Z}_{(1-\varepsilon)} = [q_Z(0.5 - 0.5(1 - \varepsilon)), q_Z(0.5 + 0.5(1 - \varepsilon))].$$

Then, imposing

$$\mathcal{Z}_{(1-\varepsilon)} \in g_x^{-1}(\mathcal{Y}) \quad (2.10)$$

guarantees satisfaction of (2.9). In fact, by definition of  $\mathcal{Z}_{(1-\varepsilon)}$ , it holds that

$$\mathbb{P}(\{\omega : Z(\omega) \in \mathcal{Z}_{(1-\varepsilon)}\}) \geq (1 - \varepsilon). \quad (2.11)$$

This approach is intuitive, simple to apply, and requires only the knowledge of an appropriate pair of quantiles of  $Z(\omega)$ . However, it might be inefficient in practice, because the bounds of  $\mathcal{Z}_{(1-\varepsilon)}$  are computed offline. Thus, there

<sup>7</sup> Recall that  $F_Z(z)$  is defined as  $F_Z(z) = \mathbb{P}(\{\omega : Z(\omega) \leq z\})$  [Murphy, 2012].

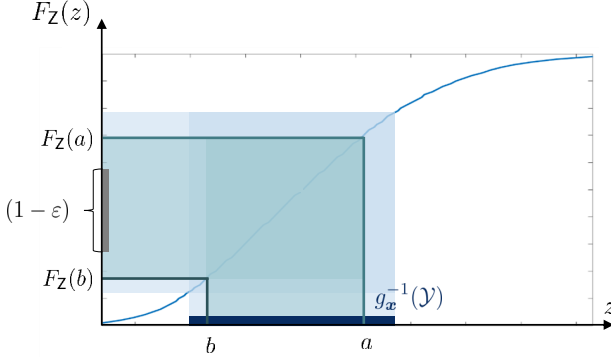


Figure 2.3: Schematic representation of the computationally tractable reformulation of chance constraint (2.9).

is no guarantee that a solution with lower cost can be achieved by a different choice of  $\mathcal{Z}_{(1-\varepsilon)}$  satisfying (2.11).

A second method to deal with (2.9) implies a direct use of the CDF  $F_Z(z)$ . Given  $F_Z(z)$ , the inequalities

$$F_Z(a) - F_Z(b) \geq (1 - \varepsilon), \quad (2.12a)$$

$$-\min(g_{\mathbf{x}}^{-1}(\mathcal{Y})) \geq -b, \quad (2.12b)$$

$$\max(g_{\mathbf{x}}^{-1}(\mathcal{Y})) \geq a, \quad (2.12c)$$

are a computationally tractable reformulation of the joint chance constraint (2.9), [Miller and Wagner, 1965]. Figure 2.3 illustrates this reformulation in order to ease its understanding. In words, the probability of the realization of  $Z$  to lay in the interval  $[a, b] \subset g_{\mathbf{x}}^{-1}(\mathcal{Y})$  should be equal or higher than  $(1 - \varepsilon)$ . As  $F_Z(z)$  is increasing, (2.12) is contemporary satisfied if

$$F_Z(\max(g_{\mathbf{x}}^{-1}(\mathcal{Y}))) - F_Z(\min(g_{\mathbf{x}}^{-1}(\mathcal{Y}))) \geq (1 - \varepsilon), \quad (2.13)$$

also illustrated in Figure 2.3. The proposed constraints formulation is similar, yet not equivalent, to the one resulting from a quantile-based approach. In fact, similar to (2.11), the satisfaction of the joint chance constraint is achieved by enforcing problem feasibility for a compact subsets of the support of  $Z$ . However, contrary to (2.11), this subsets is chosen using full information on the distribution of the random variables and does not have to be symmetric w.r.t. the expected value.

### **Advantages and Disadvantages**

The computationally tractable optimization problem obtained via approaches that do not require sampling has the advantage of addressing directly the original stochastic program. Eventual approximations are clearly defined and are not the results of a random selection. However, the application of non-sampling-based approaches is not straightforward and should be tailored to the specific case. Depending on the structure of the problem and on the nature of the uncertainty, dealing with computational tractability with non-sampling-based approaches may be impossible without introducing numerous approximations or it may lead to a high computational burden. Furthermore, non-sampling-based approaches are ineffective in case of limited information on the uncertainty (shape of the distribution, correlation, etc.). Resorting to conservative approximations to compensate for this lack of knowledge may spoil the benefits of the method.

## **2.4 Data Processing**

The last aspect of automatic optimization-based scheduling in which uncertainty plays a role is data processing. In fact, a stochastic program requires in input some information on the random parameters in terms of probabilistic forecasts. Recall that probabilistic forecasts determine ranges of plausible values and their associated probability, in contrast to point forecasts which provides only a single value [Antonanzas *et al.*, 2016]. Probabilis-

tic forecasting methods with applications in the energy sectors have been deeply investigated in recent years; see [González Ordiano *et al.*, 2018a] and [Bessa *et al.*, 2017] for a comprehensive review. The core ideas of the proposed methods can be divided in three major categories:

- based on persistence;
- based on a parametric description of the uncertainty;
- based on a non-parametric description of the uncertainty.

Forecasting algorithms based on persistence use past realizations of the uncertainty as a forecast for future realizations. These approaches select a set of past realizations among the available data and consider this set as a set of scenarios for the realization of the uncertainty; see [Namor *et al.*, 2016] for an example. Forecasting algorithms based on a parametric description of the uncertainty assume that the distribution (PDF or CDF) of the uncertain parameter follows a pre-defined shape which can be described by an analytic expression. An example involving Gaussian processes can be found in [Kou *et al.*, 2015b]. Last, forecasting algorithms based on non-parametric forecasts translate the distribution of the uncertain parameter into a set of density forecasts or into a number of quantile forecasts. Therefore, these algorithms are considered distribution-free, see [Zhang *et al.*, 2014] and references therein.

Note that the output of each forecasting method describes the uncertainty in a specific way: with a set of scenarios, with an analytic expression of the distribution, or with a number of density/quantile forecasts. At the same time, the forecast output should match the requirements on the input of the optimization problem. Some transformations can harmonize the forecast output with the optimization input, regardless of the core idea behind the forecasting algorithm. Examples are statistics to turn scenarios into quantiles, fitting to go from quantiles to CDF, sampling to obtain scenarios

from a CDF, etc. Nevertheless, these transformation are not always trivial [González Ordiano, 2019]. For example, sampling scenarios from non-parametric probabilistic forecasts requires to include the correlation among time steps at subsequent times, which is not directly considered in the non-parametric probabilistic forecasts;<sup>8</sup> see [González Ordiano, 2019] and [Pinson *et al.*, 2009] for examples of scenario generation from non-parametric probabilistic forecasts. Furthermore, some information may be lost in the transformation. In [González Ordiano *et al.*, 2018b], for example, it is shown that scenarios obtained via sampling from non-parametric forecasts are not describing the stochastic process as well as the original forecasts. Specifically, the sampled scenarios are less accurate in capturing the tails of the actual distributions.

## 2.5 Summary

Scheduling under uncertainty by means of multi-stage stochastic optimization is well investigated. However, the three aspects of the decision chain that are mostly affected by uncertainty—problem structure and models, computational tractability, and data processing—are often examined separately. This leads to the fact that promising ideas in each of these distinct fields do not naturally combine together in a scheduling algorithm. One of the major conflicts raises between forecasting algorithms and methods to deal with computational tractability. As discussed, non-sampling-based approaches are supported by a well established theory and can achieve computational tractability while providing a solution to the original problem; however, they require an explicit description of the correlation among the

---

<sup>8</sup> Forecasting the random process as a multivariate distribution (where each dimension represents a step in the forecasting horizon) would provide information on the correlation. Eventually, this information could be used to obtain linearly independent single-step random variables, by means of principal component analysis [Abdi and Williams, 2010]. However, such a forecasting model is difficult to create and computationally demanding for long forecasting horizon.

time-steps of the multivariate stochastic process, which is not provided by non-parametric forecasting techniques. On the other side, non-parametric probabilistic forecasting techniques show superior performances to other forecasting techniques in describing stochastic processes that are relevant in power system applications, such as solar and wind generation [Hong *et al.*, 2016]. The apparent conflict between computational tractability and data processing, and between model-based optimization and machine learning, is traditionally overcome by application of sampling-based methods with scenario forecasts. However, these approaches indirectly include an approximation of the uncertainty, which may deteriorate the benefits of advanced forecasting techniques on the final result. Thus, scheduling for management and operation of power system calls for alternative methods to link non-parametric probabilistic forecasting and numerical optimization without resorting to scenario forecasts. In the following chapter, we tackle this challenge for the case of aggregated power systems.

## 3 Stochastic Scheduling based on Energy Balance

In this chapter we investigate scheduling and operation of an aggregation of DERs/loads comprising both inflexible DERs with uncertain power output and a single flexible—but energy constrained—DER. The core of this chapter is an innovative algorithm to schedule the active power dispatch of the aggregated system. The novelty of the algorithm is the way it combines non-parametric probabilistic forecasts with numerical optimization without resorting to samples of the uncertain parameters. Therein, the major challenge is the difficulty of forecasting the correlation among the (possibly numerous) uncertain parameters, information required by non-sampling based approaches to deal with the computational tractability of the energy state dynamics. We tackle this issue formulating a stochastic program that does not contain any constraints involving more than one uncertain parameter or decision variable. Specifically, this formulation is obtained by introducing (approximated) energy balance equations in spite of the dynamics of the energy state.

The ideas presented in this chapter have appeared in [Appino *et al.*, 2018a] and [Appino *et al.*, 2018b].

### 3.1 Models and Requirements

In this chapter, we deal with scheduling the exchange of active power at the interface between a utility-owned power grid and a prosumer-owned aggregation of DERs comprising inflexible and uncertain generation/demand and

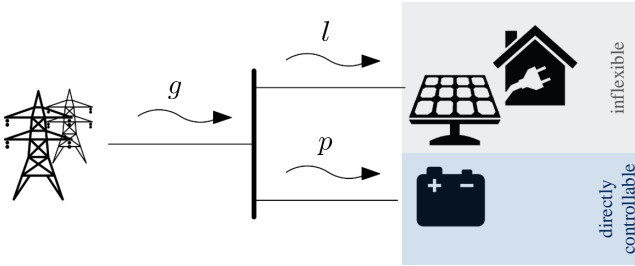


Figure 3.1: Schematic representation of a dispatchable feeder.

a single flexible, but energy-constrained, DER (Figure 3.1). Furthermore, we consider the requirement to dispatch the total power output of the aggregation accordingly to a pre-computed DS. This system can be associated to the concept of a virtual power plant or of a microgrid [IEEE PES Task Force on Microgrid Stability Analysis and Modeling, 2018]. However, for the sake of clarity, we emphasize that the focus of the present work is on the dispatch of active power, regardless of the provision of any capacity reserve or other support services *to the grid*. The recent work from Sossan *et al.* [2016] denotes a system with these characteristics and requirements as a *dispatchable feeder*; nevertheless, a commonly accepted terminology is currently lacking. Details on the models and on the requirements are described in the following subsections.

### 3.1.1 System Components

#### Inflexible Distributed Energy Resources and Loads

We denote devices (whether they are loads or generators) whose power output is either not adjustable or regulated according to independent device-specific settings as *inflexible*. This is often the case, for example, with wind turbines or PV generators, as well as with the majority of domestic loads. Here, variable  $l(k) \in \mathbb{R}$  indicates the (averaged) aggregated inflexible active power output over the  $k$ -th step, regardless of the number and nature

of devices contributing to it. A negative value for  $l(k)$  represents power injection.

### Energy-constrained Distributed Energy Resources

The term EC-DER denotes devices that can be associated to an energy state that is subject to dynamics and constraints. This energy state can represent either an amount of energy that is physically stored in the device or the energy exchanged with the EC-DER over a given time period [Evans *et al.*, 2018]. Examples of EC-DER are batteries and other types of storage, see [Zhao *et al.*, 2015], or flexible demand. Xu *et al.* [2016] formalize this concept by proposing a generic “time-varying battery” model for an EC-DER.<sup>1</sup> Therein, an integrator-like dynamic equation describes the evolution of the energy state of the EC-DER

$$e(k+1) = e(k) + \delta \cdot (p(k) - \mu |p(k)|), \quad (3.1)$$

where the variable  $p(k) \in \mathbb{R}$  is the (averaged) active power output over the  $k$ -th step,  $e(k) \in \mathbb{R}$  is the energy state at time  $k$ , and  $\mu$  is a coefficient modeling conversion losses. This model moves from ideas on energy conservation, supposing that the energy losses are directly proportional—with coefficient  $\mu$ —to the absolute value of the power output  $p(k)$ . Note that this model simplifies the actual phenomenon which occur in practice. Estimating the energy lost in operation by an EC-DER is still an open question and it is particularly challenging in the case of batteries [Li *et al.*, 2018]. Nevertheless, dynamics as in (3.1) are frequently applied in the literature concerning scheduling problems, and have proved to be a valid approximation also in real-life experiments pSossan16a. Thus, we consider (3.1) to be sufficiently accurate for the scope of the present work.

---

<sup>1</sup> Xu *et al.* [2016] use the term “flexible loads” to denote what here is called EC-DERs.

The active power output of an EC-DER can be adjusted within the limits imposed by its power and energy constraints

$$p(k) \in \mathcal{P}(k), \quad (3.2a)$$

$$e(k+1) \in \mathcal{E}(k+1), \quad (3.2b)$$

with  $\mathcal{P}(k)$  and  $\mathcal{E}(k+1)$  being closed real intervals, i.e.  $\mathcal{P}(k) = [\underline{p}(k), \bar{p}(k)] \subset \mathbb{R}$  and  $\mathcal{E}(k+1) = [\underline{e}(k+1), \bar{e}(k+1)] \subset \mathbb{R}$ .

### Interconnection with the Upper Level Grid

Variable  $g(k)$  indicates the active power exchange between the system and its corresponding upper-level grid. For the sake of simplicity, we do not consider any constraint on the value of  $g(k)$ .<sup>2</sup> All of the devices connect to the same grid-connected bus, as schematically represented in Figure 3.1. The connections are assumed to be lossless and such that the system components are able to exchange power mutually without any technical limit. Therefore, the power balance is (see Figure (3.1))

$$g(k) = p(k) + l(k). \quad (3.3)$$

### 3.1.2 Requirements

The scheme proposed in this chapter aims at dispatch-as-scheduled of the power exchange  $g(k)$  by means of a coordinated control of the system components. We consider that the dispatchable feeder acts directly on an energy market of the kind described by Morales13: operating revenues (or costs) can be directly associated to the DS through a known cost function, while deviations from the DS (imbalances) are limited by regulations or penalized in operation.

---

<sup>2</sup> Please note that adding constraints on  $g(k)$  does not change the findings outlined in the present thesis, as long as the feasible set remains non-empty.

Following this regulation, we first divide the power exchange  $g(k)$  into two components:

$$g(k) = \tilde{g}(k) + \Delta g(k), \quad (3.4)$$

where  $\tilde{g}(k)$  is the DS for the  $k$ -th step, and  $\Delta g(k)$  is the average imbalance over the  $k$ -th step.

Then, we model the operating revenues (or costs) of the DS via the following cost function  $c^{\text{DS}}(\tilde{g}(k), k) : \mathbb{R} \times \mathbb{N} \rightarrow \mathbb{R}$ ,

$$c^{\text{DS}}(\tilde{g}(k), k) = c^{\text{q}}(k)\tilde{g}^2(k) + c^{\text{l}}(k)\tilde{g}(k). \quad (3.5\text{a})$$

Here,  $c^{\text{q}}(k)$  and  $c^{\text{l}}(k)$  are (known) time-varying cost coefficients. Additionally, the term

$$c^{\text{c}}(\tilde{g}(k+1) - \tilde{g}(k))^2, \quad (3.5\text{b})$$

can be considered to penalize the incremental change of  $g(k)$  (approximating the derivative of the DS), with  $c^{\text{c}}$  being a constant weight,. We chose cost function  $c^{\text{DS}}(\tilde{g}(k), k)$  because of its generality: peak shaving and maximization of self-consumption can be considered together with price-based load shifting.<sup>3</sup> We discuss different pricing for selling and buying power from the grid later in Section 3.3.3.

With respect to the penalization of the imbalances, we analyze two different policies: i) a cost of imbalances, and ii) a limitation on the number of imbalances. The first option can be described by a cost function of  $\Delta g(k)$ ,  $c^{\text{i}}(\Delta g(k)) : \mathbb{R} \rightarrow \mathbb{R}$ ,

$$c^{\text{i}}(\Delta g(k)) = c^{\Delta \text{q}} |\Delta g(k)|^2 + c^{\Delta \text{l}} |\Delta g(k)|, \quad (3.6)$$

<sup>3</sup> Note that alternative cost functions (non-quadratic) can as well be used without compromising the validity of the method described in this chapter.

with given cost coefficients  $c^{\Delta q}$  and  $c^{\Delta l}$ . The second option translates into requiring the tracking ratio of the DS to be greater than a given security level  $(1 - \varepsilon) \in [0, 1] \subset \mathbb{R}$ , i.e.

$$r^\gamma(\{\Delta g\}_{\mathcal{K}}) \geq (1 - \varepsilon), \quad (3.7)$$

where the tracking ratio is a function  $r^\gamma : \mathbb{R}^K \rightarrow \mathbb{R}$ ,

$$r^\gamma(\{\Delta g\}_{\mathcal{K}}) = \frac{\#\{k \in \mathcal{K} : |\Delta g(k)| \leq \gamma\}}{K}, \quad (3.8)$$

with operator  $\#\{\cdot\}$  denoting the cardinality of set  $\{\cdot\}$ . Requirement (3.7) is equivalent to requiring a minimum number of time steps over the horizon  $\mathcal{K}$  in which  $|\Delta g(k)|$  does not surmount a given threshold  $\gamma$ , i.e. it poses a limit to the number of imbalances over the horizon  $\mathcal{K}$ . Note that even if the present dissertation disregard the problem of sizing the storage, the feasibility of the tracking requirement is strictly coupled with the available storage capacity. In fact, given an assigned capacity and the uncertainty surrounding  $l(k)$ , the tracking requirement may turn unfeasible for arbitrary high values of  $(1 - \varepsilon)$ . We tackle this challenge in Section 3.3.2 by allowing a relaxation of  $(1 - \varepsilon)$  whenever its value would cause infeasibility. In this manner, we decouple the sizing and the scheduling problem, allowing the application of the proposed method to any storage size. Additional comments on storage size are discussed in Section 5.2. Nevertheless, we remark that an appropriate storage size is recommended to avoid an excessive relaxation of  $(1 - \varepsilon)$ , which would undermine the meaning of having a tracking constraint at all. We refer to [Yi *et al.*, 2019] for an example of coupled consideration of both sizing and scheduling problems for energy storage.

### 3.1.3 Hierarchical Control

The flexibility provided by the EC-DER enables tracking of the DS for  $\tilde{g}(k)$ . Similar to [Olivares *et al.*, 2015] and [Lampropoulos *et al.*, 2015], we pro-

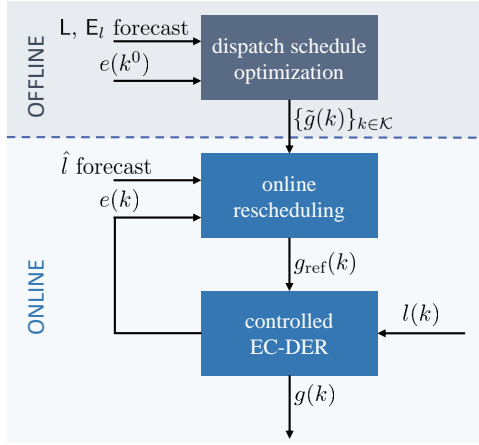


Figure 3.2: Three-level hierarchical scheduling and control scheme.

pose a hierarchical scheduling and control scheme, cf. Figure 3.2. On the highest level, a DS is computed by means of optimization. At the next level, online adjustments of the DS is performed using Model Predictive Control (MPC) [Rawlings *et al.*, 2017]. The lowest layer is the real-time controller regulating the power output of the dispatchable feeder. Note that each levels runs on a different time scale. Furthermore, observe that the knowledge of  $l(k)$  is available only at the lowest, real-time level. The DS optimization and the online rescheduling take place *before* the realization  $l(k)$  becomes known. Thus, they rely on forecasts for this value. In the following sections, we analyze these control levels one by one.

## 3.2 Online Schedule Tracking

The EC-DER is controlled in real-time to compensate for the volatility of the inflexible elements, aiming to accurate tracking of the DS. Examples of controllers of this kind can be found in [Citro *et al.*, 2011] for PV generation, and in [Zhao *et al.*, 2015] for wind turbines. This control action is

carried out after the power output  $l(k)$  is known. From a high level perspective, this controller regulates the power output of the storage at step  $k$  depending on the inflexible power output  $l(k)$ , on the reference  $g_{\text{ref}}(k)$ , and on the energy state  $e(k)$  such that the imbalance  $\Delta g(k)$  is minimized. For the sake of simplicity, consider in the first place  $g_{\text{ref}}(k) = \tilde{g}(k)$ . We will discuss the effect of on-line rescheduling later in Section 3.4. We can formalize the behavior of the EC-DER controller with the implicit control law  $h : \mathbb{R}^3 \rightarrow \mathbb{R}^2$ , mapping a realization of  $[\tilde{g}(k) \ l(k) \ e(k)]$  to its corresponding  $[p(k) \ \Delta g(k)]$ :

$$h(\tilde{g}(k), l(k), e(k)) := \arg \min_{p(k), \Delta g(k)} \Delta g^2(k) \quad \text{s.t. (3.1) – (3.4)}. \quad (3.9)$$

Problem (3.9) is a multi parametric quadratic problem. Therefore, its solution  $h(\tilde{g}(k), l(k), e(k))$  is a piece-wise affine function of the parameters [Pistikopoulos *et al.*, 2007], here not reported explicitly.

### 3.3 Dispatch Schedule Optimization

The first step of the decision process in Figure 3.2 is the computation of the DS over horizon  $\mathcal{K}$ , which is the main focus of this thesis. As discussed in Chapters 1 and 2, scheduling is often performed via numerical optimization, and the core of this process is a computationally tractable formulation of

the optimization problem. Combining the system requirements and models (3.1)-(3.9) gives<sup>4</sup>

$$\begin{aligned}
& \min_{\{\mathbf{x}\}_{\mathcal{K}}} \sum_{k \in \mathcal{K}} c^{\text{DS}}(\tilde{g}(k), k) + c^i(\Delta g(k)) \\
& \text{s.t.} \tag{3.10} \\
& e(k+1) = e(k) + \delta \cdot (p(k) - \mu |p(k)|) \quad \forall k \in \mathcal{K}, \\
& e(k^{\text{b}}) = e^0, \\
& [p(k) \ \Delta g(k)] = h(\tilde{g}(k), l(k), e(k)) \quad \forall k \in \mathcal{K}, \\
& r^\gamma(\{\Delta g\}_{\mathcal{K}}) \geq (1 - \varepsilon),
\end{aligned}$$

where  $e^0$ , is the energy state at the beginning of the DS and vector  $\mathbf{x}(k) \in \mathbb{R}^4$  collects the decision variables at  $k$ , i.e.

$$\mathbf{x}(k) := [p(k) \ e(k+1) \ \tilde{g}(k) \ \Delta g(k)].$$

Note that satisfaction of (3.1)-(3.4) is indirectly imposed via the argmin operator  $h$  defined in (3.9).

A key parameter in (3.10) is the inflexible power output  $\{l\}_{\mathcal{K}}$ . However, (3.10) should be solved before knowing the value taken by  $\{l\}_{\mathcal{K}}$ . Therefore, this parameter enters the scheduling problem as a stochastic process  $\{L\}_{\mathcal{K}}$ , as described in Chapter 2.<sup>5</sup> Furthermore, given that the DS has to be computed before  $k^{\text{b}}$ , also the initial condition  $e^0$  is an uncertain parameter,  $E^0$ . This uncertainty reflects into the decision variables. The DS  $\{\tilde{g}\}_{\mathcal{K}}$  is the decision taken upon scheduling (first-stage); thus, it is a deterministic decision variable. Instead,  $p(k)$  and  $\Delta g(k)$  depend on the realization of  $l(k)$  as well as on the initial energy state  $e^0$ . Therefore, these variables are described us-

<sup>4</sup> For the sake of notation simplicity, we do not include the penalization of the DS derivative (3.5b).

<sup>5</sup> In order to simplify the notation, from here on we drop the notation indicating the explicit dependence of a random process on the sample  $\omega$ . In other words, we denote random variable  $X(\omega, k)$  as  $X(k)$  and we denote probability  $\mathbb{P}(\{\omega : X(\omega, k) \in \mathcal{X}\})$  as  $\mathbb{P}(X(k) \in \mathcal{X})$ .

ing the stochastic processes  $\{P\}_{\mathcal{K}}$  and  $\{\Delta G\}_{\mathcal{K}}$ . Finally, the dynamics (3.1) describes a stochastic process too, because both the initial energy state and the sequence of  $\{p\}_{[k^b, \dots, k]}$  are uncertain.

Introducing the uncertainty in (3.10) leads to

$$\min_{\substack{\{\tilde{g}\}_{\mathcal{K}}, \\ \{\mathbf{x}\}_{\mathcal{K}}}} \sum_{k \in \mathcal{K}} c^{\text{DS}}(\tilde{g}(k), k) + \mathbb{E} \left[ \sum_{k \in \mathcal{K}} c^i(\Delta G(k)) \right] \quad (3.11a)$$

$$\text{s.t. } \forall k \in \mathcal{K}$$

$$E(k+1) = E(k) + \delta \cdot (P(k) - \mu |P(k)|), \quad (3.11b)$$

$$E(k^b) = E^0, \quad (3.11c)$$

$$[P(k) \Delta G(k)] = h(\tilde{g}(k), L(k), E(k)), \quad (3.11d)$$

$$\mathbb{E} \left[ \sum_{k \in \mathcal{K}} B(k) \right] \geq (1 - \varepsilon) \cdot K, \quad (3.11e)$$

where the random decision variables are collected in vector

$$\mathbf{X}(k) := [P(k) \ E(k+1) \ \Delta G(k)],$$

and  $B(k)$  is a Bernoulli random variable whose realization is

$$b(k) = \begin{cases} 1 & \text{if } |\Delta g(k)| \leq \gamma \\ 0 & \text{otherwise} \end{cases}. \quad (3.12)$$

The uncertainties affecting the cost function and the inequality constraints are dealt with as described in Chapter 2. The cost includes the *expected* cost of the imbalances. The inequalities interpret the original requirement (3.7) as  $\mathbb{E} [\sum_{\mathcal{K}} B(k)] \geq (1 - \varepsilon) \cdot K$ , requesting the expected number of time steps over  $\mathcal{K}$  without imbalances to be at least  $(1 - \varepsilon) \cdot K$ .

Problem (3.11) implements a two-stage structure where the only actual decision is the first-stage one, i.e. the DS. In fact, for a given DS, the equality

constraints are such that the realization of all the random decision variables is uniquely determined depending on the realization of  $\{\mathbf{L}\}_{\mathcal{K}}$  and  $\mathbf{E}^0$ .

Solving (3.11) requires two preliminary steps, as described in Chapter 2: forecasting of the random parameters, and rendering (3.11) computationally tractable. Non-parametric forecasts are promising in predicting  $\{\mathbf{L}\}_{\mathcal{K}}$  with separate forecasts for each time step in  $\mathcal{K}$ . In other words, they can predict  $\mathbf{L}(k)$  at each  $k$  *separately*, without any information on the correlation among these random variables: forecasting the distribution  $F_{\mathbf{L}(k)}(l)$  for each  $k \in \mathcal{K}$  is possible, but forecasting the multivariate distribution  $F_{\mathbf{L}(k^b), \dots, \mathbf{L}(k^e)}(l(k^b), \dots, l(k^e))$  is difficult. Non-sampling based approaches to computation tractability of (3.11) would require an explicit description of this correlation, because the constraints in (3.11) involve functions having correlated random variables as arguments. On the other hand, combining non-parametric forecasting methods with sampling in a suitable manner allows to generate scenarios for  $\{\mathbf{L}\}_{\mathcal{K}}$  that capture the correlation between  $\mathbf{L}(k)$  at subsequent time instants [Pinson *et al.*, 2009; González Ordiano *et al.*, 2018b]. As already mentioned in Chapter 2, this is the reason why a combination of scenario forecasting and sampling-based method is commonly used in dealing with (3.11). In contrast to this popular approach, we propose in the following a method to overcome the incompatibility of non-parametric forecasts and non-sampling based method in tackling (3.11).

### 3.3.1 Model Modification

Next, we elaborate on (3.11) to simplify computational tractability. In particular, we aim to remove the dependencies between correlated random variables in the dynamics (3.11b) and in the mapping  $h$  (3.11d). In other words, we seek for an approximated yet accurate version of (3.11) that does not include more than one random parameter and more than one random variable per constraint. The proposed modification of (3.11) can be subdivided in seven subsequent steps, addressed one by one in the following.

### Step 1: Introducing Chance Constraints

First, we elaborate on constraint (3.11e). For the sake of simplicity, consider the extreme case  $\gamma \simeq 0$ , i.e. each small deviation from the DS is considered an imbalance. Under this condition,  $b(k)$  is equal to 1 only if  $\Delta g(k) = 0$ . We address (3.11e) with a separate constraint per each time-step. Given the properties of expected values,<sup>6</sup> satisfaction of (3.11e) is achieved if

$$\mathbb{P}(B(k) = 1) \geq (1 - \varepsilon) \quad \forall k \in \mathcal{K}.$$

Summing up, from  $\gamma \simeq 0$  it follows that (3.11e) is satisfied when

$$\mathbb{P}(\Delta G(k) = 0) \geq (1 - \varepsilon) \quad \forall k \in \mathcal{K}. \quad (3.13)$$

Note that (3.13) allows to tackle (3.11e) with separate constraints per each time step. Recall that the realization of  $\Delta G(k)$  depends on the realization of  $\tilde{g}(k)$ ,  $l(k)$ , and  $e(k)$  via the piece-wise affine function  $h(\tilde{g}(k), l(k), e(k))$ , cf. (3.9). In particular,  $h(\tilde{g}(k), l(k), e(k))$  gives a  $\Delta g(k) = 0$  whenever  $\tilde{g}(k)$ ,  $l(k)$ , and  $e(k)$  are such that

$$\tilde{g}(k) - l(k) \in \mathcal{P}(k), \quad (3.14a)$$

$$e(k) + \delta \cdot ((\tilde{g}(k) - l(k)) - \mu |(\tilde{g}(k) - l(k))|) \in \mathcal{E}(k + 1). \quad (3.14b)$$

Thus, constraint (3.11e) with  $\gamma \simeq 0$  is equivalent to chance constraint

$$\mathbb{P}(P(k) \cap E(k + 1)) \geq (1 - \varepsilon) \quad \forall k \in \mathcal{K}. \quad (3.15)$$

<sup>6</sup> It holds that  $\mathbb{E}[\sum_{\mathcal{K}} B(k)] = \sum_{\mathcal{K}} \mathbb{E}[B(k)]$  which can be derived from the linearity of sum. A demonstration of this property using the definition of marginal density can be found in [Ross, 2014, Chapter 4]; however, a more rigorous demonstration requires the application of the Tonelli-Fubini's Theorem, which can be found in [Hoffmann-Jørgensen, 1994, Chapter 3].

with events  $P(k)$  and  $E(k + 1)$  defined as

$$P(k) := \tilde{g}(k) - l(k) \in \mathcal{P}(k) \quad (3.16a)$$

$$E(k + 1) := e(k) + \delta \cdot ((\tilde{g}(k) - l(k)) - \mu |(\tilde{g}(k) - l(k))|) \in \mathcal{E}(k + 1). \quad (3.16b)$$

### Step 2: Neglecting of the Cost of Imbalances

The next step in the elaboration of (3.11) involves an approximation: removing the expected cost of imbalances from the cost function of (3.11). This approximation does not take the tracking requirement out of the problem, because the requirement is still considered in the form of constraint (3.15) (equivalent to (3.13)). However, (3.15) accounts only for the *number* of imbalances and not for their *intensity*. Therefore, by neglecting the expected cost of imbalances, the possibility to penalize the intensity of the imbalances is lost.

### Step 3: Assuming Perfect Tracking of the Dispatch Schedule

Next, we proceed with manipulating the equality constraints (3.11b) and (3.11d). Once more, we introduce an approximation: we consider  $\Delta g(k)$  to be constantly equal to zero. This approximation is aligned with a desirable operation of the dispatchable feeder, as a  $\Delta g(k) = 0$  is certainly preferred. However, it also leads to a different physical interpretation of the entire set of constraint: under the assumption of  $\Delta g(k) = 0$ , chance constraint (3.15) is constraining the probability of having a deviation from the DS at  $k$  after that there have been no deviations over the time period  $\{k^0, \dots, k\}$ . This is a conservative approximation: the demanded tracking becomes higher than what originally required in (3.11e). Furthermore, it has a fundamental implication in the optimization problem: the higher the  $k$ , the more difficult it is to satisfy (3.15). To avoid over conservative solutions, a  $(1 - \varepsilon)$  decreasing with increasing  $k$  can be used in (3.13). However, it is not trivial

to determine a sequence of decreasing  $(1 - \varepsilon)$  guaranteeing that the original constraint (3.11e) is satisfied. Thus, we maintain the same  $(1 - \varepsilon)$  for all  $k \in \mathcal{K}$  and further discuss this point later in Section 3.3.2.

If  $\Delta g(k) = 0$ , then  $p(k)$  is uniquely determined by the power balance

$$p(k) = \tilde{g}(k) - l(k). \quad (3.17)$$

Thus, we replace constraint (3.11d) with

$$P(k) = \tilde{g}(k) - L(k). \quad (3.18)$$

#### Step 4: Separating Expected Values and Deviations

A further step in the elaboration of (3.11b)-(3.11d) is to introduce additional parameters and decision variables to describe  $L(k)$ ,  $P(k)$  and  $E(k)$  in terms of their expected value and deviations from expectancy. The first ones are point (or “deterministic”) parameters/decision variables, while the second ones remain random processes:

$$L(k) = \hat{l}(k) + \Delta L(k), \quad (3.19a)$$

$$P(k) = \hat{p}(k) + \Delta P(k), \quad (3.19b)$$

$$E(k) = \hat{e}(k) + \Delta E(k). \quad (3.19c)$$

Here, notation  $\hat{x}$  indicates the expected value of  $X$ . In this way, (3.11b) and (3.17) become

$$\tilde{g}(k) = \hat{p}(k) + \hat{l}(k), \quad (3.20a)$$

$$0 = \Delta P(k) + \Delta L(k), \quad (3.20b)$$

$$\hat{e}(k+1) = \hat{e}(k) + \delta \cdot (\hat{p}(k) - \mu |\hat{p}(k)|), \quad (3.20c)$$

$$\Delta E(k+1) = \Delta E(k) + \delta \cdot (\Delta P(k) - \mu |\Delta P(k)|). \quad (3.20d)$$

Note that assuming perfect tracking of the DS ( $\Delta g(k) = 0$ ) implies that the uncertainty affecting the forecasts is completely compensated by the storage; in fact, from (3.20b) it follows

$$\Delta P(k) = -\Delta L(k). \quad (3.21)$$

Furthermore, substituting constraint (3.11d) with (3.20a) and (3.21) removes from stochastic program (3.11) one of the two constraints requiring the knowledge of the correlation among random variables.

### Step 5: Neglecting the Stochastic Losses

In the next step, we introduce another approximation: negligible stochastic losses, i.e.  $\mu |\Delta P(k)| \simeq 0$ . This assumption is motivated by the fact the integral of their realizations (which can also be negative whenever the expected losses are higher than the realized ones) is often small in comparison to the stored energy. However, the severity of this approximation should be validated a posteriori, eventually introducing an appropriate counterbalancing measure. We undertake this analysis later in Chapter 5. In the case of  $\mu |\Delta P(k)| \simeq 0$ , (3.20d) becomes

$$\Delta E(k+1) = \Delta E(k) + \delta \cdot \Delta P(k).$$

Considering (3.21), we obtain

$$\Delta E(k+1) = \Delta E(k) - \delta \cdot \Delta L(k).$$

This dynamics implies that the state  $\Delta E(k+1)$  is given by its initial condition  $\Delta E(k^0)$  and the sum of  $\delta \cdot \Delta L(k)$  over the time interval from  $k^0$  to  $k$ , i.e.

$$\Delta E(k+1) = \Delta E(k^0) - \sum_{i=k^0}^k \delta \cdot \Delta L(i).$$

Note that  $e(k^0)$  is known with certainty at  $k^0$  because it can be measured. Therefore,  $\Delta E(k^0) = 0$ , and

$$\Delta E(k+1) = - \sum_{i=k^0}^k \delta \cdot \Delta L(i). \quad (3.22)$$

Summarizing, we describe the deviation from the expected energy state at  $k+1$  as the sum of all the deviation from the expected inflexible power output, starting from the moment in which the DS is computed,  $k^0$ .

### Step 6: Introducing the Energy Forecasts

The approximated stochastic dynamics (3.22) motivates the introduction of a new concept: energy as a stochastic process. Consider the sequence  $\{e_l\}_{\mathcal{K}^0}$ , with  $\mathcal{K}^0 = \{k^0 + 1, \dots, k^e\}$  and

$$e_l(k+1) = \sum_{i=k^0}^k \delta \cdot l(i), \quad e_l(k^0) = 0.$$

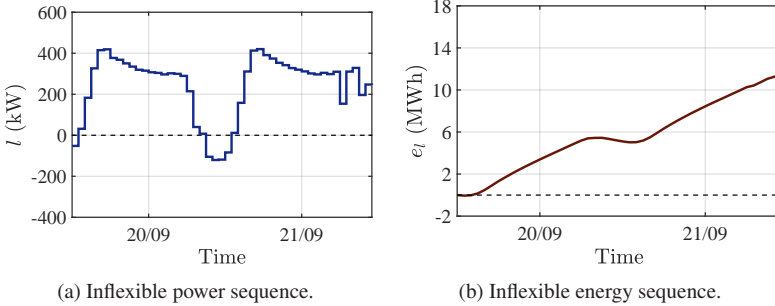


Figure 3.3: Example of inflexible power and energy sequences.

Figure 3.3b depicts an example of the sequence  $\{e_l\}_{\mathcal{K}^0}$  for an industrial case, aggregating inflexible loads and generation. Figure 3.3a shows the

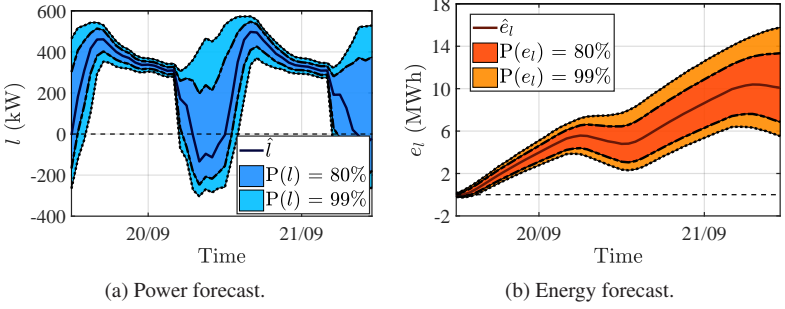


Figure 3.4: Example of probabilistic forecasts for  $l$  and  $e_l$ . Forecasts with different horizons computed at 12:00 of 19 Sep 2018.

sequence of  $l(k)$  generating the  $\{e_l\}_{\mathcal{K}^0}$  in Figure 3.3b. From a physical perspective,  $e_l(k)$  can be interpreted as the total energy exchanged with the inflexible devices up to time step  $k$ . Upon scheduling,  $e_l(k)$  is a stochastic process,  $E_l(k)$ . The variability of  $e_l(k)$  can be observed in Figure 3.4, which reports probabilistic forecasts for the time series of  $l(k)$  and  $e_l(k)$  depicted in Figure 3.3. Similarly to the case of the other stochastic processes, see (3.19), we divide  $E_l(k)$  into a deterministic and a stochastic part, i.e.  $E_l(k) = \hat{e}_l(k) + \Delta E_l(k)$ . Therefore,

$$\Delta E_l(k+1) = \sum_{i=k^0}^k \delta \cdot \Delta L(i). \quad (3.23)$$

Finally, from (3.22) and (3.23) it follows

$$\Delta E(k+1) = -\Delta E_l(k+1). \quad (3.24)$$

Once more, this equation is a natural consequence of the assumption of perfect tracking of the DS. As the power output of the storage compensates for the uncertainty affecting the inflexible power output, the uncertainty on the energy state also depends on the integrated uncertainty of the inflexible power output. Using (3.24) in place of (3.20d) in the stochastic scheduling

program allows to remove also the second of the equality constraints requiring the knowledge of correlation among random variables. In fact,  $E_l(k)$  is a stochastic process for which a forecast can be computed. This forecast includes (indirectly) the correlation among  $L(k)$  at different time instants. The approximations presented in the previous steps and the introduction of a stochastic process for energy allows to formulate (3.16b) in its equivalent form

$$\begin{aligned} E(k+1) &:= \hat{e}(k+1) + \Delta E(k+1) \in \mathcal{E}(k+1) \\ &= \hat{e}(k+1) - \Delta E_l(k+1) \in \mathcal{E}(k+1), \end{aligned}$$

which does not contain anymore the sum of correlated random variables (i.e.  $E(k+1) - \delta L(k) - \delta \mu |L(k)|$ ).

### Step 7: Separating Chance Constraints for Power and Energy

Chance constraint (3.15) requires events  $P(k)$  and  $E(k)$  to occur contemporary. However, enforcing this condition necessitates the knowledge of the correlation between  $L(k)$  and  $\Delta E_l(k+1)$ , because  $L(k)$  plays a role in event  $P(k)$  and  $\Delta E_l(k+1)$  plays a role in event  $E(k)$ . Aiming to remove any expression involving correlated random variables from (3.11), we first address *separate* chance constraints for power and energy,

$$\mathbb{P}(P(k)) \geq (1 - \varepsilon_P), \tag{3.25a}$$

$$\mathbb{P}(E(k+1)) \geq (1 - \varepsilon_E), \tag{3.25b}$$

instead of the original constraint (3.15).

Then, we require the DS to be robust against worst-case realization of the uncontrolled power output  $P(k)$ ,<sup>7</sup> i.e.  $(1 - \varepsilon_P) \simeq 1$ , which implies  $\mathbb{P}(P(k)) \simeq 1$  and  $\mathbb{P}(P(k) \cup E(k+1)) \simeq 1$ . Thus

$$\begin{aligned} \mathbb{P}(P(k) \cap E(k+1)) &= \mathbb{P}(P(k)) + \mathbb{P}(E(k+1)) - \mathbb{P}(P(k) \cup E(k+1)) \\ &\simeq \mathbb{P}(E(k+1)), \end{aligned}$$

meaning that (3.15) is respected if (3.25) is satisfied with  $(1 - \varepsilon_P) \simeq 1$  and  $(1 - \varepsilon_E) \geq (1 - \varepsilon)$ .

### Correlation-free Stochastic Scheduling

Following the previously described steps, we reformulate (3.11) as

$$\min_{\{\mathbf{x}\}_{\mathcal{K}}} \sum_{k \in \mathcal{K}} c^{\text{DS}}(\tilde{g}(k), k) \quad (3.26)$$

$$\text{s.t. } \forall k \in \mathcal{K} \quad (3.27)$$

$$\hat{e}(k+1) = \hat{e}(k) + \delta \cdot (\hat{p}(k) - \mu |\hat{p}(k)|),$$

$$\hat{e}(k^{\text{b}}) = \hat{e}^0,$$

$$\tilde{g}(k) = \hat{p}(k) + \hat{l}(k),$$

$$\mathbb{P}\left(\tilde{g}(k) - \hat{l}(k) - \Delta L(k) \in \mathcal{P}(k)\right) \geq (1 - \varepsilon_P) \simeq 1,$$

$$\mathbb{P}(\hat{e}(k+1) - \Delta E_l(k+1) \in \mathcal{E}(k+1)) \geq (1 - \varepsilon).$$

For the sake of clarity, we summarize in Table 3.1 the model approximations on which (3.26) is based.

### 3.3.2 Reformulation of Chance Constraints

The constraints defined by (3.25) entail linear combinations of decision variables and parameters. Thus, (3.25) satisfies the requirements for the appli-

<sup>7</sup> Throughout all simulations reported in Chapter 5, this worst-case choice for  $(1 - \varepsilon_P)$  does not lead to infeasibility of the scheduling problem.

cation of the approaches to tractability of chance constraints presented in Section 2.3.2.

We address computational tractability of (3.25a) using a quantile-based approach, as described in Section 2.3.2. Thus, (3.25a) becomes

$$\tilde{g}(k) - \bar{p}(k) \leq \underline{l}_{(1-\varepsilon_P)}(k), \quad (3.28)$$

$$\bar{l}_{(1-\varepsilon_P)}(k) \leq \tilde{g}(k) - \underline{p}(k), \quad (3.29)$$

with

$$\underline{l}_{(1-\varepsilon_P)}(k) = q_{\mathbf{L}(k)}(0.5 - 0.5(1 - \varepsilon_P)),$$

$$\bar{l}_{(1-\varepsilon_P)}(k) = q_{\mathbf{L}(k)}(0.5 + 0.5(1 - \varepsilon_P)).$$

The decision of using a quantile-based approach is motivated by the fact that a more advanced method would not bring any advantage: having

Table 3.1: List of approximations used in (3.26).

Initial constraint	Approximation	Description	Effect
(3.11a) Step 2	$\mathbb{E} [\sum_{k \in \mathcal{K}} c^i(\Delta G(k))] = 0$	neglect the expected cost of imbalances	impossibility of penalizing the intensity of imbalances
(3.11d) Step 3	$\Delta g(k) = 0$	perfect tracking of the dispatch schedule	constraint (3.11e) means no imbalances at $k$ after not having had imbalances over $\{k^b, \dots, k\}$
(3.11b) Step 5	$\mu  \Delta P(k)  = 0$	neglect stochastic losses	underestimation of losses

$(1 - \varepsilon_P) \simeq 1$  requires  $P(k)$  to verify for approximately the entire support of  $L(k)$ .

The case of the energy constraint (3.25b) is different. Tackling tractability of this constraint via a quantile-based approach is certainly possible. However, as already described in Section 2.3.2, this method has some drawbacks. First, considering different—even if larger—intervals with the same probability of containing the realizations of  $\Delta E_l(k+1)$  might lead to a DS that is worst than what it would have been possible. Second, the scheduling problem might be infeasible for an arbitrarily large value of  $(1 - \varepsilon)$ . This second issue is particularly relevant in the case of long-term scheduling. As already mentioned, satisfying (3.25b) becomes harder over time: the support of  $\Delta E_l(k+1)$  grows with  $k$  (see Figure 3.4b) and can become large in comparison to the available capacity. For these reasons, we propose to reformulate (3.25b) with a direct use of the CDF of  $\Delta E_l(k+1)$ ,  $F_{\Delta E_l(k+1)}(\Delta e_l)$ , as in (2.13). Introducing, for the sake of compact notation, the set

$$\mathcal{G}(\alpha) := \{ \mathcal{I} \subset \mathbb{R} \mid F_Z(\max(\mathcal{I})) - F_Z(\min(\mathcal{I})) \geq \alpha \}, \quad (3.30)$$

we reformulate (3.25b) as

$$[\hat{e}(k) - \bar{e}(k), \hat{e}(k) - \underline{e}(k)] \in \mathcal{G}((1 - \varepsilon)) \quad (3.31)$$

The reformulation of the energy constraint (3.31) contains  $(1 - \varepsilon)$  as an explicit parameter. Thus, it enables to overcome the infeasibility problem appearing towards the end of the DS by means of constraint softening [Kerigan and Maciejowski, 2000]. Specifically, (3.31) can be replaced by

$$[\hat{e}(k) - \bar{e}(k), \hat{e}(k) - \underline{e}(k)] \in \mathcal{G}((1 - \varepsilon) - \epsilon(k)), \quad (3.32a)$$

$$\epsilon(k) \geq 0, \quad (3.32b)$$

adding the penalty term  $\alpha \cdot \epsilon(k)$  to the cost function of the scheduling problem with a sufficiently large  $\alpha$  [Kerrigan and Maciejowski, 2000]. This technique maximizes the probability of satisfying the energy constraint when it is not possible to guarantee the desired security level, making this approach particularly interesting for robust optimization ( $(1 - \epsilon) \simeq 1$ ). Furthermore, it can partially counterbalance the conservativeness of the DS induced by the approximation introduced in Step 3 of Section 3.3.1.

A representation of constraint (3.32), for the case of an industrial campus with a large storage (capacity of 1.5 MWh) and high uncertainty surrounding the forecasts, is depicted in Figure 3.5. There, the dashed lines represent the storage limits and the colored areas illustrate values that the realization  $e(k)$  can take with a given probability. Graphically, constraint (3.32) means that the probability associated with the energy states enclosed within the storage limits should be at least  $(1 - \epsilon)$ , or, when this is not feasible, the highest possible. For the results depicted in Figure 3.5,  $(1 - \epsilon)$  is set to 70%. However, given the high level of uncertainty, a  $(1 - \epsilon) = 70\%$  is feasible only for the first hours of the day. Then, the area covered by the possible energy states becomes so wide that a  $(1 - \epsilon) = 70\%$  is not feasible and constraint softening is required. Specifically, the probability of having a feasible realization of  $E(k)$  (i.e. a realization comprised within the minimum and maximum storage capacity) is reduced below 40% towards the end of the schedule.

### 3.3.3 Implementation Aspects

Besides computational tractability, Problem (3.26) raises a few implementation issues on which we comment next.

#### Distinguish Among Power Directions

Different variables can be employed to distinguish opposite power flow directions. These additional variables are of interest to model different prices

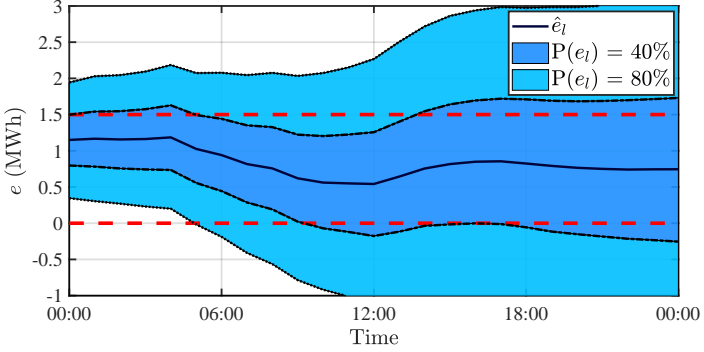


Figure 3.5: Representation of chance constraint on energy state.

for buying/selling power to the grid (differentiating between the directions of  $\tilde{g}(k)$ ), and to avoid the non-differentiability introduced by the absolute value in dynamics (3.20c) (differentiating between the directions of  $\hat{p}(k)$ ). Distinguishing between the directions of a power flow implies the introduction of two more variables and four more constraints. In general, consider power flow  $x(k)$  as composed of a non-negative component  $x^+(k)$  and a non-positive component  $x^-(k)$ . Then, the quantities  $x(k)$ ,  $x^+(k)$  and  $x^-(k)$  are subject to the following constraints

$$x^+(k) + x^-(k) = x(k), \quad (3.33a)$$

$$x^+(k) \geq 0, \quad (3.33b)$$

$$-x^-(k) \geq 0, \quad (3.33c)$$

$$x^+(k) \cdot x^-(k) = 0. \quad (3.33d)$$

that we summarize with the shorthand notation

$$[x^-(k) \ x^+(k)] \in \mathcal{F}_d(x(k)),$$

with

$$\mathcal{F}_d(x(k)) = \{ [x^-(k) \ x^+(k)] \in \mathbb{R} \mid \text{satisfy (3.33)} \} .$$

Consider the case of power flow  $\tilde{g}(k)$  and introduce variable  $\tilde{g}^+(k)$  to denote non-negative values of  $\tilde{g}(k)$  and variable  $\tilde{g}^-(k)$  to denote non-positive values of  $\tilde{g}(k)$ , with  $[\tilde{g}^-(k) \ \tilde{g}^+(k)] \in \mathcal{F}_d(\tilde{g}(k))$ . A similar discrimination can be undertaken for  $\hat{p}(k)$ , with variables  $\hat{p}^+(k)$  and  $\hat{p}^-(k)$  subject to  $[\hat{p}^-(k) \ \hat{p}^+(k)] \in \mathcal{F}_d(\hat{p}(k))$ .

Constraint (3.33d) is structurally similar to complementary conditions and it might cause problems because of its non-differentiability. Several convex relaxations for such constraints have been proposed in the literature, see [Perez *et al.*, 2013; Sossan *et al.*, 2016; Braun *et al.*, 2016]. These relaxations rely on the observation that dropping complementary conditions does often not affect the optimal solution. In other words, the convex set

$$\mathcal{F}'_d(x(k)) = \{ [x^-(k) \ x^+(k)] \in \mathbb{R} \mid \text{satisfy (3.33a) – (3.33c)} \} ,$$

is used in place of  $\mathcal{F}_d$ .

Let us discuss a practical example of this latter point. Consider a cost function  $c^{\text{DS}}$  with distinct directions of  $\tilde{g}(k)$ , i.e.

$$\begin{aligned} c^{\text{DS}+/-(\tilde{g}^+(k), \tilde{g}^-(k), k) = c^{q^+}(k) (\tilde{g}^+(k))^2 + c^{q^-}(k) (\tilde{g}^-(k))^2 \\ + c^{l^+}(k) \tilde{g}^+(k) + c^{l^-}(k) \tilde{g}^-(k), \end{aligned} \quad (3.34)$$

with cost coefficients greater or equal to zero. Additionally, apply a similar distinction to  $\hat{p}(k)$  and remove the absolute value from the dynamic equation (3.20c):

$$\hat{e}(k+1) = \hat{e}(k) + \delta \cdot (\hat{p}(k) - \mu \hat{p}^+(k) + \mu \hat{p}^-(k)) . \quad (3.35)$$

In this case, (3.33d) in  $\mathcal{F}_d(\tilde{g}(k))$  can be relaxed completely without affecting the solution because its violation would increase the cost. The same does

not apply to  $\mathcal{F}_d(\hat{p}(k))$ . In fact, given (3.35), relaxing (3.33d) in  $\mathcal{F}_d(\hat{p}(k))$  allows an unrealistic increase of the storage losses. This unrealistic energy dissipation can increase  $\hat{p}(k)$ —and, consequently,  $\tilde{g}(k)$ —without violating the capacity constraint of the storage. Given the quadratic penalization of  $\tilde{g}(k)$  in cost function (3.34), there are values under which the cost increases with decreasing  $\tilde{g}(k)$ . Thus, increasing  $\tilde{g}(k)$  by means of unrealistic conversion losses can reduce (3.34), and  $\mathcal{F}'_d(\hat{p}(k))$  cannot replace  $\mathcal{F}_d(\hat{p}(k))$  because (3.33d) is not fulfilled indirectly anyway. Nevertheless, the use of a smooth constraint relaxation is numerically advisable because the boundaries of the feasible set generated by (3.33d) are not differentiable at  $x^+(k) = x^-(k) = 0$ . To this end, we employ the set

$$\mathcal{F}''_d(x(k)) = \{ [x^-(k) \ x^+(k)] \in \mathbb{R} \mid \text{satisfy (3.33a) – (3.33c),} \\ x^+(k) \cdot x^-(k) \leq \beta, \},$$

with  $0 < \beta \ll 1$ , as an alternative relaxation of  $\mathcal{F}_d(x(k))$  that can be used for the case of  $\hat{p}(k)$ . Summarizing, different relaxations can be employed to tackle non-differentiability of constraint set  $\mathcal{F}_d(x(k))$ , depending on the properties of the problem; in this thesis we employ  $\mathcal{F}'_d(\tilde{g}(k))$  as a substitute of  $\mathcal{F}_d(\tilde{g}(k))$ , and  $\mathcal{F}''_d(\hat{p}(k))$  as a substitute of  $\mathcal{F}_d(\hat{p}(k))$ . Otherwise, one may attempt reformulation as a mixed integer problem, introducing, for example, a binary variable to model the switch of power flows, see for example [Murray *et al.*, 2018]. This choice leads to mixed-integer non-linear programs, which are not straightforward to solve [Trespalcios and Grossmann, 2014].

### Uncertainty of Initial Condition

The expected value of the energy state at  $k^b$ ,  $\hat{e}^0$ , is a parameter of the scheduling problem that requires to be estimated at  $k^0$ . A computation of  $\hat{e}^0$  coherent with the model presented in the previous section would make use

of dynamics (3.20c), a measurement of  $\hat{e}(k^0)$ , and the expected sequence of  $p(k)$  over  $\mathcal{O} = \{k^0, \dots, k^b - 1\}$ ,<sup>8</sup> i.e.

$$\hat{p}(k) = \tilde{g}(k) - \hat{l}(k) \quad \forall k \in \mathcal{O}. \quad (3.36)$$

However, this might lead to problems in practice. In fact,  $\{\tilde{g}\}_{\mathcal{O}}$  is determined at the previous scheduling iteration to guarantee feasibility of  $\{\hat{e}\}_{\mathcal{O}}$  according to a profile of  $\{\hat{l}\}_{\mathcal{O}}$  forecasted on the day before. Thus, solving (3.36) and (3.20c) with the latest forecasts for  $\{\hat{l}\}_{\mathcal{O}}$  (which is coherent with the model) might lead to an unfeasible value of  $e(k)$ . The consequence is that the computed DS can present power peaks at  $k^b$ , necessary to restore the feasibility of the energy state. To avoid this issue,  $\hat{e}^0$  should be computed using (3.36) with a power profile  $\{\hat{p}\}_{\mathcal{O}}$  in accordance to the *complete* control law

$$[\hat{p}(k) \Delta g(k)] = h \left( \tilde{g}(k), \hat{l}(k), \hat{p}(k) \right) \quad \forall k \in \mathcal{O}. \quad (3.37)$$

Even if (3.37) is not entirely coherent with the utilized model (because it allows imbalances), it ensures feasibility of the estimated  $\hat{e}^0$ .

However, the DS can still exhibit unnecessary peaks of power at the beginning of the horizon, even with a feasible  $\hat{e}^0$ . This is caused by the fact that not only  $e(k^b + 1)$  has to be feasible, but also an interval of values around it. The dimension of this interval depends on the uncertainty of  $\Delta E_l(k^b + 1)$  and on the security level  $(1 - \varepsilon)$ . To resolve this issue, we relax the energy constraint (3.32) at the beginning of the scheduling horizon utilizing a slack variable as standard in non-linear programming [Nocedal and Wright, 2006]. In other words, we add variable  $\rho(k) \geq 0$  to constraint (3.32), and penalize it linearly in the cost function with a time-dependent coefficient  $\gamma(k)$ . The relaxation should apply only at the beginning of the DS; thus,

---

<sup>8</sup> Recall that the uncertainty affecting the EC-DER is calculated by integrating the uncertainty on the forecasts starting from  $k^0$ .

coefficient  $\gamma(k)$  should increase with  $k$ . In particular, it should be equal to  $+\infty$  for all the portion of the scheduling horizon for which the constraint relaxation is not needed and therefore undesirable.

### **Length of the Optimization Horizon**

The requirement of operating the system continuously, i.e. of computing subsequent dispatch schedules, should enter the optimization problem to avoid the complete discharging of the EC-DER at the end of the DS. To this end, we consider an extended horizon  $\mathcal{K}^s$  as discussed in Chapter 2. The extension of the horizon should be such that increasing the horizon further would not influence the decision on the DS. Given the cyclic behavior of load and generation, we observed that an extension of 6 to 10 hours should suffice for the analyzed case. Alternatively, this could be achieved by adding a terminal penalty that rewards a minimum energy content towards the end of the horizon, as in [Lampropoulos *et al.*, 2015]. However, designing this penalty term is not easy.

### 3.3.4 Computationally Tractable Formulation

Finally, we summarize all the concepts discussed in this Section in the following optimization problem

$$\begin{aligned}
& \min_{\{\mathbf{x}\}_{\mathcal{K}^s}} \sum_{k \in \mathcal{K}^s} c^{\text{DS}+/-}(\tilde{g}^+(k), \tilde{g}^-(k), k) + \alpha \cdot \epsilon(k) + \gamma(k) \cdot \rho(k) \\
& \text{s.t. } \forall k \in \mathcal{K}^s \tag{3.38} \\
& \quad \hat{e}(k+1) = \hat{e}(k) + \delta \cdot (\hat{p}(k) - \mu \hat{p}^+(k) + \mu \hat{p}^-(k)), \\
& \quad \hat{e}(k^b) = \hat{e}^0, \\
& \quad \tilde{g}(k) = \hat{p}(k) + \hat{l}(k), \\
& \quad [\tilde{g}^+(k) \ \tilde{g}^-(k)] \in \mathcal{F}'_d(\tilde{g}(k)), \\
& \quad [\hat{p}^+(k) \ \hat{p}^-(k)] \in \mathcal{F}''_d(\hat{p}(k)), \\
& \quad \tilde{g}(k) - \bar{p}(k) \leq \underline{l}_{(1-\varepsilon_p)}(k), \\
& \quad \bar{l}_{(1-\varepsilon_p)}(k) \leq \tilde{g}(k) - \underline{p}(k), \\
& \quad [\hat{e}(k) - \bar{e}(k), \hat{e}(k) - \underline{e}(k)] \in \mathcal{G}((1-\varepsilon) - \epsilon(k) - \rho(k)), \\
& \quad \epsilon(k) \geq 0, \\
& \quad \rho(k) \geq 0,
\end{aligned}$$

with decision variables at  $k$  collected in vector  $\mathbf{x}(k) \in \mathbb{R}^9$ ,

$$\mathbf{x}(k) := [\tilde{g}(k) \ \tilde{g}^+(k) \ \tilde{g}^-(k) \ \epsilon(k) \ \rho(k) \ \hat{e}(k+1) \ \hat{p}(k) \ \hat{p}^+(k) \ \hat{p}^-(k)]^\top.$$

The parameters of the problem, besides the one involved by the cost function, are  $\hat{e}^0$ ,  $\{\hat{l}(k)\}_{\mathcal{K}^s}$ ,  $\{\bar{l}_{(1-\varepsilon_p)}(k)\}_{\mathcal{K}^s}$ ,  $\{\underline{l}_{(1-\varepsilon_p)}(k)\}_{\mathcal{K}^s}$ , the bounds of the intervals  $\mathcal{P}(k)$  and  $\mathcal{E}(k)$ , and the function  $F_{\Delta E_i(k)}(\cdot)$  for each  $k \in \mathcal{K}^s$ . Observe that despite the nine decision variables per time step, Problem (3.38) has (practically) only three degrees of freedom per time step (the schedule  $\tilde{g}(k)$ , the constraint softening coefficient  $\epsilon(k)$ , and the constraint relaxation

coefficient  $\rho(k)$ ).<sup>9</sup> The non-linear program (3.38) fulfills the desired requirements, i.e. it can be solved with available solvers, and its parameters can be obtained via non-parametric forecasts. Recall that a summary of the approximations on which (3.38) is based is provided in Table 3.1.

### 3.4 Online Rescheduling

The security level  $(1 - \varepsilon)$  is generally smaller than one; therefore some imbalances may be unavoidable. These imbalances are more likely to occur towards the end of the horizon, as a consequence of the already discussed approximation  $\Delta g(k) = 0$ . Excessive or extended imbalances might negatively affect the stability of the overall system, especially in case of a large scale application of the proposed method. Hence, we add an additional online optimization layer. This control layer makes use of the most recent information about the system—both in terms of power forecast and of the energy state of the EC-DER—to predict eventual upcoming energy/capacity shortage and to re-compute the power output reference accordingly. In particular, the aim of this level is to avoid sudden peaks of power deviation from the DS and to redistribute the imbalances along the entire scheduling horizon. The re-scheduling is obtained via MPC [Rawlings *et al.*, 2017]. For the sake on notation simplicity, we adopt the same discrete time notation used for the DS.<sup>10</sup> In the following, we refer to an optimization performed at time  $k$  over horizon  $\mathcal{M}(k) = \{k, k + 1, \dots, k + M\}$ . The outcome is the sequence  $\{g_{\text{ref}}\}_{\mathcal{M}(k)}$ , of which only the first value,  $g_{\text{ref}}(k)$ , is sent as reference for the lower controller, see Figure 3.2.

<sup>9</sup> There are six equality constraints, because the constraint sets  $\mathcal{F}'_d(\hat{g}(k))$  and  $\mathcal{F}''_d(\hat{p}(k))$  are implicitly including two equality constraints each.

<sup>10</sup> A different discretization with higher resolution is clearly possible, see the case study in Section 5.3.

Similar to the scheduling case, also the online optimization is performed via automatic decision making entailing numerical optimization. To this end, we formulate the optimization problem

$$\begin{aligned}
& \min_{\{\mathbf{x}\}_{\mathcal{M}(k)}} \sum_{i \in \mathcal{M}(k)} (\tilde{g}(i) - g_{\text{ref}}(i))^2 \\
& \text{s.t. } \forall i \in \mathcal{M}(k) \tag{3.39} \\
& \quad \hat{e}(i+1) = \hat{e}(i) + \delta \cdot (\hat{p}(i) - \mu \hat{p}^+(i) + \mu \hat{p}^-(i)), \\
& \quad \hat{e}(k) = e^k, \\
& \quad g_{\text{ref}}(i) = \hat{p}(i) + \hat{l}(i), \\
& \quad [\hat{p}^+(i) \ \hat{p}^-(i)] \in \mathcal{F}'_d(\hat{p}(k)), \\
& \quad \hat{p}(i) \in \mathcal{P}(i), \\
& \quad \hat{e}(i+1) \in \mathcal{E}(i+1).
\end{aligned}$$

where the decision variables are

$$\mathbf{x}(i) := [g_{\text{ref}}(i) \ \hat{p}(i) \ \hat{p}^+(i) \ \hat{p}^-(i) \ \hat{e}(i+1)]^\top \in \mathbb{R}^5.$$

Observe that out of five decision variables per time step, there is practically only one degree of freedom per time step, cf. Footnote 9. Differently from the scheduling case, we do not consider here any uncertainty. The initial condition  $e^k$  is known, as (3.39) is solved online right before the application of its output. Furthermore, we employ point forecasts for the unknown sequence  $\{\hat{l}\}_{\mathcal{M}(k)}$ . This choice is motivated by the small uncertainty affecting short-term forecasts. Additionally, recall that the use of probabilistic forecasts has the effect of allocating energy reserves to deal with the realization of the uncertainties. As these reserves have already been allocated at the highest level, it is not necessary to add further reserves during the on-line phase. Given this modeling choice, the parameters of (3.39) are:  $e^k$ ,  $\{\hat{l}(i)\}_{\mathcal{M}(k)}$ , and the intervals  $\mathcal{P}(k)$  and  $\mathcal{E}(k)$ . Last, we consider  $M \leq O$ ; in

this way, the DS for the following optimization interval is always computed before its first value is utilized in Problem (3.39). Note that, if required by the utility, Problem (3.39) could be extended with constraints forcing  $\Delta g(i)$  below a given threshold. This threshold can be either fixed or dependent on the conditions of the entire system. For this latter case, a mechanism similar to the Balance Area ACE Limit (BAAL) can be implemented [NERC, 2018].

### 3.5 Summary

Scheduling and operation of a market-integrated aggregation of flexible and inflexible generators, loads, and storage is generally structured in hierarchical decision and control steps. Among them, the computation of a day-ahead DS is particularly challenging because of the uncertainty affecting the forecasts of the future inflexible outputs. While methods such as non-parametric probabilistic forecasting can quantify this uncertainty, their integration in a computationally tractable optimization for scheduling is non-trivial. Traditionally, sampling-based methods are applied. In contrast to this approach, we propose a novel optimization-based scheduling algorithm that can make use of non-parametric probabilistic forecasting without resorting to samples. The most difficult task in designing such an algorithm is represented by the dynamic equation describing the storage, which—in a stochastic setting—contains a sum of correlated random variables (the power output at subsequent time steps is a function of the uncertain power outputs, which are time-correlated) and is non-linear (an energy loss follows from an exchange of power with the storage, regardless from the direction). Key concept of the proposed method is to accept some approximations on the system model to achieve a more complete use of the information obtained via forecasting. In particular, we overcome the previously described obstacles in the storage dynamics by substituting it with an approximated energy balance and by assuming a conservative setting where the storage compensates entirely

for the forecast uncertainty. The resulting approximated model entails only chance constraints with at most one uncertain parameter for which a non-parametric probabilistic forecast can be computed. Such constraints can be easily rendered tractable as described in Chapter 2, without losing any of the information obtained via forecasting nor recurring to any approximation on the uncertainty. On the other hand, this approach does not hold with multiple EC-DERs. In fact, with multiple EC-DERs, it is not enough to impose that the storage compensates for the uncertainty, but it is necessary also to decide in which proportion the storage devices contribute to this process. Deciding upon this point via optimization requires the consideration of constraints including multiple random decision variables, thus undermining the idea of one random decision variable per constraint. The next chapter deals with this problem by presenting a comprehensive analysis on how a DS computed with respect to a single (aggregated) storage can be dispersed in operation among multiple devices.

## 4 Aggregated Scheduling of EC-DERs

The control of a large force is the same principle as the control of a few men: it is merely a question of dividing up their numbers.

---

*Sun Tzu, The art of War*

The previous chapter describes a stochastic scheduling algorithm that allows the use of non-parametric probabilistic forecasts without sampling. One of the major limitations of this technique is that it cannot handle multiple uncertain energy states. Nevertheless, its application to a population of EC-DERs is permitted if, upon scheduling, one considers the energy states of the various resources lumped into a single one describing the entire cluster. This procedure, often referred to as “aggregation”, is common in the scientific literature, see [Xu *et al.*, 2016]. However, to the best of the author’s knowledge, a thorough discussion of its mathematical properties is still missing. In particular, it is unclear i) if or under which conditions the consideration of separate constraints for each device leads to the same results of aggregated scheduling, and, if so, ii) how to disperse in operation the aggregated DS among the various storage devices. In this chapter, we fill this theoretical gap. The ideas presented in this section have appeared in [Appino *et al.*, 2019b, 2018c].

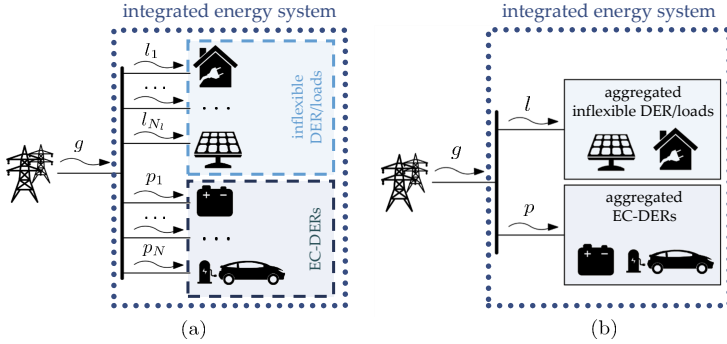


Figure 4.1: Schematic representation of an aggregated energy system.

## 4.1 Models and Requirements

In this Chapter, we recall the case of  $N$  inflexible DERs and loads, and  $N_l$  EC-DERs. We consider the case where all the inflexible DERs, loads and EC-DERs have the same owner, or where they are at least all controlled in view of the same scope: regulating the power exchange between the cluster of devices and an external grid according to a pre-computed dispatch schedule. Note that, as in the case of Chapter 3, we assume the point of view of an aggregator trading electrical energy on the day-ahead energy market. Similar to the system described in Chapter 3, all the devices are connected to the same grid-connected bus, as schematically represented in Figure 4.1a. There, variable  $g$  indicates the active power exchange between the system and its corresponding upper-level grid. The connections are assumed to be lossless and such that the system components are able to exchange power mutually without any technical limit. This assumption is justified in many cases, since, on average, about 80% of the capacity of distribution grids is unused [Priebe *et al.*, 2019]. Extending the notation introduced in Chapter 3, we denote the active power output of each  $i$ -th inflexible DER/load as  $l_i$  with  $i \in \mathcal{N}_l = \{1, \dots, N_l\}$ , and the active power output of the  $j$ -th

EC-DER with  $j \in \mathcal{N}$  as  $p_j$  with  $j \in \mathcal{N} = \{1, \dots, N\}$ . Each EC-DER is subject to a dynamics and to a power and an energy constraint

$$e_j(k+1) = e_j(k) + \delta \cdot p_j(k), \quad (4.1)$$

and

$$p_j(k) \in \mathcal{P}_j(k), \quad (4.2a)$$

$$e_j(k+1) \in \mathcal{E}_j(k+1), \quad (4.2b)$$

with  $\mathcal{P}_j(k)$  and  $\mathcal{E}_j(k)$  being closed real intervals, i.e.

$$\mathcal{P}_j(k) = [\underline{p}_j(k), \bar{p}_j(k)] \subset \mathbb{R}, \quad \mathcal{E}_j(k+1) = [\underline{e}_j(k+1), \bar{e}_j(k+1)] \subset \mathbb{R}.$$

Note that (4.1) differs from (3.1) because it neglects potential conversion losses. We discuss this point later in Section 4.6.

With respect to the requirements, we target dispatch-as-scheduled of the power exchange  $g(k)$  by means of a coordinated control of the system components as in Chapter 3. Also in this case we distinguish the DS  $\tilde{g}(k)$  from the imbalances  $\Delta g(k)$ , see (3.4), with operating revenues (or costs) that are directly associated to the DS through a known cost function,  $c^{\text{DS}}(\tilde{g}(k), k) : \mathbb{R} \times \mathbb{N} \rightarrow \mathbb{R}$ , see (3.5). However, in the following we assume perfect knowledge of  $\{l_i\}_{\mathcal{K}}$  for all  $i \in \mathcal{N}_1$ ,<sup>1</sup> implying that we do not have to be concerned with planning reserves to avoid imbalances. In other words, we consider  $\Delta g(k) = 0$  and focus on using the storage solely for energy arbitrage.

### 4.1.1 Hierarchical Control

Following the scheme described in Chapter 3, we consider a hierarchical structure for the decision and control process (cf. Figure 3.2).

<sup>1</sup> At the end of this chapter, we discuss dropping this assumption and thus extending the scheduling algorithm presented in Chapter 3 to the case of multiple EC-DERs.

In absence of random parameters, there is no need to introduce any random decision variable nor multiple decision stages. All the relevant information can be taken at once by solving the scheduling problem

$$\min_{\{\mathbf{x}\}_{\mathcal{K}}} \sum_{k \in \mathcal{K}} c^{\text{DS}}(\tilde{g}(k), k) \quad (4.3a)$$

s.t.

$$\tilde{g}(k) = \mathbf{1}^\top \mathbf{p}(k) - \mathbf{1}^\top \mathbf{l}(k) \quad \forall k \in \mathcal{K}, \quad (4.3b)$$

$$\mathbf{e}(k+1) = \mathbf{e}(k) + \delta \cdot \mathbf{p}(k) \quad \forall k \in \mathcal{K}, \quad (4.3c)$$

$$\mathbf{e}(k^{\text{b}}) = \mathbf{e}^0, \quad (4.3d)$$

$$\mathbf{p}(k) \in \times_{j \in \mathcal{N}} \mathcal{P}_j(k) \quad \forall k \in \mathcal{K}, \quad (4.3e)$$

$$\mathbf{e}(k+1) \in \times_{j \in \mathcal{N}} \mathcal{E}_j(k+1) \quad \forall k \in \mathcal{K}. \quad (4.3f)$$

Here, we use the vector notation

$$\begin{aligned} \mathbf{l}(k) &:= [l_1(k) \ \dots \ l_{N_l}(k)]^\top \in \mathbb{R}^{N_l}, \\ \mathbf{p}(k) &:= [p_1(k) \ \dots \ p_N(k)]^\top \in \mathbb{R}^N, \\ \mathbf{e}(k) &:= [e_1(k) \ \dots \ e_N(k)]^\top \in \mathbb{R}^N, \\ \mathbf{x}(k) &:= [\tilde{g}(k) \ \mathbf{p}^\top(k) \ \mathbf{e}^\top(k+1)]^\top \in \mathbb{R}^{(2N+1)}. \end{aligned}$$

Furthermore, parameter  $\mathbf{e}^0$  is the initial energy level,  $\mathbf{1}$  is a column vector of ones whose dimension follows from context, and notation  $\times_{j \in \mathcal{N}}$  indicates the cartesian product of all the sets indexed in  $\mathcal{N}$ , i.e.

$$\times_{j \in \mathcal{N}} \mathcal{P}_j(k) = \mathcal{P}_1(k) \times \dots \times \mathcal{P}_N(k) \subset \mathbb{R}^N, \quad (4.4a)$$

$$\times_{j \in \mathcal{N}} \mathcal{E}_j(k) = \mathcal{E}_1(k) \times \dots \times \mathcal{E}_N(k) \subset \mathbb{R}^N. \quad (4.4b)$$

The constraints are as follows: Equality (4.3b) is the power balance and (4.3c)-(4.3f) model the EC-DERs, see (4.1) and (4.2). Note that the sets  $\times_{j \in \mathcal{N}} \mathcal{P}_j(k)$  and  $\times_{j \in \mathcal{N}} \mathcal{E}_j(k)$  are hyperboxes of  $\mathbb{R}^N$  built upon the constraints of the single devices.

## 4.2 Scheduling with Aggregated Models

Upon solving (4.3)—and provided it is feasible— $\{\mathbf{p}(k)\}_{\mathcal{K}}$  and  $\{\mathbf{e}(k)\}_{\mathcal{K}}$  are obtained. However the DS itself, i.e.  $\{\tilde{\mathbf{g}}\}_{\mathcal{K}}$ , is the only decision variable entering the cost function directly, and the only information of interest for the coordination with the upper-level grid. Thus, the question arises whether it is possible to reduce the number of constraints and decision variables in (4.3) by means of aggregation.

The idea guiding an aggregated model is to calculate one DS for aggregated DERs instead of computing individual schedules for each DER, this way immediately reducing the number of variables. An obvious advantage of a reduced number of variables is to lower the computational burden of large-scale problems. Furthermore, aggregation is especially convenient to tackle uncertainty in multi-stage stochastic scheduling, as discussed later in Section 4.7. Examples of aggregated models for population of devices in energy applications are [Subramanian *et al.*, 2013] for energy storage systems, [Wenzel *et al.*, 2017; Zhang *et al.*, 2016; Vandael *et al.*, 2013] for plug-in electric vehicles, [Mathieu *et al.*, 2014; Hao *et al.*, 2015] for thermostatically controlled loads, and [Xu *et al.*, 2016; Bernstein *et al.*, 2015; Evans *et al.*, 2018] for heterogenous storage-like devices. Despite differences, all the cited methods build upon the same aggregation concept, summarized in the following.

To start with, the power outputs of DERs are grouped in inflexible and energy-constrained ones, see Figure 4.1b. To this end, consider the function

$$s : \mathbb{R}^{N_y} \rightarrow \mathbb{R}, \quad \mathbf{y} \mapsto y = \mathbf{1}^\top \mathbf{y}, \quad (4.5)$$

which sums—i.e. *aggregates*—the elements of a vector  $\mathbf{y} \in \mathbb{R}^{N_y}$ . Formally, its inverse

$$s^{-1} : \mathbb{R} \rightarrow \mathbb{R}^{N_y}, \quad s^{-1}(y) = \{\mathbf{y} \in \mathbb{R}^{N_y} \mid y = \mathbf{1}^\top \mathbf{y}\}, \quad (4.6)$$

is the set-valued (pre-image) map. We refer to  $s^{-1}(y) \subset \mathbb{R}_y^N$  as *the set of dispersions of  $y$  to  $\mathbf{y}$* .<sup>2</sup> The aggregated power outputs and the aggregated energy are

$$l(k) := s(\mathbf{l}(k)), \quad p(k) := s(\mathbf{p}(k)), \quad e(k) := s(\mathbf{e}(k)). \quad (4.7)$$

These aggregated variables allow re-writing (4.3) as follows:

$$\min_{\{\mathbf{x}\}_{\mathcal{K}}, \{\mathbf{p}\}_{\mathcal{K}}, \{\mathbf{e}\}_{\mathcal{K}^+}} \sum_{k \in \mathcal{K}} c^{\text{DS}}(\tilde{g}(k), k) \quad (4.8a)$$

s. t.

$$\tilde{g}(k) = p(k) - l(k) \quad \forall k \in \mathcal{K} \quad (4.8b)$$

$$\mathbf{e}(k^b) = \mathbf{e}^0, \quad (4.8c)$$

$$\mathbf{e}(k+1) = \mathbf{e}(k) + \delta \cdot \mathbf{p}(k) \quad \forall k \in \mathcal{K}, \quad (4.8d)$$

$$\mathbf{p}(k) \in \bigtimes_{j \in \mathcal{N}} \mathcal{P}_j(k) \quad \forall k \in \mathcal{K}, \quad (4.8e)$$

$$\mathbf{e}(k+1) \in \bigtimes_{j \in \mathcal{N}} \mathcal{E}(k+1) \quad \forall k \in \mathcal{K}, \quad (4.8f)$$

$$p(k) = s(\mathbf{p}(k)) \quad \forall k \in \mathcal{K}, \quad (4.8g)$$

$$e(k+1) = s(\mathbf{e}(k+1)) \quad \forall k \in \mathcal{K}, \quad (4.8h)$$

which is equivalent to (4.3) with the additional decision variables  $\{\mathbf{p}\}_{\mathcal{K}}$  and  $\{\mathbf{e}\}_{\mathcal{K}^+}$ . Note that  $\mathcal{K}^+ = \{1, \dots, K+1\} \subset \mathbb{N}$ .

<sup>2</sup> This notion is chosen to the end of avoiding confusion with *statistical distributions* of random variables, which are also discussed in this thesis.

Aggregated scheduling builds upon (4.8), by dropping the constraints on  $\mathbf{p}(k)$  and  $\mathbf{e}(k)$  and replacing them with constraints on the aggregated variables. This yields

$$\min_{\{\tilde{g}\}_{\mathcal{K}}, \{\mathbf{p}\}_{\mathcal{K}}, \{\mathbf{e}\}_{\mathcal{K}+}} \sum_{k \in \mathcal{K}} c^{\text{DS}}(\tilde{g}(k), k) \quad (4.9a)$$

s. t.

$$\tilde{g}(k) = p(k) - l(k) \quad \forall k \in \mathcal{K}, \quad (4.9b)$$

$$e(k^b) = s(\mathbf{e}^0), \quad (4.9c)$$

$$e(k+1) = e(k) + \delta \cdot p(k) \quad \forall k \in \mathcal{K}, \quad (4.9d)$$

$$p(k) \in \mathcal{P}(k) \quad \forall k \in \mathcal{K}, \quad (4.9e)$$

$$e(k+1) \in \mathcal{E}(k+1) \quad \forall k \in \mathcal{K}. \quad (4.9f)$$

The aggregated problem refrains from computing  $\{\mathbf{p}\}_{\mathcal{K}}$  and  $\{\mathbf{e}\}_{\mathcal{K}+}$  alongside with  $\{\tilde{g}\}_{\mathcal{K}}$ . However, computing of  $\{\tilde{g}\}_{\mathcal{K}}$  by using (4.9) as a substitute of (4.3) may cause issues whenever the aggregated constraints sets  $\mathcal{P}(k)$  and  $\mathcal{E}(k+1)$  do not coincide with the propagation of the feasible sets of  $\mathbf{p}(k)$  and  $\mathbf{e}(k)$  from (4.3).

Let us clarify this point with an abstraction. Conceptually, Problem (4.9) equals

$$\min_{\{\mathbf{y}\}_{\mathcal{K}+}} \sum_{k \in \mathcal{K}+} \ell(h(\mathbf{y}(k))) \quad (4.10a)$$

$$\text{s.t. } \mathbf{y}(k+1) \in \bigtimes_{j \in \mathcal{N}_y} \mathcal{Y}_j(k+1, \mathbf{y}(k)) \subset \mathbb{R}^{N_y}, \quad (4.10b)$$

where the cost function  $\ell \circ h : \mathbb{R}^{N_y} \rightarrow \mathbb{R}$  is continuous in  $\mathbf{y}$  and for all  $k \in \mathcal{K}$  the constraint set  $\bigtimes_{j \in \mathcal{N}_y} \mathcal{Y}_j(k+1, \mathbf{y}(k)) \subset \mathbb{R}^{N_y}$ , which depends both on

the time and on the state  $\mathbf{y}(k)$ , is non-empty and compact. Aggregation, as in (4.9), consists of applying the linear mapping

$$h : \mathbb{R}^{N_y} \rightarrow \mathbb{R}, \quad \mathbf{y} \mapsto y = h(\mathbf{y}),$$

to reduce the number of variables. Applying this to (4.10) yields

$$\min_{\{\mathbf{y}\}_{\mathcal{K}^+}} \sum_{k \in \mathcal{K}^+} \ell(y(k)) \quad (4.11a)$$

$$\text{s.t. } y(k+1) \in \mathcal{Y}(k+1, y(k)) \subset \mathbb{R}. \quad (4.11b)$$

Note that the cost functions of (4.10) and (4.11) are equivalent by construction. Let  $h(\times_{j \in \mathcal{N}_y} \mathcal{Y}_j)$  denote the point-wise application of  $h$  to  $\times_{j \in \mathcal{N}_y} \mathcal{Y}_j$ , i.e.

$$h \left( \times_{j \in \mathcal{N}_y} \mathcal{Y}_j \right) = \left\{ y = h(\mathbf{y}) \mid \mathbf{y} \in \times_{j \in \mathcal{N}_y} \mathcal{Y}_j \right\}.$$

The following lemma is easily obtained.

**Lemma 1** (Optimality preserving aggregation). *Let  $\{y^*\}_{\mathcal{K}^+} \in \mathbb{R}^K$  denote a solution of Problem (4.11), extended to include the initial condition  $y^0$ . If*

$$\mathcal{Y}(k+1, y(k)) \equiv h \left( \times_{j \in \mathcal{N}_y} \mathcal{Y}_j(k+1, \mathbf{y}(k)) \right), \quad (4.12)$$

for all  $k \in \mathcal{K}$ , then there exists at least a  $\{\mathbf{y}^*\}_{\mathcal{K}^+} \in \mathbb{R}^{N_y \cdot K}$  solving Problem (4.10) for which

$$\{y^*\}_{\mathcal{K}^+} = h(\{\mathbf{y}^*\}_{\mathcal{K}^+})$$

holds for arbitrary continuous choices of  $\ell : \mathbb{R} \rightarrow \mathbb{R}$ . ■

The proof of this result is straightforward and thus omitted. Observe that condition (4.12) is not easily enforced via direct calculation of

$$h\left(\bigtimes_{j \in \mathcal{N}_y} \mathcal{Y}_j(k+1, \mathbf{y}(k))\right).$$

In fact, this computation would require the knowledge of the state  $\mathbf{y}$  at each time step, knowledge that is lost during aggregation by construction. Thus, there is a need of alternative approaches characterizing the set  $\mathcal{Y}(k+1, y(k))$  such that (4.12) is satisfied. The next section presents a popular choice to achieve this computation for the sets  $\mathcal{P}(k)$  and  $\mathcal{E}(k+1)$  in (4.9).

### 4.3 Bounds for the Aggregated Model

The construction of the sets  $\mathcal{P}(k)$  and  $\mathcal{E}(k+1)$  in (4.9) is not unique. However, a common practice (see for example [Xu *et al.*, 2016]) is to consider intervals of  $\mathbb{R}$  given by the (point-wise) mapping of the hyperboxes  $\mathcal{P}(k)$  and  $\mathcal{E}(k+1)$ ,

$$\mathcal{P}(k) = s\left(\bigtimes_{j \in \mathcal{N}} \mathcal{P}_j(k)\right), \quad \mathcal{E}(k+1) = s\left(\bigtimes_{j \in \mathcal{N}} \mathcal{E}_j(k+1)\right). \quad (4.13)$$

Practically speaking, this choice leads to

$$\mathcal{P}(k) = [\underline{p}(k), \bar{p}(k)], \quad \mathcal{E}(k+1) = [\underline{e}(k+1), \bar{e}(k+1)], \quad (4.14a)$$

with

$$\underline{p}(k) = \sum_{j \in \mathcal{N}} \underline{p}_j(k), \quad \bar{p}(k) = \sum_{j \in \mathcal{N}} \bar{p}_j(k), \quad (4.14b)$$

and

$$\underline{e}(k+1) = \sum_{j \in \mathcal{N}} \underline{e}_j(k+1), \quad \bar{e}(k+1) = \sum_{j \in \mathcal{N}} \bar{e}_j(k+1). \quad (4.14c)$$

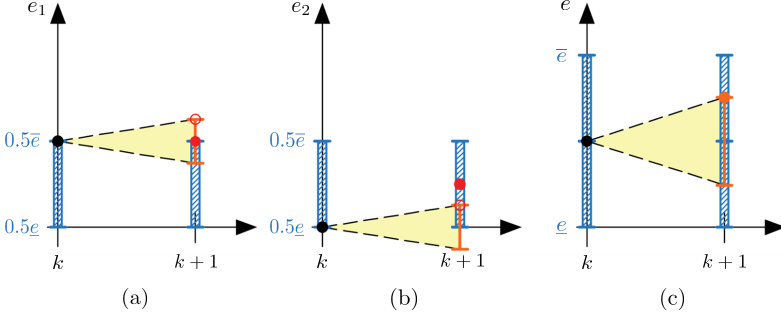


Figure 4.2: Illustration of Example 1.

In the following, we assume aggregated constraints sets  $\mathcal{P}(k)$  and  $\mathcal{E}(k+1)$  obtained via (4.13). The underlying ratio derives from interval arithmetics [Jaulin *et al.*, 2001]. Indeed, it can be shown that

$$p(k) = s(\mathbf{p}(k)) \in s\left(\bigtimes_{j \in \mathcal{N}} \mathcal{P}_j(k)\right),$$

when  $\mathbf{p}(k) \in \bigtimes_{j \in \mathcal{N}} \mathcal{P}_j(k)$ . The same applies for the aggregated energy  $e(k)$ ,

$$e(k+1) = s(e(k+1)) \in s\left(\bigtimes_{j \in \mathcal{N}} \mathcal{E}_j(k+1)\right).$$

Thus, feasibility of  $p(k)$  and  $e(k+1)$  in (4.8e)-(4.8h) implies their feasibility with respect to (4.9e)-(4.9f). Moreover, it is easy to see that if  $e(k+1)$  and  $p(k)$  satisfy (4.8d), then  $p(k)$  and  $e(k+1)$  satisfy (4.9d). To summarize, considering (4.13), the aggregated dynamics (4.9d) and the constraints (4.9e)-(4.9f) do not restrict the feasible set of (4.8). Rather, they are a relaxation of the propagation of the original constraint set in (4.3). Thus, there can be cases in which the aggregated schedules of  $p(k)$  and  $e(k+1)$  cannot be dispersed without violating individual constraints on  $\mathbf{p}(k)$  and  $\mathbf{e}(k+1)$ . We illustrate this issue with a simple example.

**Example 1** (Non-dispersable aggregation). Consider two EC-DERs, i.e.  $\mathcal{N} = \{1, 2\}$ , and two subsequent time instants,  $k$  and  $k + 1$ . For the sake of simplicity, let the EC-DERs have identical time-invariant power and energy limits, i.e.  $\mathcal{P}_1(k) = \mathcal{P}_2(k) = [0.5\underline{p}, 0.5\bar{p}] \subset \mathbb{R}$ , and  $\mathcal{E}_1(k) = \mathcal{E}_2(k) = \mathcal{E}_1(k + 1) = \mathcal{E}_2(k + 1) = [0.5\underline{e}, 0.5\bar{e}] \subset \mathbb{R}$ . Moreover, let  $\bar{p} = -\underline{p} \neq 0$  with  $2\bar{p}\delta \leq \bar{e} - \underline{e}$  and, clearly,  $\bar{e} > \underline{e}$ .

Now, consider the case in which  $e_1(k) = 0.5\bar{e}$  and  $e_2(k) = 0.5\underline{e}$ , implying  $e(k) = 0.5\underline{e} + 0.5\bar{e}$ . The constraints limiting  $e_1(k + 1)$  and  $e_2(k + 1)$  are depicted in Figure 4.2a and Figure 4.2b respectively. The striped intervals represent the feasible states according to the energy constraint; the cones indicate the states admissibly reachable from  $e_1(k)$  and  $e_2(k)$ . According to (4.13), the aggregated constraints are

$$p(k) \in [\underline{p}, \bar{p}], \quad e(k + 1) \in [\underline{e}, \bar{e}], \quad (4.15)$$

see Figure 4.2c.

For the sake of illustration, consider  $e(k + 1) = 0.5(\underline{e} + \bar{e}) + \delta \cdot \bar{p}$ ; the corresponding value of  $p(k) = \bar{p}$  follows. This choice is feasible for the aggregated model; it satisfies (4.15). In Figure 4.2c, this choice of  $e(k + 1)$  is represented by a filled circle. However, the dispersion of  $e(k + 1)$  and  $p(k)$  to individual devices leads to infeasibility on the individual side.

A feasible choice of  $\mathbf{p}(k)$ , such that  $\mathbf{p}(k) = s^{-1}(\bar{p})$  exists, it is:

$$p_1(k) = 0.5\bar{p} \in [0.5\underline{p}, 0.5\bar{p}], \quad p_2(k) = 0.5\bar{p} \in [0.5\underline{p}, 0.5\bar{p}].$$

Yet this implies

$$\begin{aligned} e_1(k + 1) &= 0.5\bar{e} + \delta \cdot 0.5\bar{p} \notin [0.5\underline{e}, 0.5\bar{e}], \\ e_2(k + 1) &= 0.5\underline{e} + \delta \cdot 0.5\bar{p} \in [0.5\underline{e}, 0.5\bar{e}], \end{aligned}$$

which violates the energy constraint of EC-DER  $j = 1$ . This can be seen in Figure 4.2a and 4.2b, where empty circles indicates energy values which sum up to  $e(k+1)$  and are reachable from  $e_1(k), e_2(k)$  but not feasible with respect to  $e_1(k+1) \in [0.5\underline{e}, 0.5\bar{e}]$ .

At the same time, a feasible choice of  $e(k+1)$  such that  $e(k+1) = s^{-1}(0.5(\underline{e} + \bar{e}) + \delta \cdot \bar{p})$  is

$$\begin{aligned} e_1(k+1) &= 0.5\bar{e} \in [0.5\underline{e}, 0.5\bar{e}], \\ e_2(k+1) &= 0.5\underline{e} + \delta \cdot \bar{p} \in [0.5\underline{e}, 0.5\bar{e}]. \end{aligned}$$

This implies  $p_1(k) = \frac{0.5(\bar{e} - \underline{e})}{\delta} = 0 \in [0.5\underline{p}, 0.5\bar{p}]$ , and

$$p_2(k) = \frac{0.5\underline{e} - (0.5(\underline{e} + \bar{e}) + \bar{p})}{\delta} \notin [0.5\underline{p}, 0.5\bar{p}],$$

which violates the power constraint of EC-DER  $j = 2$ . This is depicted in Figure 4.2a and 4.2b by filled circles, which indicate energy values summing up to  $e(k+1)$  that are feasible but not reachable for EC-DER  $j = 2$ . Hence, the chosen values for  $e(k+1)$  and  $p(k)$  are feasible for the aggregated model, but cannot be dispersed to  $\mathbf{p}(k)$  and  $e(k+1)$ . ■

Example 1 points out that an aggregated model with power and energy constraints computed as in (4.13) might lead to infeasibilities in practice. The time-wise coupling between the variables  $p_j(k)$  and  $e_j(k)$ —and, consequently, between constraints (4.2)—introduced by the discrete-time dynamics (4.1) is the main source of these infeasibilities. In other words, the constrained reachability properties of the dynamics are ignored in (4.13). Therefore, the solution of the “relaxed” aggregated problem (4.9) differs from the one of the original problem (4.3) whenever those properties play an active role in restricting the feasible space at the following time step. In order to investigate this aspect, we first derive an energy constraint that

summarizes the power and the energy constraints (4.2)—given the initial condition  $e(k^b)$ .

Given  $e_j(k)$ , the power constraint (4.2a) can be seen as an implicit constraint on  $e_j(k+1)$  because it limits the energy state that can be reached at the following step  $k+1$ . This aspect can be formalized considering the 1-step reachable set of (4.1), which is

$$e_j(k) \oplus \delta \cdot \mathcal{P}_j(k). \quad (4.16)$$

Here  $\oplus$  denotes the Minkowski sum.<sup>3</sup> Note a slight abuse of notation: for the sake of compact notation, the set  $\{e_j(k)\}$  is indicated with its sole element  $e_j(k)$ . However, not all  $e_j(k+1) \in e_j(k) \oplus \delta \cdot \mathcal{P}_j(k)$  are feasible with respect to the energy constraint at  $k+1$ , (4.2b). Combining (4.1) and (4.2) leads to

$$e_j(k+1) \in \mathcal{R}_j(k+1, e_j(k)), \quad (4.17)$$

where

$$\mathcal{R}_j(k+1, e_j(k)) := \mathcal{E}_j(k+1) \cap (e_j(k) \oplus \delta \cdot \mathcal{P}_j(k)). \quad (4.18)$$

The set  $\mathcal{R}_j(k+1, e_j(k))$  is the interval of feasible and reachable  $e_j(k+1)$  given  $e_j(k)$ . To ease readability, we will omit the explicit dependency of the interval  $\mathcal{R}_j(k+1, e_j(k))$  on  $e_j(k)$  in the sequel. Evidently, one needs to avoid cases in which the intersection in (4.18) is the empty set. To this end, we consider the following assumption.

**Assumption 1** (Consistency of constraints). *For all  $j \in \mathcal{N}$  EC-DERs and all  $k \in \mathcal{K}$ , let the sampling time  $\delta$  and the intervals  $\mathcal{P}_j(k)$ ,  $\mathcal{E}_j(k)$ , and  $\mathcal{E}_j(k+1)$  be such that for all  $e_j(k) \in \mathcal{E}_j(k)$*

$$\mathcal{E}_j(k+1) \cap (e_j(k) \oplus \delta \cdot \mathcal{P}_j(k)) \neq \emptyset \quad (4.19)$$

<sup>3</sup> Recall that the Minkowski sum between two sets  $\mathcal{A}$  and  $\mathcal{B}$  is defined as  $\mathcal{A} \oplus \mathcal{B} = \{a+b \mid a \in \mathcal{A}, b \in \mathcal{B}\}$ .

holds. ■

This condition can be regarded as controlled forward invariance of the entire (time-varying) state constraint set  $\mathcal{E}_j(k)$ ,  $k \in \mathcal{K}$ . Practically speaking, it can be satisfied by reducing the state constraints—i.e. if there are no feasible  $e_j(k+1)$  reachable from  $e_j(k)$ , then this  $e_j(k)$  should be excluded from  $\mathcal{E}_j(k)$ —or by enlarging the set  $\delta \cdot \mathcal{P}_j(k)$  by considering a different time-discretization—and, consequently, a different time step  $\delta$ .

Under Assumption 1, the bounds of

$$\mathcal{R}_j(k+1) = [\underline{e}_j^r(k+1), \bar{e}_j^r(k+1)] \quad (4.20a)$$

are

$$\underline{e}_j^r(k+1) = \max \left\{ \underline{e}_j(k+1), e_j(k) + \delta \cdot \underline{p}_j(k) \right\}, \quad (4.20b)$$

$$\bar{e}_j^r(k+1) = \min \left\{ \bar{e}_j(k+1), e_j(k) + \delta \cdot \bar{p}_j(k) \right\}; \quad (4.20c)$$

which follows from standard tools of interval arithmetics [Jaulin *et al.*, 2001]. Going back to Example 1, a sketch of  $\mathcal{R}_1(k+1)$  and  $\mathcal{R}_2(k+1)$  is shown in Figure 4.3a and Figure 4.3b. Therein, these intervals are depicted by crossed intervals.

An energy constraint summarizing the power and the energy constraints can be elaborated also for the aggregated states. This model requires a joint power and energy constraint (per time step), i.e.

$$e(k+1) \in \mathcal{R}(k+1, e(k)), \quad (4.21)$$

with

$$\mathcal{R}(k+1, e(k)) := \mathcal{E}(k+1) \cap (e(k) \oplus \delta \cdot \mathcal{P}(k)).$$

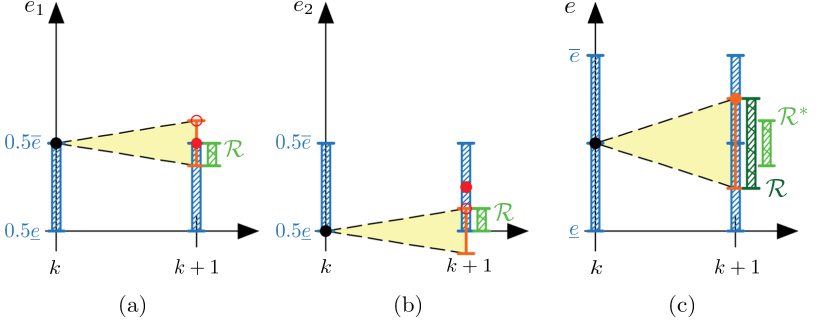


Figure 4.3: Illustration of the feasible and reachable energy states in Example 1.

Henceforth, we simplify the notation by dropping in the following the explicit dependency of  $\mathcal{R}(k+1, e(k))$  on  $e(k)$ . Similar to (4.20), the bounds of

$$\mathcal{R}(k+1) = [\underline{e}^r(k+1), \bar{e}^r(k+1)] \quad (4.22a)$$

are

$$\underline{e}^r(k+1) = \max \left\{ \underline{e}(k+1), e(k) + \delta \cdot \underline{p}(k) \right\}, \quad (4.22b)$$

$$\bar{e}^r(k+1) = \min \left\{ \bar{e}(k+1), e(k) + \delta \cdot \bar{p}(k) \right\}. \quad (4.22c)$$

However, given  $e(k)$ , the actual aggregation of the feasible and reachable energy intervals of each EC-DER  $\mathcal{R}_j(k+1)$  gives

$$\mathcal{R}^*(k+1) := s \left( \bigtimes_{j \in \mathcal{N}} \mathcal{R}_j(k+1) \right). \quad (4.23)$$

The propagation of set  $\bigtimes_{j \in \mathcal{N}} \mathcal{R}_j(k+1)$  with  $s$  from (4.5) is again to be understood as the point-wise image. Considering (4.20), this can be written as

$$s \left( \bigtimes_{j \in \mathcal{N}} \mathcal{R}_j(k+1) \right) = \left[ \sum_{j \in \mathcal{N}} \underline{e}_j^r(k+1), \sum_{j \in \mathcal{N}} \bar{e}_j^r(k+1) \right].$$

Next, we investigate the relation between the bounds of  $s \left( \times_{j \in \mathcal{N}} \mathcal{R}_j(k+1) \right)$  and  $\mathcal{R}^*(k+1)$ . The application of (4.13) to (4.22) implies the following inequalities

$$\underline{e}^r(k+1) \leq \sum_{j \in \mathcal{N}} \underline{e}_j^r(k+1), \quad (4.24a)$$

$$\bar{e}^r(k+1) \geq \sum_{j \in \mathcal{N}} \bar{e}_j^r(k+1). \quad (4.24b)$$

Consequently, we have that

$$\mathcal{R}(k+1) \supseteq \mathcal{R}^*(k+1). \quad (4.25)$$

Specifically, there are values of  $e(k+1)$  which are feasible for (4.9b)-(4.9c) but not for (4.8b)-(4.8c) every time that one of the inequalities (4.24) holds strictly. Practically speaking, there are values of  $e(k+1)$  that are feasible for the aggregated model but that cannot be dispersed into a feasible  $e(k+1)$ . This is the case of Example 1, illustrated in Figure 4.3c. It can be seen that the interval  $\mathcal{R}^*(k+1)$  is a “narrower” subset of  $\mathcal{R}(k+1)$ . The  $e(k+1)$  chosen in Example 1 is feasible and reachable according to the aggregated model, as it is contained within  $\mathcal{R}(k+1)$ . However, this solution is unfeasible for the complete constraint set, because it lays *outside* of the interval  $\mathcal{R}^*(k+1)$ .

To summarize, the aggregated constraints from (4.13) might undesirably enlarge the feasible space of  $p(k)$  and  $e(k)$ . Recalling the abstract problem presented at the end of Section 4.2, this is the case if

$$\mathcal{Y}(k+1, y(k)) \supseteq h \left( \times_{j \in \mathcal{N}_y} \mathcal{Y}_j(k+1, \mathbf{y}(k)) \right), \quad (4.26)$$

which violates condition (4.12) of Lemma 1. Subsequently we present sufficient conditions under which the aggregated constraints equal the propagation of the original constraints.

## 4.4 Ensuring Schedule Feasibility

From Lemma 1, the aggregation preserves the optimality of the solution if and only if

$$\mathcal{R}(k+1) \equiv \mathcal{R}^*(k+1). \quad (4.27)$$

In the previous section we have showed that  $\mathcal{R}(k+1)$  obtained by application of (4.13) does not guarantee (4.27). A natural consequence would be to find a different way to compute  $\mathcal{R}(k+1)$  such that (4.27) holds. In contrast, we propose to pursue a reversed approach. Instead of computing a “narrower”  $\mathcal{R}(k+1)$  such that (4.27) is satisfied, we suppose the existence of an  $e(k)$ —whose elements sum up to the selected  $e(k)$ —for which (4.27) holds for a  $\mathcal{R}(k+1)$  with aggregated bounds computed via (4.13). Example 2 demonstrates this.

**Example 2.** Consider the setting of Example 1, but with  $e_1(k) = e_2(k) = 0.25(\bar{e} + \underline{e})$ . Figure 4.4 depicts this case. Therein,  $\mathcal{R}(k+1)$  and  $\mathcal{R}^*(k+1)$  are equivalent and  $e(k+1) = 0.5(\bar{e} + \underline{e})$ —which is feasible and reachable for the aggregated model as discussed in Example 1—is feasible and reachable with respect to the constraints of each EC-DER:

$$\begin{aligned} p_1(k) &= 0.5\bar{p} \in [0.5\underline{p}, 0.5\bar{p}], & p_2(k) &= 0.5\bar{p} \in [0.5\underline{p}, 0.5\bar{p}], \\ e_1(k+1) &= 0.25(\bar{e} + \underline{e}) + \delta \cdot 0.5\bar{p} \in [0.5\underline{e}, 0.5\bar{e}], \\ e_2(k+1) &= 0.25(\bar{e} + \underline{e}) + \delta \cdot 0.5\bar{p} \in [0.5\underline{e}, 0.5\bar{e}]. \end{aligned} \quad \blacksquare$$

Comparison of Examples 1 and 2 points out that certain feasible dispersions of  $e(k)$  are preferable over others. The energy states  $e_1(k)$  and  $e_2(k)$  are a feasible dispersion of aggregated energy  $e(k)$  both in Example 1 and

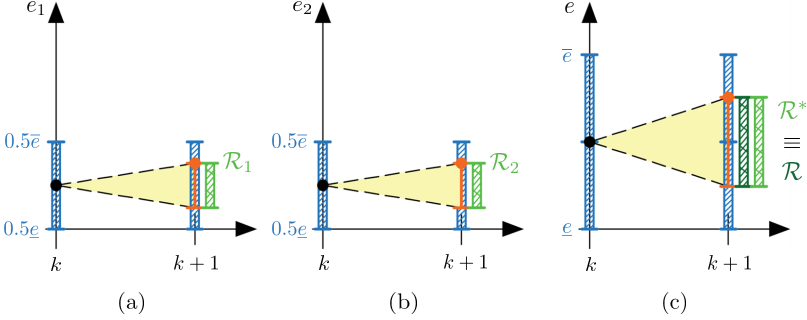


Figure 4.4: Illustration of Example 2.

in Example 2. However, the values for  $e_1(k)$  and  $e_2(k)$  chosen in Example 1 compromise the existence of a feasible dispersion of the desired (aggregated feasible)  $e(k+1)$ . The same  $e(k+1)$  has instead a feasible dispersion with the values of  $e_1(k)$  and  $e_2(k)$  chosen in Example 2.

Let us rephrase this observation using the abstraction from Section 4.2. Given a value of  $y(k)$ , we define

$$h^{-1}(y(k)) = \left\{ \mathbf{y}(k) \in \prod_{j \in \mathcal{N}_y} \mathcal{Y}_j(k, \mathbf{y}(k-1)) \mid h(\mathbf{y}(k)) = y(k) \right\}$$

as the set of feasible pre-images of  $y(k)$  with respect to the mapping  $h$ . If the set  $h^{-1}(y(k))$  is not a singleton, each of its elements maps to  $y(k)$ . However, some of those can restrict the feasible set at the next time step,  $\prod_{j \in \mathcal{N}_y} \mathcal{Y}_j(k+1, \mathbf{y}(k))$ , more than others. Hence, given a set  $\mathcal{Y}(k+1, y(k))$  for which (4.26) holds, satisfaction of (4.12) depends on  $\mathbf{y}(k) \in h^{-1}(y(k))$ , because the set  $h(\prod_{j \in \mathcal{N}_y} \mathcal{Y}_j(k+1, \mathbf{y}(k)))$  varies with  $\mathbf{y}(k)$ .

Motivated by these considerations, we denote

$$\tilde{\mathcal{E}}(k, e(k)) := \prod_{j \in \mathcal{N}} \mathcal{E}_j(k) \cap s^{-1}(e(k)),$$

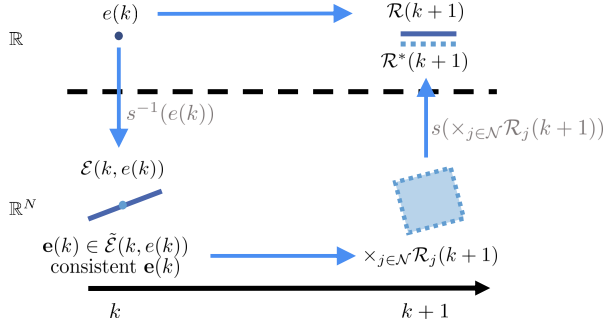


Figure 4.5: Graphical representation of a consistent dispersion of  $e(k)$ .

as the set of feasible dispersions of  $e(k)$ .

**Definition 1** (Consistent dispersion of  $e(k)$ ). *Given  $e(k)$ , the vector  $e(k)$  is said to be a consistent dispersion of  $e(k)$  at time  $k + 1$ , if  $e(k) \in \mathcal{E}(k, e(k))$  and*

$$\mathcal{R}(k + 1) \equiv \mathcal{R}^*(k + 1),$$

with  $\mathcal{R}(k + 1)$  as in (4.22) and  $\mathcal{R}^*(k + 1)$  from (4.23). ■

The meaning of consistent  $e(k)$  is illustrated in Figure 4.5. Starting from the top-left corner, Figure 4.5 shows that an aggregated state  $e(k)$  can be dispersed in different ways, namely all the points in  $\tilde{\mathcal{E}}(k, e(k))$ . Among them, a consistent dispersion of the aggregated state  $e(k)$  leads to a feasible and reachable set  $\times_{j \in \mathcal{N}} \mathcal{R}_j(k + 1)$  (on the right) whose propagation on the aggregated space,  $\mathcal{R}^*(k + 1)$ , is equivalent to the aggregated feasible and reachable set obtained via direct computation, i.e. from  $e(k)$  and relative aggregated constraints as in (4.13). Considering the complete problem, the DS  $\{\tilde{g}_j\}_{\mathcal{K}}$  can be computed via (4.9) as much as via (4.8) if  $e(k)$  is a consistent dispersion of  $e(k)$  for all  $k \in \mathcal{K}$ , because the conditions of Lemma 1 are satisfied at each time step.

**Remark 1** (Dispersions and two-stage scheduling). Introducing the concept of a consistent dispersion helps understanding why (4.9) is successfully ap-

plied, cf. [Xu *et al.*, 2016; Appino *et al.*, 2018c]. Therein, hierarchical control is often used to solve (4.8) in a sequential manner. First, (4.9) is used (with (4.13)) on an upper level to provide long-term aggregated schedules. Second, a lower level feedback control (e.g. MPC) assigns the dispersion of the aggregated energy state in a way that guarantees the feasibility of the pre-computed DS over the subsequent time-steps. Essentially, this controller consistently disperses the aggregated DS.

## 4.5 Existence and Computation of Consistent Dispersions

The considerations above motivate investigation of the existence of a consistent dispersion. To this end, we make the following assumption.

**Assumption 2** (Forward Invariance and Reachability of Energy Constraints). *For all  $j \in \mathcal{N}$  and all  $k \in \mathcal{K}$ , let the sampling time  $\delta$  and the intervals  $\mathcal{P}_j(k)$ ,  $\mathcal{E}_j(k)$  and  $\mathcal{E}_j(k+1)$  be such that there exists at least one  $e_j(k) \in \mathcal{E}_j(k)$  for which*

$$e_j(k) \oplus \delta \cdot \mathcal{P}_j(k) \subseteq \mathcal{E}_j(k+1), \quad (4.28a)$$

$$(\mathcal{E}_j(k) \oplus \delta \cdot \mathcal{P}_j(k)) \supseteq \mathcal{E}_j(k+1), \quad (4.28b)$$

*holds.* ■

Condition (4.28a) implies that there exists a controlled invariant (time-varying) subset of  $\mathcal{E}_j(k)$ , and furthermore that there exists a subset of  $\mathcal{E}_j(k)$  from which all reachable states are feasible. The second part (4.28b) instead requires that the entire set  $\mathcal{E}_j(k+1)$  is contained in the reachable set  $\mathcal{E}_j(k) \oplus \delta \cdot \mathcal{P}_j(k)$ .

Moreover, consider  $d_l : \mathbb{N} \times \mathbb{R}^N \rightarrow \mathbb{R}$  given by

$$d_l(k, \mathbf{e}(k)) = \sum_{j \in \mathcal{N}} - \left( e_j(k) + \delta \cdot \underline{p}_j(k) + \right. \\ \left. - \max \left\{ e_j(k) + \delta \cdot \underline{p}_j(k), \underline{e}_j(k+1) \right\} \right), \quad (4.29a)$$

and  $d_u : \mathbb{N} \times \mathbb{R}^N \rightarrow \mathbb{R}$  given by

$$d_u(k, \mathbf{e}(k)) = \sum_{j \in \mathcal{N}} \left( e_j(k) + \delta \cdot \bar{p}_j(k) + \right. \\ \left. - \min \left\{ e_j(k) + \delta \cdot \bar{p}_j(k), \bar{e}_j(k+1) \right\} \right). \quad (4.29b)$$

**Theorem 1** (Existence of a consistent dispersion).

Suppose Assumptions 1 and 2 hold. If

$$\mathbf{e}(k) \in \arg \min_{\mathbf{e}(k) \in \mathcal{E}(k, \mathbf{e}(k))} (d_l(k, \mathbf{e}(k)) + d_u(k, \mathbf{e}(k))) \quad (4.30)$$

with  $d_l$  and  $d_u$  from (4.29), then  $\mathcal{R}(k+1)$  from (4.22) and  $\mathcal{R}^*(k+1)$  from (4.23) satisfy

$$\mathcal{R}(k+1) \equiv \mathcal{R}^*(k+1),$$

i.e.  $\mathbf{e}(k)$  is a consistent dispersion of  $\mathbf{e}(k)$  at time  $k+1$ . ■

The proof of Theorem 1 will be given in Section 4.5.1. Note that Assumption 2 is quite mild. Set relation (4.28a) can, for example, be enforced by reducing the set  $\delta \cdot \mathcal{P}_j(k)$ . Set relation (4.28b), instead, requires to exclude all the values of  $\mathbf{e}(k+1)$  that are feasible from an energy perspective but that cannot be reached from any feasible  $\mathbf{e}(k)$ . Note that (4.28b) is trivially fulfilled when  $\mathcal{E}_j(k)$  is constant (or decreasing with respect to set-inclusion) provided 0 belongs to  $\mathcal{P}_j(k)$ . Similar to the case of Assumption 1, this latter aspect is an additional modeling effort that is normally avoided, but

that is fundamental in case of aggregation. In short, Assumption 2 can be seen as requiring that the set of feasible energy states of each device does not “change too much” from one time step to the next, which can be obtained by excluding never-reachable states and increasing the granularity of the time-discretization. In this sense, Assumptions 1 and 2 are indirectly coupling the power and the energy constraints (4.2). Note that the use of time-varying power constraints is particularly useful to avoid that the most stringent energy constraint limits the power constraint over the entire scheduling horizon.

Furthermore, observe that cost function  $d_l(k, e(k)) + d_u(k, e(k))$  as stated in Theorem 1 involves the energy state  $e(k)$  *only* at time step  $k$ . This means that the computation of a consistent dispersion is independent from the knowledge of  $e(h)$  with  $h \neq k$ . Thus,  $e(k)$  (and consequently the vector  $\mathbf{p}(k-1)$  leading to  $e(k)$  from  $e(k-1)$ ) can be determined at each  $k$  by a lower-level controller without any need for information about past or future states of the system. This has two important consequences. On the one hand, it avoids any dependency between dispersion at subsequent time instants in the scheduling problem, which complicates dealing with eventual random decision variables and parameters. On the other hand, the computation of  $e(k)$  does not require any load forecasts nor MPC strategies (the long-term perspective is already accounted for in the aggregated DS). However, we remark that the main results are: i) that a combination of energy states that is feasible with respect to the constraints of the individual EC-DERs (4.3c)-(4.3f) exists whenever the aggregated energy state is feasible with respect to the aggregated constraints (4.9d)-(4.9f) and (4.13), and ii) that such a feasible realization can be computed online. In fact, other methods to determine—*online*—a consistent dispersion of the aggregated energy state can be applied alternatively to the one proposed in Theorem (1), e.g. MPC as mentioned in Remark 1. These alternative techniques might be useful to discriminate among consistent dispersions whenever there exist multiple ones, i.e. whenever function  $(d_l(k, e(k)) + d_u(k, e(k)))$  is not strictly

convex. Note that while a consistent dispersion  $e(k)$  implies that the set of feasible dispersion  $\tilde{\mathcal{E}}(k, e(k))$  is not empty, it does not guarantee that a consistent dispersion at  $k + 1$  exists. We address this point in the following theorem.

**Theorem 2** (Recursive existence of consistent dispersions). *Suppose Assumptions 1 and 2 hold. If  $e(k + 1) \in \mathcal{E}(k + 1)$  and  $e(k)$  is a consistent dispersion of  $e(k)$ , then there exists at least one consistent dispersion of  $e(k + 1)$ .* ■

The proof of Theorem 2 will be given in Section 4.5.1. An important consequence of Theorem 2 is that given that the initial  $e(k^b)$  is a consistent dispersion of  $e(k^b)$ , then a consistent dispersion of  $\{p\}_{\mathcal{K}}$  and  $\{e\}_{\mathcal{K}+}$  is always possible as long as (4.9b)-(4.9c) hold with (4.13). In other words, the aggregated DS can always be tracked. Furthermore, note that while the existence of a consistent dispersion is a property of the entire system, the requirements of Assumptions 1 and 2 involve each EC-DER *separately*, in line with the task of aggregating heterogeneous devices.

Besides justifying the use of aggregated scheduling (4.9) in presence of a consistent dispersion of the aggregated energy state, Theorem 1 and Theorem 2 lead to further considerations in more general problems. We will discuss this in Section 4.5.2 after providing the proofs in the next section.

## 4.5.1 Proofs of Theorem 1 & 2

*Proof of Theorem 1.*

The main idea behind the proof of Theorem 1 is showing that the bounds of the real intervals  $\mathcal{R}(k + 1)$  and  $\mathcal{R}^*(k + 1)$  coincide when  $e(k)$  satisfies (4.30). If the bounds of  $\mathcal{R}(k + 1)$  and  $\mathcal{R}^*(k + 1)$  coincides, then  $\mathcal{R}(k + 1) \equiv \mathcal{R}^*(k + 1)$ . First we prove technical lemmata to then turn towards the proof of Theorem 1.

From (4.22) it follows that there are two possible cases for each of the two bounds of  $\mathcal{R}(k + 1)$ :

- Case (i):

$$e(k) + \delta \cdot \underline{p}(k) \geq \underline{e}(k+1), \quad (4.31a)$$

respectively,

$$e(k) + \delta \cdot \bar{p}(k) \leq \bar{e}(k+1). \quad (4.31b)$$

- Case (ii):

$$e(k) + \delta \cdot \bar{p}(k) > \bar{e}(k+1), \quad (4.32a)$$

respectively,

$$e(k) + \delta \cdot \underline{p}(k) < \bar{e}(k+1). \quad (4.32b)$$

Observe that, differently from Case (i), the inequalities in Case (ii) are strict. Furthermore, note that the feasible and reachable states at time  $k$  are limited by the reachability (power) constraint (??) in Case (i), and by the feasibility (energy) constraint in Case (ii). We analyze both cases in two technical lemmata.

**Lemma 2** (Case (i)). *Suppose Assumptions 1 and 2 hold and let  $e(k)$  satisfy (4.30).*

- (a) *If (4.31a) holds, then the lower bound  $\underline{e}^r(k+1)$  of  $\mathcal{R}(k+1)$  from (4.22) and the lower bound  $\sum_{j \in \mathcal{N}} \underline{e}_j^r(k+1)$  of  $\mathcal{R}^*(k+1)$  from (4.23) satisfy*

$$\underline{e}^r(k+1) = \sum_{j \in \mathcal{N}} \underline{e}_j^r(k+1).$$

- (b) *If (4.31b) holds, then the upper bound  $\bar{e}^r(k+1)$  of  $\mathcal{R}(k+1)$  from (4.22) and the upper bound  $\sum_{j \in \mathcal{N}} \bar{e}_j^r(k+1)$  of  $\mathcal{R}^*(k+1)$  from (4.23) satisfy*

$$\bar{e}^r(k+1) = \sum_{j \in \mathcal{N}} \bar{e}_j^r(k+1).$$

*Proof.* First, consider the lower-bound case (a), i.e. that (4.31a) holds. From  $e(k) + \delta \cdot \underline{p}(k) \geq \underline{e}(k+1)$ , we have

$$e(k) \geq -\delta \cdot \underline{p}(k) + \underline{e}(k+1).$$

Thus, for a  $e(k) \in \mathcal{E}(k+1) = s(\times_{j \in \mathcal{N}} \mathcal{E}_j(k+1))$  there exists a  $e(k) = s^{-1}(e(k))$  such that

$$e_j(k) \geq -\delta \cdot \underline{p}_j(k) + \underline{e}_j(k+1) \quad \forall j \in \mathcal{N}, \quad (4.33)$$

Equation (4.28a) in Assumption 2 implies that there is at least one  $e(k)$  feasible for (4.3c)-(4.3f) for which

$$e_j(k) \geq -\delta \cdot \underline{p}_j(k) + \underline{e}_j(k+1) \quad \forall j \in \mathcal{N}.$$

Thus, that there exists at least one feasible  $e(k) = s^{-1}(e(k))$  for which (4.33) holds. In other words, there exists a  $e(k) \in \tilde{\mathcal{E}}(k, e(k))$  satisfying (4.33).

Observe that  $d_l(k, e(k))$  reaches its global minimum, which is zero, for any  $e(k)$  satisfying (4.33). Furthermore, from (4.28a) in Assumption 2 it holds that

$$\bar{e}_j(k+1) - \delta \cdot \bar{p}_j(k) \geq \underline{e}_j(k+1) - \delta \cdot \underline{p}_j(k). \quad (4.34)$$

This implies that diminishing the values of any  $e_j(k)$  below  $-\delta \cdot \underline{p}_j(k) + \underline{e}_j(k+1)$  does not reduce the value of  $d_u(e(k), k)$ . Therefore, (4.30) for Case (i)-(a) implies (4.33).

In turn, it follows from (4.33) that

$$e_j(k) + \delta \cdot \underline{p}_j(k) \geq \underline{e}_j(k+1) \quad \forall j \in \mathcal{N}.$$

Therefore, the lower bound of  $\mathcal{R}^*(k+1)$  is equal to

$$\sum_{j \in \mathcal{N}} \underline{e}_j^r(k+1) = \sum_{j \in \mathcal{N}} e_j(k) + \delta \cdot \sum_{j \in \mathcal{N}} \underline{p}_j(k) = \underline{e}^r(k+1).$$

The second part of Case (i)— $e(k) + \delta \cdot \bar{p}(k) \leq \bar{e}(k+1)$ —follows mutatis mutandis and it is skipped for the sake of brevity.  $\square$

**Lemma 3** (Case (ii)). *Suppose Assumptions 1 and 2 hold and let  $e(k)$  satisfy (4.30).*

(a) *If (4.32a) holds, then the lower bound  $\underline{e}^r(k+1)$  of  $\mathcal{R}(k+1)$  from (4.22) and the lower bound  $\sum_{j \in \mathcal{N}} \underline{e}_j^r(k+1)$  of  $\mathcal{R}^*(k+1)$  from (4.23) satisfy*

$$\underline{e}^r(k+1) = \sum_{j \in \mathcal{N}} \underline{e}_j^r(k+1).$$

(b) *If (4.32b) holds, then the upper bound  $\bar{e}^r(k+1)$  of  $\mathcal{R}(k+1)$  from (4.22) and the upper bound  $\sum_{j \in \mathcal{N}} \bar{e}_j^r(k+1)$  of  $\mathcal{R}^*(k+1)$  from (4.23) satisfy*

$$\bar{e}^r(k+1) = \sum_{j \in \mathcal{N}} \bar{e}_j^r(k+1).$$

*Proof (by contradiction).* First, consider the lower-bound case (b), i.e. that (4.32a) holds. Assume that there is a group of devices  $\mathcal{I} \subset \mathcal{N}$  for which

$$e_i(k) + \delta \cdot \underline{p}_i(k) > \underline{e}_i(k+1), \quad \forall i \in \mathcal{I} \quad (4.35)$$

and another group of devices  $\mathcal{H} = \mathcal{N} \setminus \mathcal{I}$  for which

$$e_h(k) + \delta \cdot \underline{p}_h(k) \leq \underline{e}_h(k+1), \quad \forall h \in \mathcal{H}. \quad (4.36)$$

From (4.7) it follows that

$$e(k) = \sum_{\mathcal{I}} e_i(k) + \sum_{\mathcal{H}} e_h(k).$$

Suppose that  $\mathcal{H} = \emptyset$ , then (4.32a) is false and we fall back to Case (i). Hence  $\mathcal{H} \neq \emptyset$ . Moreover, for at least one  $\hat{h} \in \mathcal{H}$ , Inequality (4.36) holds strictly (otherwise we again fall back to Case (i)).

Consider a small positive increment  $\Delta > 0$  for which  $\hat{e}_{\hat{h}}(k) = e_{\hat{h}}(k) + \Delta$  still satisfies (4.36). The increment of  $\hat{e}_{\hat{h}}(k)$  is always allowed. In fact, given Assumption 2, we have

$$\bar{e}_{\hat{h}}(k) + \delta \cdot \underline{p}_{\hat{h}}(k) \geq \underline{e}_{\hat{h}}(k + 1).$$

Thus, from (4.36) (which is strictly satisfied for  $\hat{h}$ ), it follows that  $e_{\hat{h}}(k) < \bar{e}_{\hat{h}}(k)$ . Next, consider w.l.o.g. one EC-DER  $\hat{i} \in \mathcal{I}$  for which the energy  $\hat{e}_{\hat{i}}(k) = e_{\hat{i}}(k) - \Delta$  is decreased such that  $\hat{e}_{\hat{i}}(k)$  still satisfies (4.35). This reduction is always possible: given Assumption 2 we have

$$e_{\hat{i}}(k) + \delta \cdot \underline{p}_{\hat{i}}(k) \leq \underline{e}_{\hat{i}}(k + 1);$$

thus, (4.35) implies  $e_{\hat{i}}(k) > \underline{e}_{\hat{i}}(k)$ .

Increasing the energy at EC-DER  $\hat{h}$  and reducing it at the same time at EC-DER  $\hat{i}$  maintains the satisfaction of equality (4.7), as

$$e(k) = -\Delta + \sum_{\mathcal{I}} e_i(k) + \sum_{\mathcal{H}} e_h(k) + \Delta.$$

However,  $d_l(\hat{e}(k), k) < d_l(e(k), k)$ . Moreover,  $d_u(\hat{e}(k), k) \leq d_u(e(k), k)$ . In fact, the increment of  $e_{\hat{h}}(k)$  cannot increase  $d_u(e(k), k)$ , because the contribution of the components  $e_h(k)$  to  $d_u(e(k), k)$  is zero: given (4.34), then  $\hat{e}_{\hat{h}}(k) \leq \bar{e}_{\hat{h}}(k + 1) - \delta \cdot \bar{p}_{\hat{h}}(k)$ . Thus,  $e(k)$  does not minimize

$d_l(e(k), k) + d_u(e(k), k)$ . We arrive at a contradiction, i.e.  $\mathcal{I} \neq \emptyset$  contradicts (4.30). Hence we arrive at  $\mathcal{I} = \emptyset$  if (4.30) holds.

Given that (4.36) hold for all the EC-DERs, then the lower bound of  $\mathcal{R}^*(k+1)$  is equal to

$$\sum_{j \in \mathcal{N}} e_j^r(k+1) = \sum_{j \in \mathcal{N}} e_j(k+1) = \underline{e}^r(k+1).$$

Summing up, the lower bounds of  $\mathcal{R}(k+1)$  and  $\mathcal{R}^*(k+1)$  also match in Case (ii)-(a) under (4.30). In a similar fashion, it can be shown that the upper bound of  $\mathcal{R}(k+1)$  equals the upper bound of  $\mathcal{R}^*(k+1)$  in Case (ii)-(b) under (4.30).  $\square$

Now we can finalize the proof of the theorem. As we have seen in Lemma 2 for Case (i) and in Lemma 3 for Case (ii), if (4.30) holds, then the upper and lower bound of  $\mathcal{R}(k+1)$  and  $\mathcal{R}^*(k+1)$  coincide, leading to  $\mathcal{R}(k+1) \equiv \mathcal{R}^*(k+1)$ . This finishes the proof of Theorem 1.  $\square$

### *Proof of Theorem 2.*

By construction, if  $e(k)$  is a consistent dispersion of  $e(k)$  and  $e(k+1) \in \mathcal{R}(k+1)$ , then there exist at least a feasible dispersion of  $e(k+1)$ , cf. Definition 1. Thus, the set  $\mathcal{E}(k+1, e(k+1))$  is not empty. The cost function  $d_l(k+1, e(k+1)) + d_u(k+1, e(k+1))$  is real-valued and continuous and the set  $\tilde{\mathcal{E}}(k+1, e(k+1))$  is compact. Thus, by virtue of the extreme values theorem, the function  $d_l(k+1, e(k+1)) + d_u(k+1, e(k+1))$  attains a minimum over  $\tilde{\mathcal{E}}(k+1, e(k+1))$  meaning that at least one minimizer  $e(k+1)$  exists. Consequently, applying Theorem 1, there exist a consistent dispersion of  $e(k+1)$ .  $\square$

## 4.5.2 Discussion

Theorems 1 and 2 indicate the following approach to scheduling problems in the form of (4.3):

- (i) Check/impose consistency of constraints (4.3c)-(4.3d) to Assumptions 1 and 2.
- (ii) Aggregate decision variables and constraint sets via mapping  $s$ , as in (4.7) and (4.13).
- (iii) Solve (4.9) to compute the DS  $\{\tilde{g}\}_{\mathcal{K}}$ .
- (iv) Guarantee feasibility of the aggregated DS by dispersing the aggregated variables such that (4.30) holds.

Next, we show how the results from Theorem 1 and 2 can be used to extend the applicability of the scheduling algorithm analyzed in Chapter 3 to an aggregation of EC-DERs and inflexible loads/generators. To this end, we analyze three aspects neglected in (4.3): non-linearities in the EC-DERs dynamics (4.1) caused by conversion losses, uncertain  $\{l_i\}_{\mathcal{K}}$  for all  $i \in \mathcal{N}_1$ , and aggregations of EC-DERs with time-varying connections.

## 4.6 Aggregation and Conversion Losses

Consider a dynamic model of the energy state including conversion losses as in (3.1), i.e.

$$e_j(k+1) = e_j(k) + \delta \cdot (p_j(k) - \mu_j |p_j(k)|), \quad (4.37)$$

where the coefficient  $\mu_j$  describes the amount of energy that is lost in conversion.

Next, consider an alternative—yet equivalent—model describing the conversion losses in terms of lost power. First, we define

$$t_j(k) = p_j(k) - \mu_j \cdot |p_j(k)|, \quad (4.38)$$

as the actual power exchange with the storage. Then, we introduce  $t_j(k)$  into (4.37), which gives

$$e_j(k+1) = e_j(k) + \delta \cdot t_j(k). \quad (4.39)$$

Given (4.38), the power constraint (4.2a) can be equivalently expressed as a constraint on  $t_j(k)$ , i.e.

$$\mathcal{T}(k) = \left\{ \mathbf{t}(k) \mid \exists \mathbf{p}(k) \in \prod_{j \in \mathcal{N}} \mathcal{P}_j(k) \text{ satisfy (4.38)} \right\}. \quad (4.40)$$

In other words, conversion losses modify the boundaries of the set of reachable states at  $k+1$ . Note that  $\mathcal{T}(k)$  is a closed real interval.

Finally, consider the scheduling problem (4.8) including conversion losses as modeled by (4.38)-(4.40),

$$\min_{\substack{\{\tilde{g}\}_{\mathcal{K}}, \{\mathbf{t}\}_{\mathcal{K}}, \{\mathbf{e}\}_{\mathcal{K}+}, \\ \{\mathbf{t}\}_{\mathcal{K}}, \{\mathbf{e}\}_{\mathcal{K}+}}} \sum_{k \in \mathcal{K}} c^{\text{DS}}(\tilde{g}(k), k) \quad (4.41a)$$

$$\text{s. t. } \forall k \in \mathcal{K}$$

$$\tilde{g}(k) = t(k) - l(k) + p_{\text{loss}}(k), \quad (4.41b)$$

$$\mathbf{e}(k+1) = \mathbf{e}(k) + \delta \cdot \mathbf{t}(k) \quad \mathbf{e}(k^{\text{b}}) = \mathbf{e}^0, \quad (4.41c)$$

$$e(k+1) = s(e(k+1)), \quad (4.41d)$$

$$\mathbf{t}(k) \in \prod_{j \in \mathcal{N}} \mathcal{T}_j(k), \quad (4.41e)$$

$$\mathbf{e}(k+1) \in \prod_{j \in \mathcal{N}} \mathcal{E}_j(k+1), \quad (4.41f)$$

$$t(k) = s(\mathbf{t}(k)), \quad (4.41g)$$

$$p_{\text{loss}}(k) = f(\mathbf{t}(k)). \quad (4.41h)$$

The value  $p_{\text{loss}}(k)$  aggregates the total conversion losses (in terms of power) resulting from  $\mathbf{t}(k)$ . Equation (4.41h) is the only practical difference be-

tween problem (4.41) and (4.8). Thus, the question arises if the solution of (4.41) can be approached in two steps (aggregated scheduling and subsequent dispersion), as for (4.8), without compromising the result.

The aggregated version of (4.41) would be

$$\min_{\{\tilde{g}\}_{\mathcal{K}}, \{t\}_{\mathcal{K}}, \{e\}_{\mathcal{K}^+}} \sum_{k \in \mathcal{K}} c^{\text{DS}}(\tilde{g}(k), k) \quad (4.42a)$$

$$\text{s. t. } \forall k \in \mathcal{K}$$

$$\tilde{g}(k) = t(k) - l(k) - f_{\text{agg}}(t(k)), \quad (4.42b)$$

$$e(k+1) = e(k) + \delta \cdot t(k), \quad e(k^b) = s(e^0), \quad (4.42c)$$

$$t(k) \in \mathcal{T}(k), \quad (4.42d)$$

$$e(k+1) \in \mathcal{E}(k+1). \quad (4.42e)$$

Observe that constraints (4.41c)-(4.41d) and (4.42c)-(4.42e) have the exact same structure of the corresponding ones in (4.8) and (4.9). Therefore, the idea of a consistent dispersion and the statements of Theorems 1 and 2 still hold. The main difficulty is represented here by enforcement of the equivalence between (4.42b) and (4.41b), (4.41h).

Consider a symmetric system where the losses are the same on each device and independent of  $p_j(k)$ , i.e.  $\mu_j = \mu$  for all  $j \in \mathcal{N}$ . Furthermore, consider the absence of mutual exchange of power among devices, i.e.  $\text{sign}(p_j(k)) = \text{sign}(p_i(k))$  for all  $\{j, i\} \in \mathcal{N} \times \mathcal{N}$ . Then, defining

$$f_{\text{agg}}(t(k)) = \begin{cases} \frac{\mu}{1-\mu} t(k) & \text{if } t(k) \geq 0 \\ \frac{-\mu}{1+\mu} t(k) & \text{if } t(k) < 0 \end{cases}, \quad (4.43)$$

the equivalence  $f_{\text{agg}}(t(k)) = f(\mathbf{t}(k))$  holds exactly for each  $t(k) \in \mathcal{T}(k)$ . Thus, in this specific case, (4.42b) is equivalent to (4.41b), (4.41h), and aggregation as in (4.42) leads to the same solution of (4.41). However, in general  $f_{\text{agg}}(t(k))$  can only approximate  $f(\mathbf{t}(k))$  and the solution of (4.42)

deviates from the one of the original problem (4.41) depending on this approximation. This aspect might compromise the effectiveness of aggregation. Eventually, aggregation of groups of EC-DERs with similar conversion losses can reduce the severity of the approximation at the price of a slightly higher number of variables in the aggregated problem.

Note that we use the transformation  $p_j(k) \rightarrow t_j(k)$  only to show under which conditions Theorems 1 and 2 hold when conversion losses are considered. For the discussed case of  $\mu_j = \mu$  for all  $j \in \mathcal{N}$ , this transformation is unnecessary in practice. Aggregation can be done directly on  $p_j(k)$  with using (3.1) as aggregated dynamics.

## 4.7 Aggregation and Uncertainty

The assumption of perfect knowledge of the inflexible power outputs upon scheduling,  $\{l_i\}_{\mathcal{K}}$  for all  $i \in \mathcal{N}_1$ , is unrealistic. As discussed in Chapter 3, a better representation of the inflexible power outputs is in terms of random variables, which leads to a stochastic version of (4.3) where all the decision variables representing the power outputs and the energy states of the EC-DERs are stochastic variables. Similarly to (3.11), we interpret this problem by moving from inequalities on the single devices to a chance constraint

limiting the number of deviations from the schedule, and by considering the cost function in terms of its expected value. This leads to

$$\begin{aligned}
& \min_{\substack{\{\tilde{g}\}_{\mathcal{K}}, \\ \{\mathbf{X}\}_{\mathcal{K}}}} \sum_{k \in \mathcal{K}} c^{\text{DS}}(\tilde{g}(k), k) + \mathbb{E} \left[ \sum_{k \in \mathcal{K}} c^i(\Delta \mathbf{G}(k)) \right] \\
& \text{s.t. } \forall k \in \mathcal{K} \\
& \quad \mathbf{E}_j(k+1) = \mathbf{E}_j(k) + \delta \cdot \mathbf{P}_j(k), \quad \forall j \in \mathcal{N} \\
& \quad \mathbf{E}_j(k^{\text{b}}) = \mathbf{E}_j^0, \quad \forall j \in \mathcal{N} \\
& \quad [\mathbf{P}^\top(k) \Delta \mathbf{G}(k)] = h'(\tilde{g}(k), \mathbf{L}^\top(k), \mathbf{E}^\top(k)) \\
& \quad \mathbb{E} \left[ \sum_{\mathcal{K}} \mathbf{B}(k) \right] \geq (1 - \varepsilon) \cdot K,
\end{aligned} \tag{4.44}$$

where the random decision variables are collected in vector

$$\mathbf{X}(k) := \left[ \mathbf{P}^\top(k) \mathbf{E}^\top(k+1) \Delta \mathbf{G}(k) \right]^\top,$$

and  $\mathbf{B}(k)$  is defined as for (3.11). Problem (4.44) is more challenging than (3.11): the more parameters, the more difficult it is to compute their multivariate distribution; the more correlated random variables, the harder it is to obtain a tractable formulation of the stochastic program. Thus, one may wonder whether aggregation allows to reduce the number of random variables, and eventually to elaborate the problem with the reasoning presented in Chapter 3 (based on avoiding chance constraints with multiple random variables and multiple random parameters). To this end, let us include the forecast uncertainty in the aggregated scheduling problem (4.9) instead of on (4.3). By doing so, we shift from multiple to a single aggregated uncertain power output,  $\mathbf{L}(k)$ . At the same time, we can consider the aggregated EC-DER to compensate for the uncertainty stemming from  $\mathbf{L}(k)$ . In this framework, (4.44) is reduced to (3.11), and the same reasoning and approximations detailed in Section 3.3.1 can be applied directly—the constraints

of the aggregated EC-DER are equal to the ones of a single EC-DER, which is the case considered in Chapter 3. Practically speaking, we consider—upon scheduling—that the power required to maintain  $g(k)$  at  $\tilde{g}(k)$  will be provided by *some* devices, leaving the decision on *which* specific device provides this power to a subsequent decision stage, taking place *after* scheduling. Note that this model matches particularly well a multi-stage decision structure. Planning an aggregated response to the uncertainty models a greater freedom in subsequent choices than responses to the uncertainty that are fixed at the first stage for each decision variable (and usually affine, cf. Section 3.2). In case of scheduling for power dispatch, this additional freedom translates in the need of fewer reserves for the compensation of imbalances, because the EC-DERs respond to the uncertainty *collectively* instead of reacting to “individually assigned” uncertainties (which would require individual and conservative energy reserves).

However, it remains to clarify whether the statistical properties of the resulting DS hold with consideration of multiple EC-DERs and how the uncertainty affecting the aggregated power output and energy state should be dispersed among the various devices. From Theorem 2 it follows that, as long the dispersion of the aggregated energy state at the previous time step is consistent, whatever feasible realization of the uncertain aggregated energy state has a feasible dispersion. Thus, the statistical properties of the DS are preserved. Additionally, Theorem 1 suggests how to derive a realization of the uncertain dispersed energy states from a realization of the aggregated energy state. In other words, determining a-priori the relation between the realization of the uncertain energy states and of the uncertain inflexible outputs is not necessary, because such realization can be computed online following Theorem 1. Alternatively, if there are reasons to prefer a consistent dispersion over another, an MPC scheme can be implemented to disperse the aggregated energy state. This situation occurs, for example, in the case study presented in Chapter 6.

## 4.8 Time-Varying Connections

### 4.8.1 Aggregated Model with Time-Varying Connections

The last aspect of practical relevance that should be considered in aggregated scheduling is the possibility that some devices are not connected for the entire duration of the DS. This is, for example, the case of charging stations for PEVs, where the PEVs can arrive and leave within the time spanned by a DS. It should be mentioned that there exists several works proposing to exploit the storage of PEVs for the benefit of the system by means of appropriate charging strategies; see [Mukherjee and Gupta, 2015] and references therein. The interest on the topic is motivated by the fact that vehicles inherently rely on storage for their transportation function and on average they are in-use only for 4% of the time [Kempton and Tomić, 2005]; thus PEVs are promising in providing capacity reserves and storage to power systems. To account for this situation, we extend the model presented in Section 4.1. To this end, we introduce set  $\mathcal{N}_{\mathcal{K}}$  collecting all the indexes associated with the EC-DERs connecting for at least one  $k \in \mathcal{K}$  and the set  $\mathcal{N}_{\mathcal{K}}(k) \subset \mathcal{N}_{\mathcal{K}}$  containing the indexes of the EC-DERs connected at  $k$ . The active power balance is

$$g(k) = l(k) + \sum_{j \in \mathcal{N}_{\mathcal{K}}(k)} p_j(k). \quad (4.45)$$

In this framework,  $e_j(k)$ ,  $j \in \mathcal{N}_{\mathcal{K}}$ , exists only within the interval  $[k_j^a, k_j^d]$ , where  $k_j^a$  and  $k_j^d$  denote the arrival and departure times of the  $j$ -th EC-DER, respectively. Furthermore, we consider the ordered index sets  $\mathcal{A}_{\mathcal{K}}(k) = \{j \in \mathcal{N}_{\mathcal{K}} | k_j^a \leq k\}$ , modeling the EC-DERs arriving until  $k$ , and  $\mathcal{D}_{\mathcal{K}}(k) = \{j \in \mathcal{N}_{\mathcal{K}} | k_j^d \leq k\}$ , representing the EC-DERs leaving until  $k$ .

Whenever an EC-DER connects to the aggregation, it brings the energy already stored in its battery into the system. At the same time, an EC-DER disconnecting removes from the system a quantity of energy equivalent to the one stored in its battery. This sudden injection or absorption of energy is

not represented in the aggregated dynamics (4.9d). Thus, we extend (4.9d) as

$$e(k+1) = e(k) + \sum_{j \in \mathcal{I}(k)} e_j(k_j^a) + \delta \cdot p(k), \quad (4.46)$$

where  $\mathcal{I}(k) = \{j \in \mathcal{N}_{\mathcal{K}} | k_j^a = k\}$  is the set of EC-DERs arriving at  $k$ . This dynamics is similar to (4.9d), with the inclusion of sudden energy increases at each  $k_j^a$ . This energy addition accounts for the fact that when an EC-DER connects, the energy stored in its battery is immediately added to the energy stored in the aggregated system. Observe that we employ different models for the connection and the disconnection of an EC-DER, as the energy decrease caused by an EC-DER disconnecting is not modeled in (4.46). We further discuss this aspect later.

The bounds for the set of feasible aggregated power and energy,  $\mathcal{P}(k)$  and  $\mathcal{E}(k+1)$ , should as well consider the possibility of connecting/disconnecting devices. We compute the bounds of  $\mathcal{P}(k)$ , following (4.14b), as the sum of the ones of the devices connected at time  $k$ ,

$$\underline{p}(k) = \sum_{j \in \mathcal{N}_{\mathcal{K}}(k)} \underline{p}_j, \quad \bar{p}(k) = \sum_{j \in \mathcal{N}_{\mathcal{K}}(k)} \bar{p}_j.$$

For the energy constraints instead, we use a model that is slightly different from (4.14c), i.e.

$$\bar{e}(k) = \bar{e}(k-1) + \sum_{j \in \mathcal{A}_{\mathcal{K}}(k)} \bar{e}_j, \quad (4.47a)$$

$$\underline{e}(k) = \underline{e}(k-1) + \sum_{j \in \mathcal{A}_{\mathcal{K}}(k)} \underline{e}_j + \sum_{j \in \mathcal{D}_{\mathcal{K}}(k)} e_j^{\min}, \quad (4.47b)$$

with

$$\bar{e}(k^0) = \bar{e}_0 + \sum_{j \in \mathcal{A}_{\mathcal{K}}(k^0)} \bar{e}_j, \quad \underline{e}(k^0) = \underline{e}_0 + \sum_{j \in \mathcal{A}_{\mathcal{K}}(k^0)} \underline{e}_j.$$

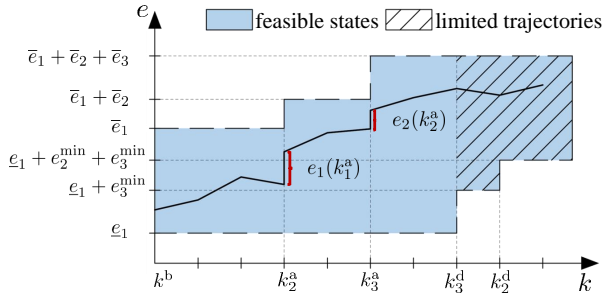


Figure 4.6: Example of aggregated energy state and of its bounds (time-varying battery).

For the sake of shorthand notation, we employ the notation  $e_j^{\min}$  to indicate the minimum amount of energy that has to be stored in the  $j$ -th EC-DER upon disconnection,  $\underline{e}_j(k_j^d)$ . An example of the energy constraint of a time-varying battery is depicted in Figure 4.6. Once more, connection and disconnection of an EC-DER are modeled in different ways.

Summarizing, the arrival of the  $j$ -th EC-DER corresponds to an increment of both lower and upper capacity limits in (4.47) together with an “energy addition” of  $e_j(k_j^a)$  in (4.46). This model does not compromise the feasibility of the aggregated schedule when the power and energy constraints of EC-DER  $j$  satisfy Assumptions 1 and 2, and  $e_j(k_j^a)$  forms a feasible dispersion of  $e(k_j^a)$  together with the energy state of the other connected devices.<sup>4</sup> An equivalent model for the departure of an EC-DER would be a reduction of the boundaries  $\underline{e}(k_j^d)$  and  $\bar{e}(k_j^d)$  at  $k_j^d$  and a subtraction of  $e_j(k_j^d)$  from  $e(k_j^d - 1)$ . However, this latter model would require the precise knowledge of  $e_j(k_j^d)$ , which is lost in aggregation. The aggregated model does not distinguish among the energy states of its single components: once an EC-DER connects, its available storage capacity is added to the aggregation and its energy state becomes indistinguishable from the ones of the other

<sup>4</sup> Theorem 1 and Theorem 2 address step-wise properties, and are indifferent to a change in the number of devices along the scheduling horizon.

devices. Thus, the disconnection of an EC-DER cannot be appropriately modeled. We consider instead as if the EC-DER would remain connected with  $\mathcal{P}_j(k) = [0, 0]$  and  $\mathcal{E}_j(k) = [e_j^{\min}, \bar{e}(k_j^d)]$  for all  $k > k_j^d$ . This choice solves the issue of having unknown departure energy states  $e_j(k_j^d)$ , but it introduces an additional challenge. In fact, it can be easily seen that the modified constraints for disconnecting devices do not satisfy Assumption 2. This is because the storage capacity  $\mathcal{E}(k) = [e_j^{\min}, \bar{e}(k_j^d)]$  and any eventual excess of energy  $e_j(k_j^d) - e_j^{\min}$  are still included in the aggregated model after the disconnection of the  $j$ -th EC-DER, even if not physically accessible ( $p_j(k) = 0$ ). Consequently, not every trajectory connecting feasible states  $e$  after the first disconnection of a device is actually a feasible trajectory, as illustrated in Figure 4.6.

Summarizing, aggregated scheduling is justified in case of EC-DERs connecting within the scheduling horizon, but it can lead to problems whenever some EC-DERs are disconnecting within the scheduling horizon. Nonetheless, the proposed aggregation can still be applied to many practical cases with disconnecting devices by adding few corrections. For example, take an aggregation including a Battery Energy Storage System (BESS) and a charging station for PEVs. Furthermore, assume a situation in which charging the  $j$ -th PEV over its  $e_j^{\min}$  should be avoided as much as possible because it does not bring any additional revenues (which is the case considered in the simulation study reported later in Chapter 6). In this context, the PEVs should store any eventual excess of energy only if the BESS is fully charged; denoting the BESS with index 1, this leads to a  $e_j(k_j^d) > e_j^{\min}$ ,  $j \neq 1$ , only if  $e_1(k_1^d) = \bar{e}_1$ .<sup>5</sup> One recurring error in this case is scheduling an excessive discharge at the end of the horizon. We address this issue as

---

<sup>5</sup> In case of an aggregation that includes only PEVs, the priority should go to the PEV leaving last.

follows. Let  $k_{j'}^d$  indicate the departure time of the last vehicle leaving, i.e.  $k_{j'}^d = \max \{k_j^d, j \in \{\mathcal{N}_K \setminus \{1\}\}\}$ . Then, including constraint

$$e(k^e) - e(k_{j'}^d) \leq \bar{e}_1 - \underline{e}_1, \quad (4.48)$$

in the aggregated scheduling problem guarantees that not more than the energy excess stored in the BESS is scheduled to be transferred to the utility grid after that the last PEV has left.<sup>6</sup> While introducing this additional constraint does not entirely solve the problem of disconnecting devices, it can suffice to obtain a feasible aggregated schedule, as shown by the results reported in Chapter 6.

## 4.8.2 Additional Sources of Uncertainty

Additional uncertainties can arise from the (often unknown) parameters of the devices connecting after the computation of the DS [Lee *et al.*, 2012]. Going back to the example of the charging station, the parameters of the connecting PEVs can be unknown, and so can be their connection/disconnection times and their energy state upon connection. Here, we focus on the uncertainty surrounding the energy state of connecting devices, which we denote as random variable  $E_v(k_v^a)$  with realization  $e_v(k_v^a)$ , and on how to integrate this additional uncertainty to the one stemming from uncertain power output discussed in Section 4.7. In particular, we assume that the aggregated EC-DER compensates not only for the uncertainties surrounding the generation forecasts but also for the uncertainty characterizing the energy state of arriving EC-DERs.

Recall that we regard the aggregated EC-DER to compensate for the uncertain power output as described in Chapter (3), i.e.  $\Delta P(k) = -\Delta L(k)$ ,

<sup>6</sup> In case uncertainty is considered, this constraint should be imposed to the expected value, i.e. to  $\hat{e}(k^e) - \hat{e}(k_{j'}^d)$

see (3.21). The main difference with Chapter 3 is that dynamics (4.46) substitutes (3.1). Including the uncertainty, this becomes

$$E(k+1) = E(k) + \sum_{v \in \mathcal{I}(k)} E_v(k_v^a) + \delta \cdot P(k). \quad (4.49)$$

As already discussed in Chapter 3, the summation of correlated random variables causes difficulties in an optimization problem. The use of an approximated energy balance may help also in this case.

Separating the deterministic and stochastic components of (4.49) as in (3.19) leads to

$$\hat{e}(k+1) = \hat{e}(k) + \delta \cdot \hat{p}(k), \quad (4.50a)$$

$$\Delta E(k+1) = \Delta E(k) + \sum_{v \in \mathcal{I}(k)} E_v(k_v^a) + \delta \cdot \Delta P(k). \quad (4.50b)$$

Note that (4.50a) is equivalent to (3.20c), as it excludes the “energy increment” caused by arriving EC-DERs. Indeed, the “energy increment”  $E_v(k_v^a)$  is a stochastic variable affecting only the stochastic component of (4.49), see (4.50b).

Further elaboration of (4.50b) (similar to Step 5 in Section 3.3.1) gives

$$\begin{aligned} \Delta E(k+1) &= \Delta E(k) + \delta \cdot \Delta P(k) + \sum_{v \in \mathcal{I}(k)} E_v(k_v^a) \\ &= \Delta E(k) - \delta \cdot \Delta L(k) + \sum_{v \in \mathcal{I}(k)} E_v(k_v^a) \\ &= -\delta \sum_{i=k^b}^k \Delta L(i) + \sum_{v \in \mathcal{A}_{\mathcal{K}}(k)} E_v(k_v^a). \end{aligned}$$

with initial condition  $\Delta E(k^b) = 0$ . Recall the notation  $\Delta E_l(k)$  from (3.23). Then

$$\Delta E(k) = -\Delta E_l(k) + \sum_{v \in \mathcal{A}_{\mathcal{K}}(k)} E_v(k_v^a). \quad (4.51)$$

Note that the energy state of each EC-DER and the uncontrolled load/generation refer to completely different devices. Thus, it is reasonable to consider that  $\Delta E_l(k)$  and  $E_v(k_v^a)$  are independent, and that so are  $E_j(k_j^a)$  and  $E_h(k_h^a)$  with  $j \neq h$ . Therefore,  $f_{\Delta E(k)}(\Delta e)$ , is given by the convolution of  $f_{\Delta E_l(k)}(\Delta e_l)$  and  $f_{E_v}(e_v)$  for each  $v \in \mathcal{A}_{\mathcal{K}}(k)$  [Carlton *et al.*, 2017]. In other words,  $f_{\Delta E(k)}(\Delta e) = \tilde{f}_{\max(\mathcal{A}_{\mathcal{K}}(k))}^k$  with

$$\tilde{f}_j^k = \tilde{f}_{j-1}^k * f_{E_v}(y), j \in \mathcal{A}_{\mathcal{K}}(k) \text{ and } \tilde{f}_0 = f_{\Delta E_l(k)}(-y), \quad (4.52)$$

where  $*$  indicates the operation of convolution and the support of  $f_{E_v}(y)$  and  $f_{\Delta E_l(k)}(y)$  is trivially extended to the real line by setting them to zero outside of their original support.

To ease the understanding, we illustrate the stochastic energy constraint (3.32) for aggregated EC-DERs with time-varying connections in Figure 4.7. The full line represents the expected state of charge  $\hat{e}(k)$ , the colored areas represent values that the realization  $e(k)$  can take with a certain probability, and the dashed lines depict the energy limits. Figure 4.7 is the equivalent of Figure 3.5: the probability associated to the energy states laying within the energy limits has to be at least  $(1 - \varepsilon)$ . However, differently from Figure 3.5, in Figure 4.7 the energy limits are time-varying. One could also observe the sudden increase in the energy states corresponding to the arrival of one or more EC-DERs at respective time instants.

## 4.9 Summary

Aggregated modeling is a promising option to extend the applicability of the scheduling algorithm proposed in Chapter 3 to a system including hetero-

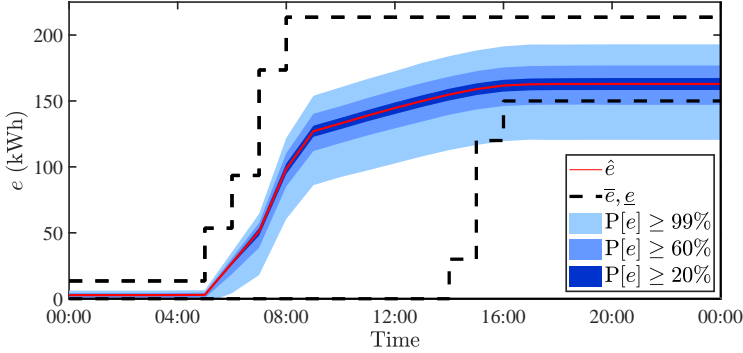


Figure 4.7: Scheduling for a DCS: graphical representation of the stochastic energy state  $E(k)$  and of its corresponding constraint with  $(1 - \varepsilon) = 0.75$ .

geneous EC-DERs. Aggregated models are well studied and often applied in the literature, because they reduce the number of parameters and decision variables in the scheduling problem, lowering the computation burden and improving the management of the uncertainties. However, feasible intervals for the aggregated power and energy state determined by summing the feasible intervals of each device in the cluster may extend the feasible space to values that cannot be attained in practice. Understanding to which extent this relaxation influences the result of an optimization problem for scheduling is pivotal to a successful application of aggregated modeling on power systems with uncertain power outputs. To this end, we show in this chapter that, whenever the energy states of the individual devices satisfy a specific (collective) property—that we define as *consistent dispersion of the aggregated energy state*—the aggregation does not alter the feasible set at the subsequent time-step and thus it does not imply a loss of optimality. Furthermore, we prove that a consistent dispersion always exists under mild assumptions on the constraints of the various devices, considered separately. Our findings justify the application of the algorithm described in Chapter 3 to schedule the aggregated dispatch of a cluster of heteroge-

neous flexible and inflexible distributed energy resources, without any loss of optimality or robustness. Additionally, we show that conversion losses, uncertain power outputs and time-varying connections of EC-DERs can all be considered in this scheduling scheme. Next, we investigate the results of applying the proposed scheduling and operation scheme to realistic and real systems, looking at cases comprising both a single EC-DER (Chapter 5) and a time-varying population of EC-DERs (Chapter 6).



## 5 Case Studies on a single EC-DER

The theories which I have expressed there, and which appear to you to be so chimerical, are really extremely practical—so practical that I depend upon them for my bread and cheese.

---

*A. C. Doyle, A Study in Scarlet*

This chapter reports the results obtained applying the scheduling and control scheme described in Chapter 3 to a number of diverse case studies. The focus is on a system with a single EC-DER as described in Chapter 3, see Figure 3.1. The chosen cases involve diverse settings, allowing to test different properties of the algorithm. The first case study concerns a household equipped with battery storage and PV generation. There, we evaluate the performance of the algorithm with respect to state-of-the-art methods based on deterministic and scenario-based forecasts. The second case study involves an industrial campus equipped with a large-scale solar field and battery storage. Scope of this study is to investigate the scalability of the proposed method to industrial-size systems together with the response of the algorithm to actual market prices. The third case study refers to an experimental generation system that couples PV panels and battery storage. The scope of this study is to validate the proposed scheme in real-life experiments. The results presented in this section have appeared in [Appino *et al.*, 2018b, 2019a].

## 5.1 Case Study 1: Simulation of a Household

The first case study entails simulations of prosumption at household level. The scope of this test case is to assess the performance of the proposed scheduling algorithm with respect to state-of-the-art ones. In the following, we first report the characteristics of the case study, of the data and of the tools employed in the simulations. Then, we detail the results and comment on them.

### 5.1.1 Description of the Case study

A household with a rooftop PV generator controlled at his maximum power point and a domestic BESS represents the case study for simulation. The data of PV production and load consumption are retrieved from the freely available dataset provided by Ausgrid [Ratnam *et al.*, 2015]. The dataset offers the time series of the load and PV generation profile of 300 Australian households with installed rooftop PV systems for the time frame of 1 Jul 2010 to 30 Jun 2013. Specifically, the data utilized here concerns household 109. The technical specifications of the BESS come from the catalog of a commercial producer.<sup>1</sup> Considering only the usable capacity, these are:  $\underline{e} = 0$  kWh,  $\bar{e} = 13.5$  kWh,  $\underline{p} = -5$  kW,  $\bar{p} = 5$  kW,  $\mu = 5\%$ . Note that the power and energy constraints in Chapter 3 allow time-varying limits; however, a BESS has time-invariant constraints. Furthermore, we remark that we choose a BESS with a capacity that is relatively small for the proposed application, aiming to illustrate the benefits of the proposed scheme in challenging conditions. Finally, note that we arbitrarily initialize the energy state of the BESS at the beginning of each simulated period to 6 kWh.

Consider the following regulation for the operation of the system. The power exchange with the higher level grid is adjusted according to a day-ahead DS. The scheduling horizon spans midnight to midnight and it is di-

---

<sup>1</sup> [www.tesla.com/powerwall](http://www.tesla.com/powerwall) [Accessed: 15-Jan-2018]

vided into 24 steps of 1 hour, i.e.  $K = 24$ ,  $O = 12$  and  $\delta = 1\text{h}$ . The cost of the DS follows (3.34), with time invariant coefficients  $c^{q+} = 0.05 \frac{\text{€}\cdot\text{h}}{\text{kW}^2}$ ,  $c^{q-} = 0.05 \frac{\text{€}\cdot\text{h}}{\text{kW}^2}$ ,  $c^{l+} = 0.3 \frac{\text{€}\cdot\text{h}}{\text{kW}}$ ,  $c^{l-} = 0.15 \frac{\text{€}\cdot\text{h}}{\text{kW}}$ . These values reflect a pricing policy rewarding self-consumption and load leveling. No penalization of the derivative, cf. (3.5b), is considered in this case. Regarding the imbalances, their cost is as in (3.6). We analyze two different pricing policies, denoted in the following as *C1* and *C2*, where the tariff of imbalances is twice (policy *C1*) and ten times (policy *C2*) as high as the one of the DS (considering both power excess and power shortage as purchased power), i.e.

$$C1: c^i(\Delta g(k)) = 2c^{q+} |\Delta g(k)|^2 + 2c^{l+} |\Delta g(k)|, \quad (5.1)$$

$$C2: c^i(\Delta g(k)) = 10c^{q+} |\Delta g(k)|^2 + 10c^{l+} |\Delta g(k)|. \quad (5.2)$$

Additionally to these pricing schemes, we require a minimum tracking ratio  $r^\gamma(\{\Delta g\}_K)$ , see (3.8), with  $\gamma = 10^{-4}$  and values for  $(1 - \varepsilon)$  ranging from 0.42 to 0.72.

### 5.1.2 Simulation Setup

The simulations cover five different weeks in the time frame going between 1 Feb 2010 and 30 Jun 2013. To the end of covering the effects of seasonal changes, these weeks have been selected in different months.

For each day, we simulate the hierarchical scheme depicted in Figure 3.2. First, we compute a DS with discrete time steps of one hour. In this process, we use only the information practically available at midday of the previous day, in accordance to the considered day-ahead market regulation. Then, we simulate the effects of the DS by computing sequentially the power outputs and the energy state at each hour of the day. Specifically, we account for the on-line rescheduling at each simulated hour by solving an additional optimization, using the information available at the beginning of that hour, see Section 3.4. The output of this optimization is then used together with the

realization of the uncertain load (with one-hour resolution) to compute the power outputs and the energy state over the hour under analysis. These values provide the input for the next iteration. Note that we arbitrarily initialize the energy state of the BESS at the beginning of each simulated week to 6 kWh.

The simulations are carried out in MATLAB, employing standard open-source optimization tools developed in the systems and control community to solve the scheduling problems. Specifically, we use CasADi [Andersson, 2013] with the IPOPT [Wächter and Biegler, 2006]. All the computations have been performed using a PC with an Intel® Core™ i5-6400 CPU at 2.70 GHz and 8.00 GB RAM.

### 5.1.3 Forecasts

Considering an extension of the scheduling interval of  $S = 6\text{h}$ , the optimization problem requires forecasts of  $\{L(k)\}_{\mathcal{K}^a}$  and  $\{E_l(k)\}_{\mathcal{K}^a}$  with  $\mathcal{K}^a = \mathcal{O} \cup \mathcal{K} \cup \mathcal{S}$  for  $O + K + S = 42\text{h}$  hours. These forecasts are requested at every DS computation, i.e. every day at 12:00. Furthermore, the online rescheduling requires hourly updates the forecasts of  $\{\hat{l}(k)\}_{\mathcal{M}}$ . The forecasts are obtained as follows:

#### Load and Generation Power Forecasts

The structure of the data-driven models is selected to be a polynomial of at most degree three. With the selected structure, 99 data-driven quantile regressions ranging from the 0.01 to the 0.99 quantiles in 0.01 intervals are trained for several forecast horizons ranging from 1h to 48h.<sup>2</sup> All power forecasting models are trained with current and past power values as well as current and past values of other time series as input. Those extra time series contain maximal, minimal, and mean power values obtained by assuming

---

<sup>2</sup> PV generation forecasting models are trained only on values considered to be day values, i.e. all night values are automatically eliminated from the utilized training set.

power time series to be periodic. The values of these additional time series are promising for the estimation of forecast uncertainties. Please note that all forecasts are only based on historical power time series, since the Ausgrid dataset does not contain weather forecast data. For further information regarding weather-free forecasting models refer to [González Ordiano *et al.*, 2016]. The polynomials are created for the four most relevant features, selected by a forward feature selection. The method and constraints (to assure positive power/energy values and no quantile crossing) are described in [González Ordiano *et al.*, accepted]. The quantile regressions for the different forecast horizons are combined into a forecasting model able to deliver at 12:00 every day forecasts for the next 48 hours and to update their forecast every hour.

### Load and Generation Energy Forecasts

After obtaining the probabilistic power forecasts, the quantile regression for the median is applied to the training data. The power forecasts obtained at 12:00 for the next 48 hours are integrated and utilized as input for the creation of 99 data-driven quantile regressions (using the same method and constraints as before). These regressions predict the quantiles of the future energy values for the same periods as the utilized power forecasts.

#### Forecasts for $\{L(k)\}_{\mathcal{K}^a}$ and $\{E_l(k)\}_{\mathcal{K}^a}$

The quantile regressions for both  $\{L(k)\}_{\mathcal{K}^a}$  and  $\{E_l(k)\}_{\mathcal{K}^a}$ —which represent the sum of load and PV generation, whereby the generation is considered to be a negative load—are obtained by convolution of the generation and load forecasts (under the assumption that load and generation are statistically independent and that their quantile regressions correctly approximate the distribution functions of their future values). The regressions describing the median are assumed to be forecasting models approximating the expecting values  $\{\hat{l}(k)\}_{\mathcal{K}^a}$  and  $\{\hat{e}_l(k)\}_{\mathcal{K}^a}$ . Pairs of the obtained quan-

tile regressions—centered on the regression describing the median—can be combined to create intervals,  $\left[ \bar{l}_{(1-\varepsilon_p)}(k), \bar{l}_{(1-\varepsilon_p)}(k) \right]$ , with a given probability that future values of  $\{L(k)\}_{\mathcal{K}^a}$  will lay inside, cf. (3.28). Finally, the quantiles of  $\{\Delta E_l(k)\}_{\mathcal{K}^a}$  are used to fit the parameters of two logistic functions whose sum is utilized as a description of  $F_{\Delta E_l(k)}(\Delta e_l)$ . The fitting is undertaken using a least-squares optimization. Extensive numerical studies have shown that the choice of a logistic function with six parameters  $[a_1 \dots a_6]$ , i.e.

$$F_{\Delta E_l(k)}(\Delta e_l) = \frac{a_1}{1 + e^{-a_2(\Delta e_l - a_3)}} + \frac{a_4}{1 + e^{-a_5(\Delta e_l - a_6)}}, \quad (5.3)$$

is able to reproduce the skewness of the quantiles. Other choices, e.g. hyperbolic tangent, arctangent or specific algebraic functions, have shown poorer results.

All utilized forecasting models are created with the open-source MATLAB toolbox SciXMiner [Mikut *et al.*, 2017].<sup>3</sup> The data from 1 Sep 2010 to 1 Dec 2012 is used for the data-driven training of the forecasting model. The models are then applied to the remaining data.

### 5.1.4 Benchmarks

Besides the scheduling algorithm described in Chapter 3 and denoted in the following as Probabilistic Forecast Scheduling (PFS), we simulate and compare the effects of other two scheduling algorithms. For the sake of readability, we indicate the deterministic cost of the DS as

$$C^{\text{DS}} := \sum_{k \in \mathcal{K}^s} c^{\text{DS}+/}(\tilde{g}^+(k), \tilde{g}^-(k), k) \in \mathbb{R},$$

<sup>3</sup> [www.sourceforge.net/projects/scixminer/](http://www.sourceforge.net/projects/scixminer/)

and the expected cost of imbalances as

$$C^i := \sum_{k \in \mathcal{K}^s} \sum_{\omega' \in \mathcal{S}'} \pi^{\omega'} \cdot c^i \left( \Delta g^{\omega'}(k) \right) \in \mathbb{R}.$$

### Deterministic Forecast Scheduling

The first technique is to ignore the uncertainty and solve a deterministic scheduling problem similar to (3.10), without the consideration of imbalances and with differentiation of power directions, i.e.

$$\begin{aligned} & \min_{\{\mathbf{x}\}_{\mathcal{K}^s}} C^{\text{DS}} \\ & \text{s.t. } \forall k \in \mathcal{K}^s, \\ & \quad \tilde{g}(k) = p(k) + \hat{l}(k), \\ & \quad e(k+1) = e(k) + \delta \cdot (p(k) - \mu p^+(k) + \mu p^-(k)), \\ & \quad e(k^{\text{b}}) = e^0, \\ & \quad [\tilde{g}^+(k), \tilde{g}^-(k)] \in \mathcal{F}'_d(\tilde{g}(k)), \\ & \quad [p^+(k), p^-(k)] \in \mathcal{F}''_d(p(k)), \\ & \quad p(k) \in \mathcal{P}(k), \\ & \quad e(k+1) \in \mathcal{E}(k+1), \end{aligned}$$

with decision variables collected in the vector

$$\mathbf{x}(k) = [\tilde{g}(k) \ \tilde{g}^+(k) \ \tilde{g}^-(k) \ e(k+1) \ p(k) \ p^+(k) \ p^-(k)]^{\text{T}} \in \mathbb{R}^7.$$

The value of  $\left\{ \hat{l}(k) \right\}_{\mathcal{K}^{\text{a}}}$  is estimated as described in the previous Section. We denote this scheduling technique as Deterministic Forecast Scheduling (DFS). The aim of comparing PFS to DFS is to evaluate the effects of considering forecast uncertainty in the scheduling algorithm.

## Scenario Forecast Scheduling

The second benchmark scheduling scheme that we consider consist in solving (3.11) without constraint (3.11e) by means of sampling, as described in Section 2.3.1.

$$\begin{aligned}
& \min_{\substack{\{\mathbf{x}\}_{\mathcal{K}^s}, \\ \{\mathbf{x}^{\omega'}\}_{\mathcal{K}^s} \forall \omega' \in \mathcal{S}'}} C^{\text{DS}} + C^{\text{i}} \\
& \text{s.t. } \forall k \in \mathcal{K}^s, \forall \omega' \in \mathcal{S}' \\
& \quad \tilde{g}(k) = p^{\omega'}(k) + l^{\omega'}(k), \\
& \quad e^{\omega'}(k+1) = e^{\omega'}(k) + \delta \cdot \left( p^{\omega'}(k) - \mu p^{+, \omega'}(k) + \mu p^{-, \omega'}(k) \right), \\
& \quad e^{\omega'}(k^{\text{b}}) = e^0, \\
& \quad [\tilde{g}^+(k), \tilde{g}^-(k)] \in \mathcal{F}'_d(\tilde{g}(k)), \\
& \quad [p^{+, \omega'}(k), p^{-, \omega'}(k)] \in \mathcal{F}''_d(p^{\omega'}(k)), \\
& \quad p^{\omega'}(k) \in \mathcal{P}(k), \\
& \quad e^{\omega'}(k+1) \in \mathcal{E}(k+1),
\end{aligned}$$

with scenario-independent decision variables collected in vector

$$\mathbf{x}(k) = [\tilde{g}(k) \tilde{g}^+(k) \tilde{g}^-(k)]^{\top} \in \mathbb{R}^3,$$

and scenario-dependent decision variables grouped in vector

$$\mathbf{x}^{\omega'}(k) = \left[ e^{\omega'}(k+1) p^{\omega'}(k) p^{+, \omega'}(k) p^{-, \omega'}(k) \Delta g^{\omega'}(k) \right]^{\top} \in \mathbb{R}^5 \quad \forall \omega' \in \mathcal{S}'.$$

We denote this scheduling technique as Scenario Forecast Scheduling (SFS). We choose this technique as a benchmark because of its large utilization in the existing literature. However, the insight of comparing SFS to PFS is twofold. On one side, it allows to assess the performance of the proposed

PFS against a state-of-the-art technique. On the other, it provides an estimate of the severity of the approximations included in (3.38) and listed in Table 3.1. In fact, sampling techniques do not require approximations. In particular, excluding constraint (3.11e) leads to a formulation of the optimization problem for SFS where the requirement of limiting the imbalances is restricted to pure cost considerations. Recall that a cost-aware allocation of the energy reserves to compensate for imbalances is neglected in the PFS, see Table 3.1. Therefore, the a-priori expectation is to use the cost achieved by the SFS as a benchmark for the minimum achievable total cost with consideration of the uncertainty. If so, comparing the total costs obtained by the PFS with the one achieved by the SFS can quantify the consequences of the approximations in Table 3.1.

Similar to the case of probabilistic forecasts, we generate scenarios of  $\{l^i(k)\}_{\mathcal{K}^a}$  by applying quantile regressions as described in [González Ordiano, 2019]. In this case the regressions predict the quantiles of the power value an hour into the future. Each scenario is created (i) by randomly selecting one of the predicted quantiles, (ii) by using it as input of the one-hour-ahead quantile regressions, and (iii) by repeating the first two steps for the length of the extended scheduling horizon. We extract 100 equiprobable scenarios.<sup>4</sup> Then, we apply the algorithm presented in [Conejo *et al.*, 2010] to reduce the number of scenarios to  $S' = 30$  and assign a weight  $\pi_i$  to each of them.

## Discussion

Note that the forecast-dependent parameters are computed using the same technique for all the analyzed algorithms. In particular, we train data-driven quantile regressions from which we obtain the parameters required in input by each scheme. This way, we target a fair comparison of the scheduling schemes that is as independent as possible from the performance of

<sup>4</sup> We selected the number of samples empirically: increasing the number of samples over this value did not have a significant impact on the solution.

the forecasting algorithm. Nevertheless, the engineering choices on problem structure and models, computational tractability, and data processing in the design of a scheduling algorithm are strongly interconnected, and contribute jointly to the final outcome, as mentioned in Chapter 2. Thus, it can be practically impossible to ascribe the results to a single, specific algorithmic choice. We comment further on this point while presenting the results.

### 5.1.5 Results

The average computation times required to solve the considered scheduling problems are reported in Table 5.1. One can see that all three variants are solved within fractions of a second (DFS and PFS) or within a few seconds (SFS). Thus, the computational load does not appear to be an implementation barrier for any of the scheduling formulations.

The average values of  $r^\gamma(\{\Delta g\}_\mathcal{K})$  resulting from the different scheduling schemes are depicted in Figure 5.1 and detailed in Table 5.1. Additionally, Table 5.1 lists also the average amount of energy required daily from the grid to compensate for the imbalances; this energy has to be considered as the total daily energy request, regardless of whether it was absorbed or injected

Table 5.1: Simulation of a household results, lowest costs in bold.

	DFS	PFS						SFS	
$(1 - \varepsilon)$ or $C1/C2$	-	0.42	0.48	0.54	0.60	0.66	0.72	$C1$	$C2$
computation time (s)	0.07	0.41	0.43	0.41	0.42	0.43	0.43	5.33	3.81
$r^\gamma(\{\Delta g\}_\mathcal{K})$	0.45	0.60	0.68	0.71	0.75	0.75	0.78	0.61	0.71
balancing energy (kWh)	5.82	4.39	3.56	3.10	2.86	2.79	2.66	4.81	3.56
cost $\{\bar{g}\}_\mathcal{K}$ (€)	<b>4.86</b>	5.48	5.87	6.29	6.68	6.84	6.96	5.40	6.24
cost $\{\Delta g(k)\}_\mathcal{K}$ $C1$ (€)	4.06	3.07	2.51	2.19	2.02	1.98	<b>1.90</b>	3.41	-
cost total $C1$ (€)	8.92	8.55	<b>8.38</b>	8.48	8.70	8.83	8.86	8.81	-
cost $\{\Delta g(k)\}_\mathcal{K}$ $C2$ (€)	27.77	19.86	16.56	14.46	13.53	13.43	<b>13.10</b>	-	17.51
cost total $C2$ (€)	30.36	25.34	22.42	20.75	20.21	20.27	<b>20.06</b>	-	23.39

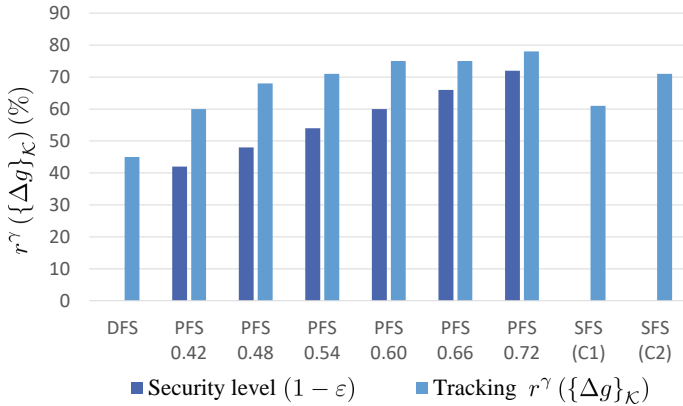


Figure 5.1: Simulation of a household: tracking of the DS, sorted by scheduling scheme.

into the grid. The detailed imbalances profile for three different cases over a week is depicted in Figure 5.2.

The DFS has the worst tracking performance. This can be noticed both from Figure 5.1 and Figure 5.2. The PFS, instead, always achieves the desired outcome of meeting the security level, i.e.  $r^\gamma(\{\Delta g\}_K) \geq (1 - \varepsilon)$ . Furthermore, the imbalances are such to include both positive and negative deviations from the schedule. In the SFS the tracking ratio depends on the pricing policy of the imbalances. This is aligned with the motivations behind the SFS, aiming at the best trade off between the DS cost and the expected cost of imbalances.

However, while the SFS achieves indeed a total cost lower than the one of the DFS, the minimum total cost is unexpectedly obtained by the PFS with an appropriate security level in both pricing policies *C1* and *C2*. This result is evident in Figure 5.3 on Page 124, which illustrates the average total cost achieved under different scheduling schemes decomposed in its schedule-dependent and its imbalance-dependent parts. Detailed costs are also reported in Table 5.1. Observing Figure 5.3, it can be inferred that en-

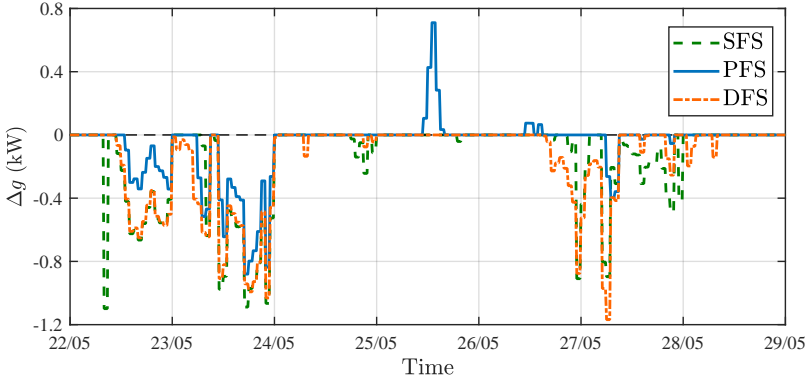


Figure 5.2: Simulation of a household: comparison of imbalances profiles over a simulated week. Cost case  $C1$ , PFS with  $(1 - \varepsilon) = 0.54$ .

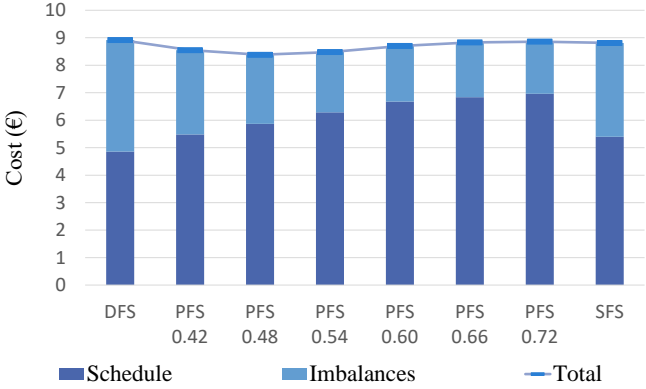
hancing the internal reserves raise the cost of the DS, while reducing the cost of imbalances. When the sole PFS is considered, these opposite tendencies result in a total cost varying with  $(1 - \varepsilon)$ . The value for  $(1 - \varepsilon)$  that achieves the minimum cost under policy  $C1$ ,  $(1 - \varepsilon) = 0.48$ , lays within the selected range. The explanation is rather simple: the increase in the cost of the DS caused by high values of  $(1 - \varepsilon)$  overcomes the savings attained by a higher reliability under this policy. Likewise, low values of  $(1 - \varepsilon)$  cause expensive imbalances that spoil the benefits deriving from a low-cost DS. In the case of policy  $C2$ , instead, the minimum cost is achieved by the highest security level, i.e.  $(1 - \varepsilon) = 0.72$ . In this case, the imbalances are so expensive in comparison to the cost of the DS that reducing them by raising the requirement on the security level is worth the increase in the cost of the DS. To conclude, the value of  $(1 - \varepsilon)$ , whenever not imposed by requirement, can be regarded as a schedule parameter, which regulates the total cost depending on the specific policy. Consequently, even if the proposed algorithm is designed to achieve a given security level and not to minimize the total cost, this latter scope can still be fulfilled with an appropriate tuning of  $(1 - \varepsilon)$ . Additionally, the PFS can reduce the total cost even further than

a SFS specifically designed for the purpose; Figure 5.3 indicates that this happens for both considered pricing policies,  $C1$  and  $C2$ . This phenomenon can be explained considering that the SFS has the limitations already discussed in Chapter 2 connected to the approximation of the uncertainty to a set of realizations. These limitations do not affect the PFS, where infinite possible realizations of  $\{l(k)\}_{\mathcal{K}}$  are considered without any assumption on an optimized redistribution of imbalances. Observe that the PFS does not obtain a lower cost than the SFS for each value of  $(1 - \varepsilon)$ , and that such a value (or range of values) differs with the pricing policies of the imbalances. The best  $(1 - \varepsilon)$  is thus circumstantial, a function of the pricing policy that is difficult to compute analytically. Nevertheless,  $(1 - \varepsilon)$  can be tuned on a specific case by means of simulation.

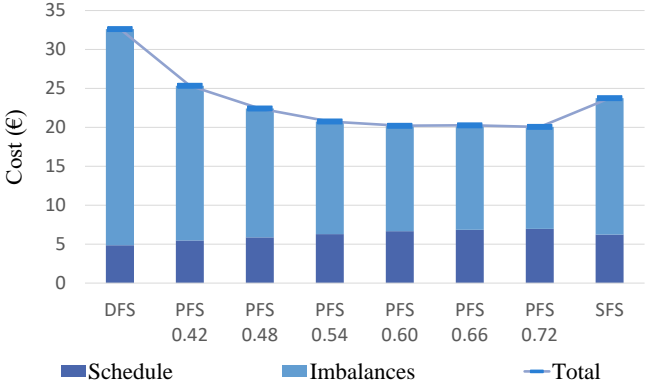
Figure 5.4 describes the profiles of the energy state for the different cases. Therein, it can be noticed that the PFS improves the allocation of energy reserve in comparison to the other methods, as it leads to a complete exploitation of the BESS capacity.

Finally, we report the power output profiles over the same week applying different scheduling procedures in Figure 5.5. There, the dotted line represents the baseline profile  $\{l(k)\}_{\mathcal{K}}$ , the dashed line represents the DS  $\{\tilde{g}\}_{\mathcal{K}}$ , and the full line the actual profile  $\{g(k)\}_{\mathcal{K}}$ . Even in this case one can see that while the DFS leads to the DS with minimum cost, this DS cannot be tracked as efficiently as the one computed using the PFS. In contrast, both the SFS and the PFS try to balance these two aspects, with PFS attaining a better behavior.

In conclusion, the PFS satisfies efficiently both requirements of limiting the number of imbalances and of minimizing the total operating cost. Additionally, the PFS outperforms the benchmark algorithms (DFS and SFS) under all the analyzed aspects of the case study.



(a) Imbalance pricing policy C1



(b) Imbalance pricing policy C2

Figure 5.3: Simulation of a household: average daily cost under different imbalance pricing policies, sorted by scheduling scheme.

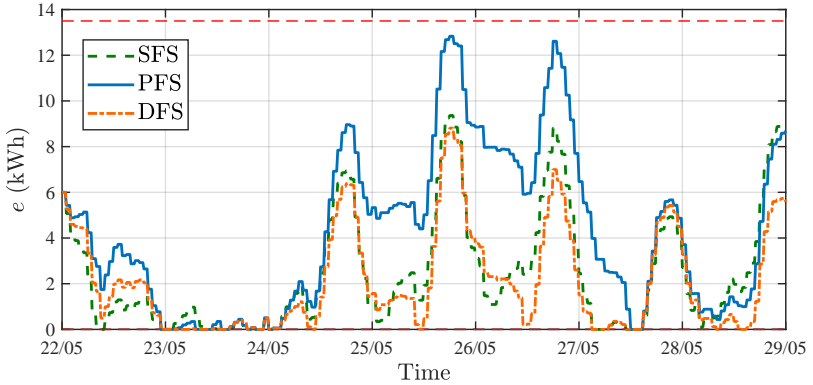
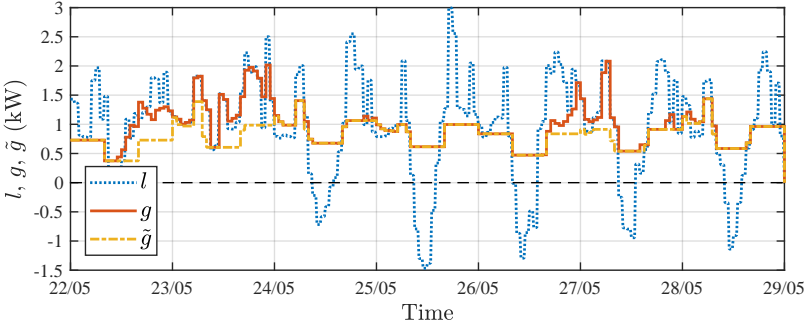


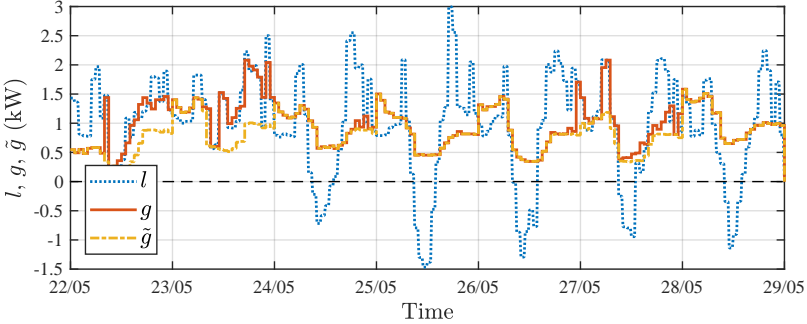
Figure 5.4: Simulation of a household: comparison of energy state profiles over a simulated week. Cost case  $C1$ , PFS with  $(1 - \varepsilon) = 0.54$ .

### 5.1.6 Summary

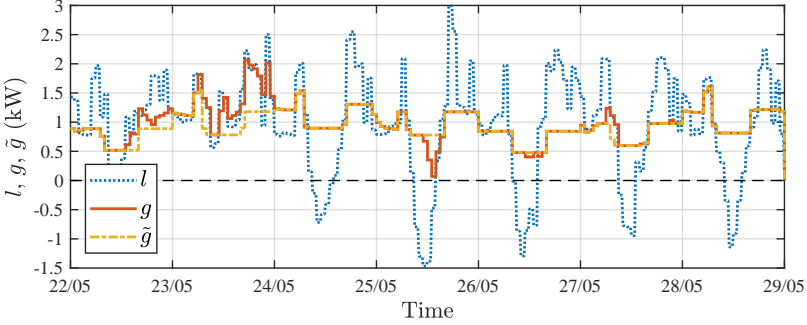
The results of the first case study show that the proposed PFS algorithm not only meets the desired requirements, but it performs better than state-of-the-art scheduling algorithms, too. This latter aspect is particular important in supporting one of the core-concepts of this thesis, i.e. the idea that an attentive handling of the uncertainty at the expense of some approximations in the mathematical description of the system and of its requirement can improve the overall scheduling performance in comparison to an opposite case (i.e. precise system and requirement modeling, uncertainties approximated by a set of realization). In fact, the PFS obtains better results than the SFS also under the aspects that are mostly affected by its approximations. While the SFS is expected to perform best cost-wise, because it accounts for the actual cost of schedule and imbalances, it is instead the PFS that obtains the lowest cost, despite the indirect consideration of the imbalance price. Motivated by these promising results, we carry on the analysis of the proposed scheduling algorithm by investigating its application to a larger, industrial-size setting.



(a) Deterministic forecast scheduling



(b) Scenario forecast scheduling



(c) Probabilistic forecast scheduling

Figure 5.5: Simulation of a household: power profiles of the inflexible load  $l$ , of the power exchange with the grid  $g$ , and of the DS  $\tilde{g}$  over a simulated week. Cost case  $C1$ , PFS with  $(1 - \varepsilon) = 0.54$ .

## 5.2 Case Study 2: Simulation of an Industrial Campus

The second case study in this Chapter concerns simulations of an industrial campus, using a realistic cost function for the DS based on the actual day-ahead prices in the German electric energy market. After assessing the goodness of the proposed scheduling algorithm against state-of-the-art schemes, we address different research questions in this section. Is the proposed algorithm scalable to large prosumption? Can it balance energy-arbitrage and reserve allocation with realistic prices? Which are the benefits of using external inputs in the forecasting process, e.g. weather information? Similar to the previous case, we first report the characteristics of the selected system, of the data, and of the tools employed in the simulations. Then, we report the results and comment on them.

### 5.2.1 Description of the Case Study

The case study involves an industrial-size campus, specifically the KIT campus north [Hagenmeyer *et al.*, 2016]. We consider a system composed of three elements: the aggregated electric load of a medium voltage substation serving office buildings and laboratories, a large-scale PV generator tracking its maximum power point, and a large-scale BESS. Even in this case, we consider a simplified model that lumps these three elements in one node, accounting solely for the exchange of active power at the interfaces with the high voltage transmission grid. The characteristics of the devices and all the data concerning consumption, generation, and weather are taken from on-site measurements. In detail, the load is the active power consumption at one of the medium-voltage substation of the distribution grid of the campus, with a yearly average value of 365 kW and peak consumption of 722 kW. The substation is serving office buildings, with a base load of about 350 kW. During the central hours of the day (working hours), the load increases

to ca. 600 kW or 700 kW of peak load. The PV data stems from the 1 MW peak PV plant of the campus, located at 49.1°N, 8.44°E. Practically, this data is obtained by scaling the measurements of an instrumented 10 kW peak PV array with an inclination of 30° and an orientation of -15°, for which weather information are available. The outcome of this choice is that we suppose as if the entire solar field face south-east, with the peak of production shifted towards the morning. The BESS is a Li-ion BESS with 1.5 MWh of usable capacity and it is capable of delivering a maximum of 1.8 MW of power. Regarding conversion losses, we consider a  $\mu = 0.1$  [Barry and Thomas, 2017]. We arbitrarily initialize the energy state of the BESS at the beginning of each simulated period (covering several days) to 750 kWh (storage half full).

As in the previous case-study, the scheduling should balance the use of the BESS between two opposite requirements. On one side, the BESS should maintain sufficient energy reserves (in terms of energy excess and available free storage) to compensate for forecast uncertainty in tracking the DS. On the other side, the available storage should be used for energy arbitrage. The tracking requirement translates in enforcing a minimum tracking ratio, cf. constraint (3.8), with values of  $(1 - \varepsilon)$  ranging from 0.50 to 0.80. This case study does not include a pricing scheme for the imbalances. Regarding the energy arbitrage, we consider the power exchange with the grid as priced (or rewarded) as in the German day-ahead energy market. We consider a DS of 24 hours with hourly time step, i.e.  $K = 24$  and  $\delta = 1\text{h}$ . The DS has to be computed at midday of the previous day,  $O = 12$ . Despite the market prices change day by day, there exists a daily trend. Figure 5.6 reports the average daily profile of the price for a time period with low energy prices (from 29 Apr 2018 to 12 May 2018) and for a time period with high energy prices (from 07 Oct 2018 to 20 Oct 2018).<sup>5</sup> While exhibiting different values,

---

<sup>5</sup> <https://www.epexspot.com/en/market-data/dayaheadauction>

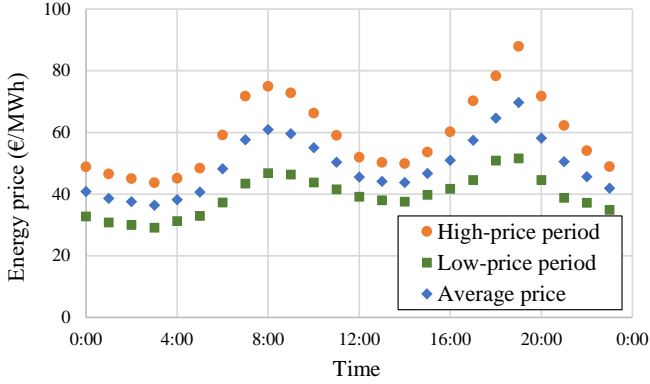


Figure 5.6: Trend of energy prices for a day in different time periods of 2018 at the EPEX day-ahead market (German market).

these two profiles follow the same trend, peaking at the same time of the day. Motivated by these observations, we consider a cost of the DS equal to

$$c^{\text{DS}}(\tilde{g}(k), k) = c^l(k)\tilde{g}(k). \quad (5.4)$$

Here, the time-varying cost coefficient  $c^l(k)$  equals a price of energy that averages the one of the high and of the low price period. This average price profile is also depicted in Figure 5.6.

## 5.2.2 Simulation Setup

The simulations cover four different periods of six days each, ranging from summer to autumn: six days in August, six days in September, six days in October and six days in November. For each case, we consider a range of values for  $(1 - \varepsilon)$ . As in the first case study, we run multiple calculation per each day to mimic the hierarchical scheme depicted in Figure 3.2. The DS is calculated once a day at 12:00, with a horizon extension of  $S = 6$ . The power outputs and the energy state are instead computed sequentially with higher granularity; specifically, we consider discrete time steps of 15 min-

utes each. The on-line rescheduling is performed every 15 minutes, using the information available at that point in time. The output of this optimization and the realization of the uncertain load/generation (with a 15-minutes resolution) contribute to the calculation of the energy state and of the power outputs, which are then used as starting point for the following iteration. The simulations are carried out in MATLAB, employing CasADi [Andersson, 2013] with the IPOPT [Wächter and Biegler, 2006]. All the computations have been performed using a PC with an Intel® Core™ i5-6400 CPU at 2.70 GHz and 8.00 GB RAM.

### 5.2.3 Forecasts

As in the previous cases, probabilistic forecasts for the sequences of inflexible power and energy over  $\mathcal{K}^a$ ,  $\{l\}_{\mathcal{K}^a}$  and  $\{e_l\}_{\mathcal{K}^a}$ , are required in the scheduling problem. Similar to the case study in Section 5.1, the total inflexible load  $l$  is divided into consumption and PV generation (modeled as negative load). The forecasts in terms of power are obtained using quantile regressions based either on polynomials with a maximum degree of two, in the case of consumption, or artificial neural networks (i.e. multi-layer perceptrons with six hidden neurons), in the case of PV generation [González Ordiano *et al.*, accepted]. The load forecasting models use information of the past month of load measurements as input. The PV generation models have as input the PV power generated over the last 24 hours and the corresponding weather forecasts, which use in turn solar irradiation and temperature forecast data from the GFS model<sup>6</sup> (as in [Barry and Thomas, 2017]). The forecasts in terms of energy are created based on the power forecasts as in Section 5.1.3. Finally, the forecasts of the total aggregated load  $l$  in terms of power and energy are obtained by combining the PV generation and load forecasts via a convolution operation for each time step. Note that the use of weather inputs reduces the uncertainty affecting the forecasts in compar-

---

<sup>6</sup> Available: <ftp://ftp.ncep.noaa.gov/pub/data/nccf/com/gfs/prod/>.

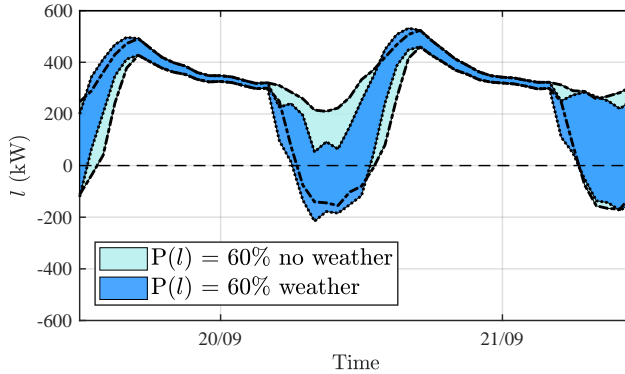


Figure 5.7: Comparison of probabilistic forecasts for a campus load (consumption + PV generation) with and without weather input.

ison to a purely auto-regressive forecast. This can be observed in Figure 5.7, which illustrates the probabilistic forecasts of  $L$  used for scheduling of a given day with and without the consideration of the weather input.

## 5.2.4 Results

Figure 5.9a on Page 135 depicts the power profiles of  $l(k)$ ,  $g(k)$  and  $\tilde{g}(k)$  over the September days for a  $(1 - \varepsilon) = 0.7$ . The DS profile shows that the scheduling algorithm balances between using the storage as a reserve and using it for energy arbitrage. On days with higher production (and, therefore, higher volatility), such as 24 Sep 2018, the DS  $\tilde{g}(k)$  follows the profile of  $l(k)$ : the BESS capacity is used almost entirely as reserve because of the high uncertainty. On days with lower production, instead, such as 22 Sep 2018, the BESS is used also for energy arbitrage: the system purchases additional energy during the price minimum in the early morning and resells it around the morning price peak.<sup>7</sup> This behavior can be observed also in Figure 5.9b on Page 135, representing the trend of the energy state of the

<sup>7</sup> The morning price minimum is around 4:00, while the morning price peak occurs at 8:00, see Figure 5.6.

BESS. Therein, the morning energy arbitrage assume the form of a peak in the energy state, mostly evident on 22 Sep 2018.

Why does this energy arbitrage occur only in the morning? One has to consider that the uncertainty on the energy forecasts grows in time and that the DS has to be computed at 12:00 of the day before. Observe from Figure 5.7 that the PV generation is the main source of uncertainty. Despite the use of weather information in forecasting, the uncertainty affecting the energy forecasts in the period of interest (from midnight to midnight) remains quite high, especially at the end of the scheduling period. Specifically, the possible energy states span intervals in the order of 5 MWh around midnight of the following day. The uncertainty becomes so high that it can be hardly compensated even when using the storage only as a reserve. Consequently, the further in the future the DS is planned, the lower becomes the possibility of using the storage for energy arbitrage while guaranteeing the required tracking at the same time. These results indicates that the scheduling horizon can be directly linked to a cost of reserves.

For similar reasons, the use of the storage for energy arbitrage is increased in months with low generation, for example November. This can be observed in Figure 5.10a on Page 136, which shows results that are conceptually equivalent to the ones of Figure 5.9a, but for a November week. The cause of the additional energy arbitrage can be found in the relatively low solar generation in this period, resulting in a lower uncertainty compared to the summer case and, consequently, in a greater amount of the BESS storage capacity that can be used for energy arbitrage. Alternatively, the scheduler can be influenced towards energy arbitrage by selecting lower  $(1 - \varepsilon)$ . For an extreme comparison, we report in Figure 5.11 on Page 137 the same type of data of Figure 5.9, but for a  $(1 - \varepsilon) = 0.4$ . An increased used of the available capacity for energy arbitrage—at the cost of numerous imbalances—is evident (note that the power profiles in 5.11 are reported in MW, and not in kW as in the previous figures).

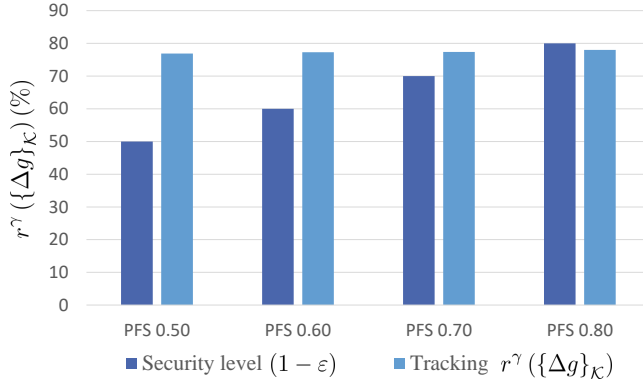


Figure 5.8: Simulation of an industrial campus: tracking of the DS with different values of  $(1 - \varepsilon)$ .

The influence of  $(1 - \varepsilon)$  on the amount of imbalances can be observed in Figure 5.8 and in Table 5.2, reporting the average daily values of  $r^\gamma(\{\Delta g\}_K)$  for different choices of  $(1 - \varepsilon)$ . Note that constraint (3.8)— $r^\gamma(\{\Delta g\}_K) \geq (1 - \varepsilon)$ —is satisfied for  $(1 - \varepsilon)$  ranging from 0.50 to 0.70, implying that the tracking requirement is achieved. That is not the case for a  $(1 - \varepsilon) = 0.80$ . As already mentioned, the storage capacity of the BESS is small relatively to the uncertainty affecting the forecasts of the inflexible power output. Therefore, arbitrary values of  $r^\gamma(\{\Delta g\}_K)$  cannot be reached: over a certain value of  $(1 - \varepsilon)$ , the scheduling algorithm can only pursue the DS that can be tracked with the highest probability. This is also the probable cause of the small increment of  $r^\gamma(\{\Delta g\}_K)$  with increasing  $(1 - \varepsilon)$ . This example illustrates the importance of the constraint softening presented in Section 3.3.2. Assessing a-priori the feasibility of a given value of  $(1 - \varepsilon)$  is difficult, because it depends on the forecast uncertainty, which varies daily. Without constraint softening, the scheduling problem would fail in computing a DS each time the selected  $(1 - \varepsilon)$  is unfeasible, and this would compromise the robustness of the scheduling and control scheme.

Table 5.2: Simulation of an industrial campus results.

$(1 - \varepsilon)$	0.50	0.60	0.70	0.80
$r^\gamma(\{\Delta g\}_{\mathcal{K}})$	0.769	0.773	0.774	0.780
$c^{\text{DS,p}}(\{\tilde{g}\}_{\mathcal{K}}) (\text{€})$	-56.14	-56.95	-56.99	-61.46

Table 5.2 details also the values of  $c^{\text{DS}}(\{\tilde{g}\}_{\mathcal{K}})$  with varying  $(1 - \varepsilon)$ . As already mentioned, higher values of  $(1 - \varepsilon)$  imply higher costs of the DS. This is caused by a reduced energy arbitrage in favor of choices for  $\{\tilde{g}\}_{\mathcal{K}}$  that are more conservative and thus able to achieve higher  $r^\gamma(\{\Delta g\}_{\mathcal{K}})$ .

### 5.2.5 Summary

This second case study points out an interesting aspect connected to the increase of large-scale generation from renewable energy sources. While the uncertainty affecting the forecasts of a “traditional” large-scale load (e.g. power absorbed at a medium voltage substation of an industrial campus) is small relatively to the expected load, the uncertainty affecting the forecasts of PV generation grows with the dimension of the generator to a considerable percentage of the expected value—even when weather inputs are considered. In fact, the large-scale load is composed of many, uncoordinated small loads, whose deviation from expectation can take opposite direction, balancing out when only the total load is considered. On the contrary, large-scale uncontrolled PV generation is composed of small generators that behave similarly, because subject to the same weather condition. Consequently, dispatching PV generation robustly over a day-long time period requires larger energy reserves in comparison with the case of “traditional” load, especially towards the end of the DS. The results presented in this section show that the proposed scheduling algorithm can efficiently cope with this challenge. First, it can balance using the BESS for both

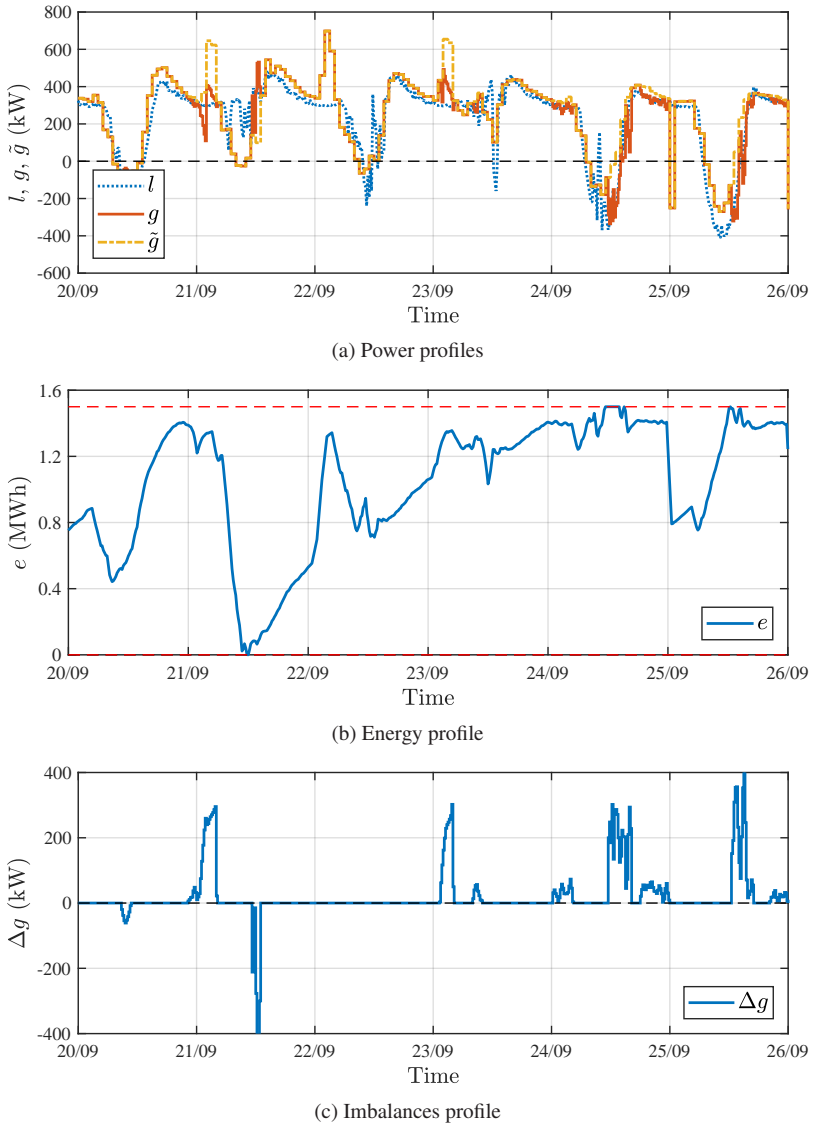
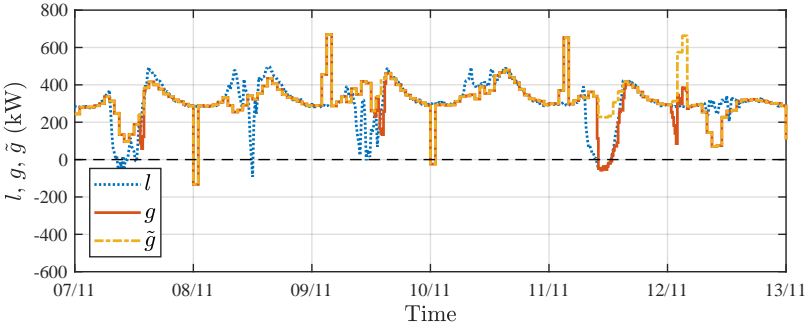
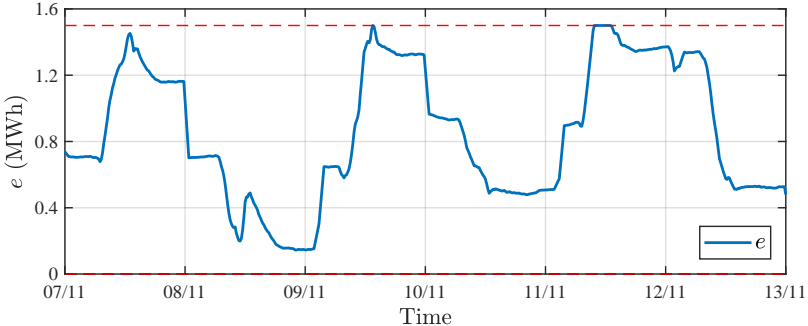


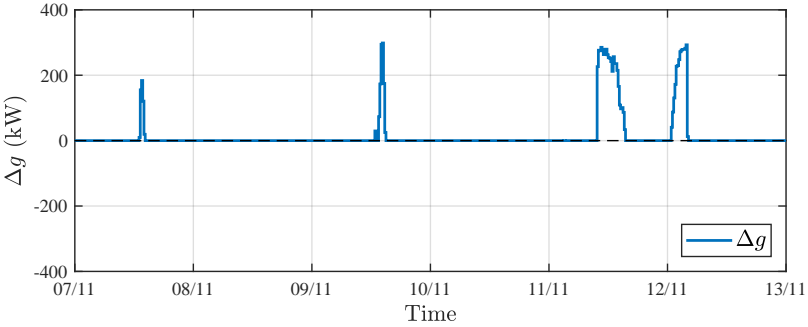
Figure 5.9: Simulation of an industrial campus: power and energy profiles over a simulated week in September 2018 with  $(1 - \varepsilon) = 0.70$ .



(a) Power profiles



(b) Energy profile



(c) Imbalances profile

Figure 5.10: Simulation of an industrial campus: power and energy profiles over a simulated week in November 2018 with  $(1 - \epsilon) = 0.70$ .

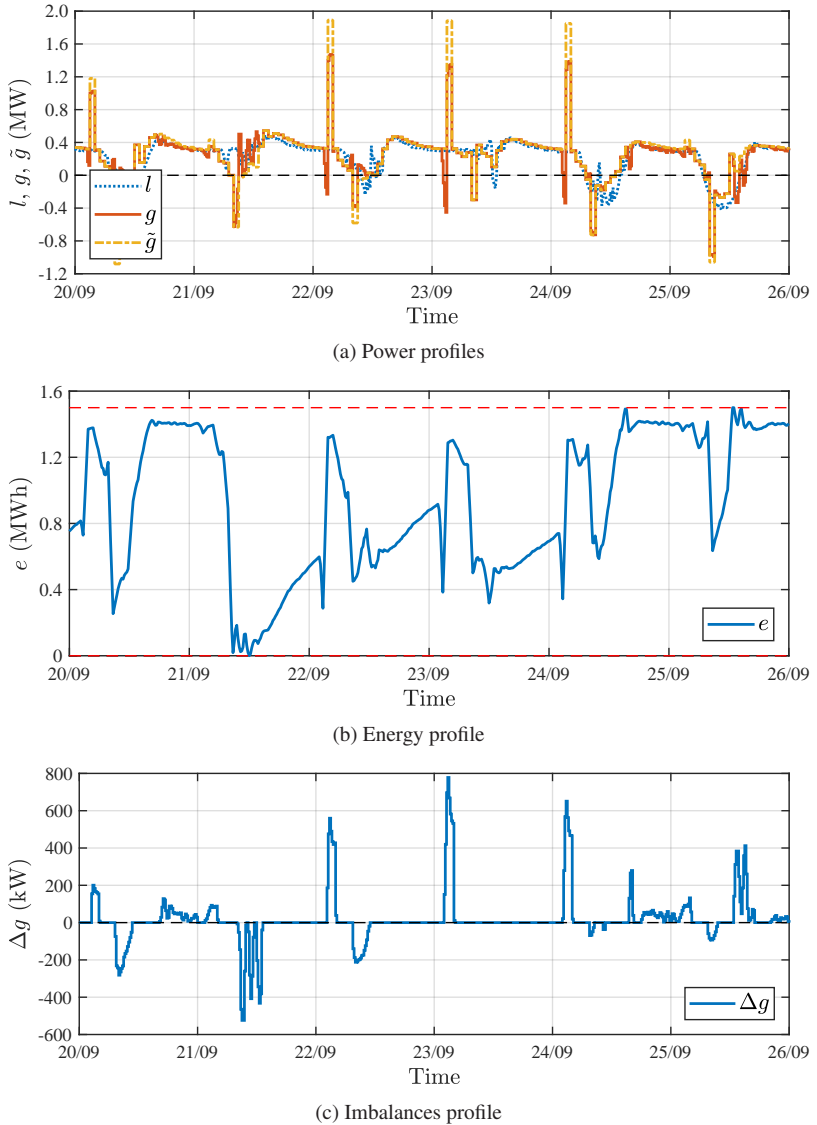


Figure 5.11: Simulation of an industrial campus: power and energy profiles over a simulated week in September 2018 with  $(1 - \epsilon) = 0.40$ .

energy-arbitrage and reserve provision, adapting to the growing uncertainty during the day. Second, it can respond to the degree of robustness desired by the user. Finally, it can deal with security levels that are higher than what practically allowed by the forecast uncertainty without running into scheduling failures.

After having assessed the potential of the proposed scheduling algorithm by simulation, it is left to research whether the response of a real-life system would be aligned with simulation. We tackle this research question in the next section, where an experimental application of the proposed scheduling is presented.

### **5.3 Case Study 3: Experimental Dispatch of Solar Generation**

The third case study compares simulation results to experimental measurements. The experiment allows evaluation of two aspects that are neglected in simulation: an accurate model of storage losses and the intra-step fluctuation of PV generation. In the following, we first describe the considered system, then we report and comment on the results.

#### **5.3.1 Description of the Case Study**

Similar to the case study presented in Section 5.2, we utilize some equipment allocated at the KIT campus north [Hagenmeyer *et al.*, 2016]. As in the previous case, we model the hardware assuming a single bus bar and we target dispatch-as-scheduled of the total active power output of the system. However, we consider in this case a system composed only of uncertain PV generation and a BESS. The power exchange with the external grid is not directly measured, but rather calculated by summing the power output of the generator and of the BESS. The PV generator is the same instrumented 10 kW peak PV array described in Section 5.2.1; no scaling has been applied in

this case. The BESS is Li-ion with a capacity of 25 kWh; we constrain the energy state to remain between  $\underline{e} = 5\text{kWh}$  and  $\bar{e} = 22.5\text{kWh}$  to reduce aging of the battery [Keil *et al.*, 2016].<sup>8</sup> The BESS interfaces with the AC grid via a DC/AC converter with a power output adjustable in the range between  $\underline{p} = -30\text{kW}$  and  $\bar{p} = 30\text{kW}$ . A low level controller is in place to track the reference power  $g_{\text{ref}}$ , as described in Section 3.2. Further information on the implemented controller can be found in [Barry and Thomas, 2017]. The measurements of both the PV generation and the power output of the BESS have a sampling time of 500 ms.

The scheduling requirements are as in Section 5.2.1. The tracking requirement imposes a security level  $(1 - \varepsilon) = 0.70$ , with no explicit consideration of an imbalance price. The revenues coming from the dispatched power follows the day-ahead pricing scheme described in Section 5.2.1, with hourly prices varying as depicted in Figure 5.6 on Page 129. We perform online rescheduling every 15 minutes, as described in Section 3.4.

It has to be mentioned that the equipment used in the experiment has been designed as a pilot project aiming at a different scope than schedule compliance. In particular, the converter is designed to deliver high power and it is highly inefficient when working within a relatively low power range—which is the case when tracking the schedule. Figure 5.12 depicts the efficiency of the AC/DC conversion for battery charging.<sup>9</sup> We have estimated, from previous prototypical implementations, that the round trip efficiency of the BESS is of about 60% ( $\mu = 0.2$ ) when controlled to track a typical DS. Furthermore, the converter cannot deliver power in the range  $0\text{kW} \leq p \leq 1\text{kW}$ , and in the range  $-1\text{kW} \leq p \leq 0\text{kW}$ . Therefore, whenever the difference between the DS and the actual power output is lower than 1 kW (in absolute value), the schedule cannot be tracked. To summarize, while the installed

<sup>8</sup> These bounds have been suggested by the operators of the battery.

<sup>9</sup> We maintain in Figure 5.12 the original sign convention from [Barry and Thomas, 2017], which is opposite to the one utilized in the present thesis.

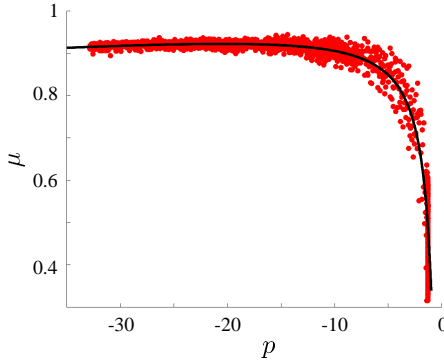


Figure 5.12: Conversion efficiency of the AC/DC conversion for battery charging; adapted from [Barry and Thomas, 2017].

converter enables a control targeting schedule compliance, it is highly inefficient and incapable of precise tracking.

### 5.3.2 Implementation Aspects

#### Measurements of the Energy State

The proposed algorithm relies on the measurement of the energy state  $e$ , which is used as a feedback for the online rescheduling (see Figure 3.2). Furthermore, measurements of this value are needed to evaluate the results. However, this quantity is not directly accessible. In the literature there exists a large body of work addressing the problem of estimating this value from directly measurable quantities (e.g. voltage and current at the terminals of the battery), but the investigation is still ongoing, see [Li *et al.*, 2017] and references therein. In the present work, we employ a simple technique based on the estimation of the State Of Charge (SOC), which is provided by the battery manufacturer. We performed charging and discharging cycles from  $\text{SOC} = 5\%$  to  $\text{SOC} = 95\%$  at constant power for different power levels. For each cycle, we measured the power exchanged with the battery on the DC side of the storage converter (so to exclude the conversion losses from

the measure), and use this measurement to estimate the energy state of the BESS. This way, we could associate a SOC to a correspondent energy state for each charging and discharging process, allowing creation of a lookup table that allows the energy state to be estimated from the available SOC information. Note that different energy states may correspond to the same SOC, depending on the redistribution of charges within this storage. This redistribution is influenced by the charging/discharging profile and implies a spread of energy states mapping to the same SOC that grows with the SOC itself up to more than 1kWh. We considered the average energy state in this range in the creation of the lookup table.

### Unusable Operating Region

The equipment utilized in this case study requires further elaboration of the scheduling problem (3.38). In particular, given the impossibility of operating the BESS within the ranges  $0\text{kW} \leq p \leq 1\text{kW}$  and  $-1\text{kW} \leq p \leq 0\text{kW}$ , we modify the storage constraint such that at least the expected power output of the storage  $\hat{p}$  lays outside this interval. This does not ensure that  $p$  will remain outside of this range, but it can simplify the operation of the system.

To this end, we substitute (3.33b), (3.33c) and (3.33d) in  $\mathcal{F}'_d(\hat{p}(k))$  with

$$z(k)\bar{p}(k) \geq \hat{p}^+(k) \geq z(k), \quad (5.5a)$$

$$(-1 + z(k)) \geq \hat{p}^-(k) \geq (1 - z(k))\underline{p}(k), \quad (5.5b)$$

$$z(k) \in \{0, 1\}. \quad (5.5c)$$

Adding the binary decision variable  $z(k)$  renders the scheduling problem a mixed-integer non-linear program, which is not easy to solve [Trespalcios and Grossmann, 2014]. Furthermore, (5.5) does not allow  $\hat{p} = 0$ . Thus, we first solve (3.38) without the constraint substitution detailed in (5.5). Then, we set up the scheduling problem comprising the decision integer

variable  $z(k)$ , initializing  $z(k) = 1$  whenever the solution of Problem (3.38) indicates a positive  $\hat{p}$ , and  $z(k) = 0$  otherwise. Additionally, we neglect (5.5) and force  $\hat{p} = 0$  whenever the solution of Problem (3.38) indicates a  $-1\text{kW} \leq \hat{p} \leq 1\text{kW}$  in the range between -1 kW and 1 kW.

## Forecasts

The forecasting models for both offline scheduling and online re-scheduling are created as described in Section 5.2.1.

### 5.3.3 Simulation and Experimental Setup

First, we simulate the behavior of the considered system under the scheduling and control scheme proposed in Chapter 3 as in Section 5.2.2 for the time period from 18 Sep 2018 to 22 Sep 2018. In particular, we consider a discrete-time setting with  $\delta = 0.25\text{h}$ , and compute the energy state according to (3.1).<sup>10</sup> Then, we observe the behavior of the experimental system over the same time period, with the same scheduling and control scheme. The only difference with the simulation is that, instead of computing  $e(k+1)$  starting from  $g_{\text{ref}}(k)$ ,  $l(k)$ , and  $e(k)$  using the simplified model (3.9) and (3.1), the signals are sent to the actual equipment and  $e(k+1)$  can be estimated as described in Section 5.3.2. In other words, we utilize the BESS within a hardware-in-the-loop framework. Note that the chosen time period involves a range of meteorological conditions. This way, we can observe the response of the controlled system in different situations, including both clear sky and cloudy days. The optimization problems are solved in MATLAB, using CasADi [Andersson, 2013] with IPOPT [Wächter and Biegler, 2006] for the non-linear program and quadratic program, and with Bonmin [Bonami *et al.*, 2008] for the mixed-integer non-linear program.

---

<sup>10</sup> Given the linear model used to approximate the conversion losses in (3.1), simulating the behavior of the system between two subsequent rescheduling events is meaningless, because it would give the same results of the average model at the sampled times.

### 5.3.4 Results

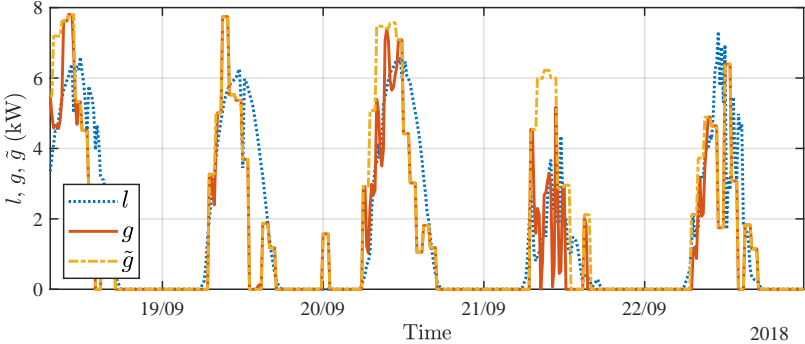
We divide the analysis of the results in two parts. In the first part, we compare the results of the experiment to the ones of the simulation. In the second part, we take a closer look to the experimental results.

#### Comparing Simulation and Experiment

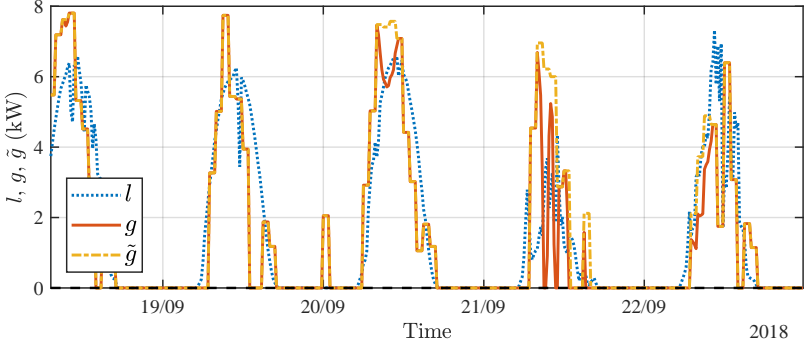
In this section, we compare experimental and simulation results. For the sake of a fair comparison, we consider  $\delta = 0.25$  h in both cases. Similarly to previous sections, Figure 5.13 reports the profiles of  $l$ ,  $g_{\text{ref}}$ , and  $\tilde{g}$  obtained both in experiment and in simulation. We compare two aspects: the DS, and the imbalances.

First, we discuss the DS. From comparative observation of Figures 5.13a and 5.13b, it can be seen that the profiles for  $\tilde{g}$  obtained in the experiment are similar to the ones obtained in simulation. To quantify this aspect, we calculate the revenues of the DS as in Section 5.3, using (5.4) and the time-varying price depicted in Figure 5.6. The total revenues over the considered time periods are of 2.02 € in the simulation and of 2.00 € in the experiment, i.e. the experimental revenues are 99 % of the simulation revenues. From this we can deduce that the simulation provides a good estimation of the revenues that can be achieved in practice.

The case of the imbalances is slightly different. Figure 5.14 depicts the imbalance profiles over the considered time period, both for the experiment and for the simulation. These imbalances have been computed comparing the reference signal  $g_{\text{ref}}$  resulting from online rescheduling and the DS  $\tilde{g}$  at the same time step. In this context, we assume perfect tracking of  $g_{\text{ref}}$  both in the simulation and in the experiment. We comment on further tracking errors observed in the experiment in the next section. Both experiment and simulation indicate that the desired tracking ratio of  $r^\gamma(\{\Delta g\}_{\mathcal{K}}) = 70\%$  is obtained and exceeded, with a  $r^\gamma(\{\Delta g\}_{\mathcal{K}}) = 90\%$  in the simulation and of  $r^\gamma(\{\Delta g\}_{\mathcal{K}}) = 86\%$  in the experiment. However, the tracking ratio in the



(a) Experimental results



(b) Simulation Results

Figure 5.13: Experimental dispatching: power profiles of the inflexible load  $l$ , of the power exchange with the grid  $g$ , and of the DS  $\tilde{g}$ .

experiment is 4% lower than what expected from simulation. Figure 5.14 indicates that the imbalance profiles are similar in cloudy days (e.g. the 21 Sep 2018), but they differ in clear sky days (e.g. the 20 Sep 2018). In this latter case, the imbalances are more numerous and more severe in the experiment (denoted with superscript ER) than in the simulation (denoted with superscript SR). The reason is that in these days the online rescheduling plans deviations from the DS more often than expected in simulation, because of a mismatch between the model of a BESS utilized in simulation, and the behavior of the real system. This mismatch can be imputed to multiple causes. At a first glance, the fact that the experimental energy state is almost always lower than the simulated one seems to indicate an underestimation of conversion losses. This effect can be attenuated by increasing  $\mu$  or by adding a corrective term to (3.1). However, this mismatch should be mostly imputed to an erroneous estimation of the energy state itself. In fact, it can be observed that, on the one hand, the experimental energy state deviates from the simulated one whenever the storage discharge but, on the other hand, the experimental energy state returns to the simulated value during charging. It is as if the error made in estimating the energy state during discharging is compensated during charging. Thus, an improved method to estimate the energy state would probably reduce the mismatch between the simulated and the experimental profiles.

Online rescheduling is able to correct the errors in the storage model and thus maintains the energy state within the required bounds, at the cost of imbalances. This is shown in Figure 5.15, depicting the energy state profiles in the experiment and in the simulation. One can observe that even if the two profiles diverge from time to time, the experimental profile remains almost always above the lower bound of 5 kW. Nonetheless, forecasting errors at the rescheduling stage may cause slight constraint violation in both the experiment and in the simulation. This is evident in the late evening of 21 Sep 2018. Note that—because of the already discussed model mismatch—the fluctuations of the energy state measured experimentally are more severe

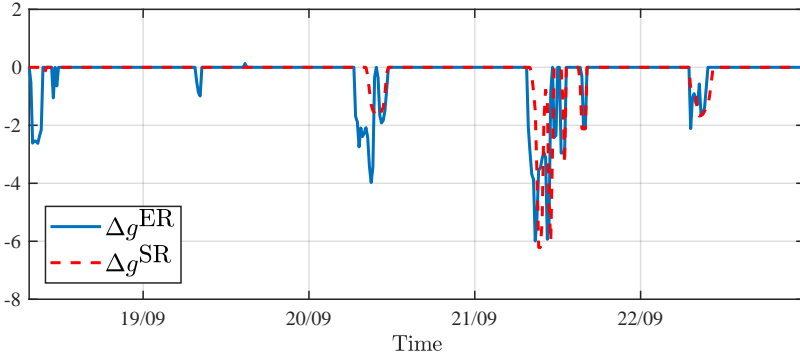


Figure 5.14: Experimental dispatching: imbalances profiles, comparison of simulation and experimental results.

than the ones seen in simulation. Furthermore, the BESS is set up to turn off after sunset whenever  $\tilde{g} = 0$ . Thus, after the last violation of the energy constraint on the evening of 21 Sep 2018 caused by forecasting errors, the online rescheduling is able to bring the energy state above the required lower bound only on the following morning. To summarize, the ER point out the need for some corrections in the implemented control system. First, an increase in the frequency of rescheduling would reduce the impact of forecasting errors, avoiding constraint violation. Second, the system should be turned off at night only if  $\tilde{g} = 0$  and the energy state is within the desired bounds.

To conclude, the experimental results show that a simulation may underestimate the amount and severity of imbalances that would occur in reality, particularly in clear-sky days. However, this underestimation is mild (4%) and the required tracking ratio is also reached in the experimental setting. Regarding the DS, the experimental results are aligned with the simulation results. Overall, the experimental results confirm the properties of the method observed in simulation. However, further experiments on different

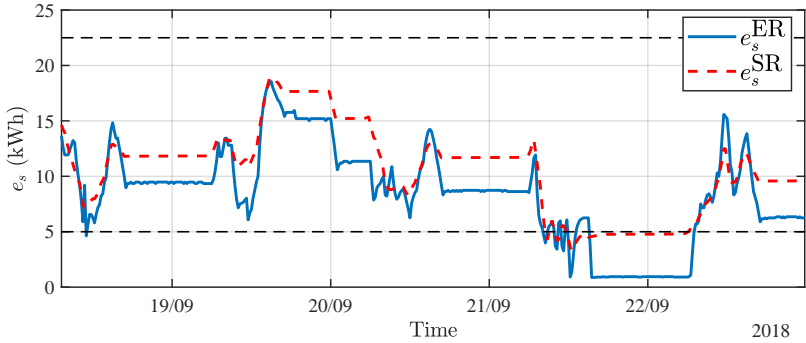


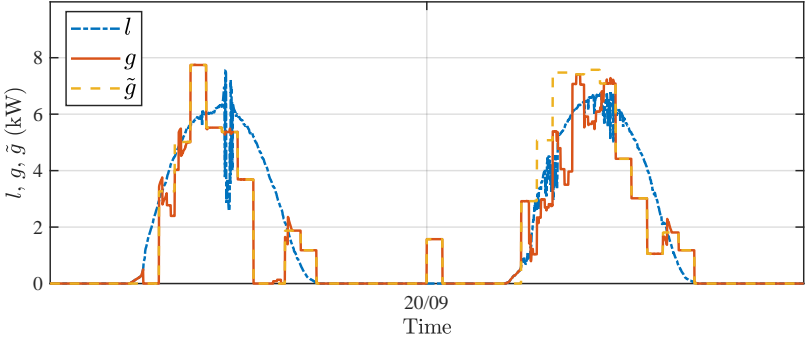
Figure 5.15: Experimental dispatching: stored energy profiles, comparison of simulation and experimental results.

systems (purposely designed for schedule compliance) would be beneficial to confirm this trend.

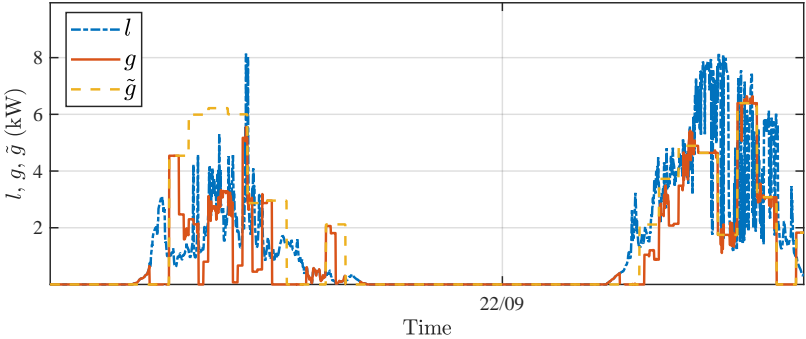
### Experimental Profiles

In this section, we report and comment on the experimental results with a sampling period of 1 minute. Figure 5.16 reports the power profile; this figure is equivalent to Figure 5.13a with a higher resolution. Figure 5.16, and in particular Figure 5.16b, illustrates that the fast fluctuations in the PV generation are almost entirely averaged out by the BESS, which is one of the main benefits of the proposed control strategy for the external grid. Note that this effect is independent from the imbalances: the BESS counterbalances the fluctuations of the PV generator even when deviations from the DS are planned.

Figure 5.16 also illustrates the limits of the used equipment: the BESS fails in providing accurate tracking every time the difference between  $\tilde{g}$  and  $l$  is smaller than 1 kW in absolute value. For the sake of completeness, we report the SOC profile with sampling period of 1 minute in Figure 5.17.



(a) Sunny days



(b) Cloudy days

Figure 5.16: Experimental dispatching: power profiles of the inflexible load  $l$ , of the power exchange with the grid  $g$ , and of the DS  $\tilde{g}$ , sampling period of 1 minute.

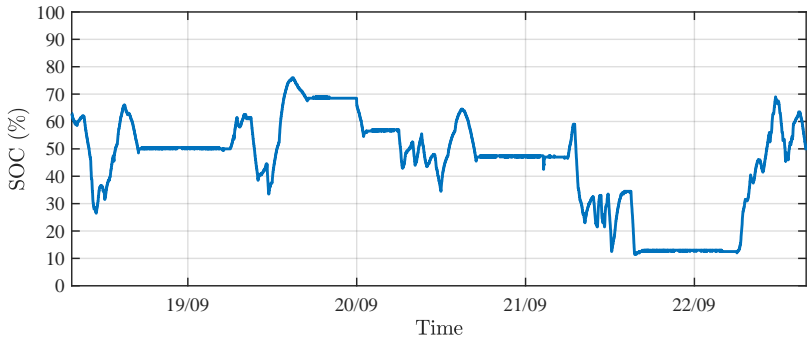


Figure 5.17: Experimental dispatching: state of charge profile, sampling period of 1 minute

### 5.3.5 Summary

This third case study corroborates the findings discussed in the previous sections by means of real-life measurements on an experimental set up. In particular, we compare simulation and experimental results on a dispatchable solar generator. The comparison indicates that the simulations are accurate in reproducing the DS that would be computed in real-life. At the same time, it shows that the simplified storage model used in simulation and the difficulties of evaluating the energy state of the BESS may cause an underestimation of the number and of the severity of imbalances. However, this underestimation is mild and does not compromise previous findings. The experimental results also indicate that the online rescheduling should be performed frequently enough to avoid forecasting errors to cause the violation of any constraint. Last, the proposed hierarchical control strategy is able to counterbalance locally the volatility of solar generation, thus lowering the power balancing burden on the external grid.

## 5.4 Summary

In this chapter, we analyze the performance of the scheduling algorithm proposed in Chapter 3 in different settings, both by means of simulations and of real-life experiments. The results indicate that the proposed scheme can cope with the system requirements, that it can achieve better revenues/costs in comparison with state-of-the-art scheduling based on sampling and scenario forecasts, and that it is applicable to real systems independently of their scale. However, all the analyzed cases included only one EC-DER with time-invariant power and energy constraints (specifically, a single BESS). The case study examined in the next chapter overcomes this restriction, investigating the effects of the proposed scheduling algorithm on a system comprising a population of EC-DER changing over time.

## 6 Case Study on a Population of EC-DERs

The case study presented in this chapter extends the analysis of the proposed scheduling algorithm to multiple EC-DERs. The purpose is to provide an example of how the algorithm presented in Chapter 3 can be applied to multiple EC-DERs by using the findings on aggregated models described in Chapter 4. The specific system considered here groups together a BESS, PEVs, and inflexible and volatile PV generation into what we define a DCS. The idea behind a DCS is to use the storage provided by both the BESS and the PEVs to dispatch the active power exchange between an external power network and the group of devices comprised in the station itself. Computation of a day-ahead DS for a DCS is a challenging problem that requires consideration not only of multiple storage devices, but also of multiple sources of uncertainties. In particular, the uncertainty affecting the connection of PEVs should be regarded in addition to the uncertainty of the forecasts of the power output of the PV generator. The ideas presented in this section have appeared in [Appino *et al.*, 2018c].

### 6.1 General Modeling of a Dispatchable Charging Station

#### 6.1.1 Device Models

The considered DCS is composed of a charging station for PEVs, a BESS and a generator exploiting intermittent renewable energy sources, such as a PV generator. All the devices are connected to the same bus, as depicted

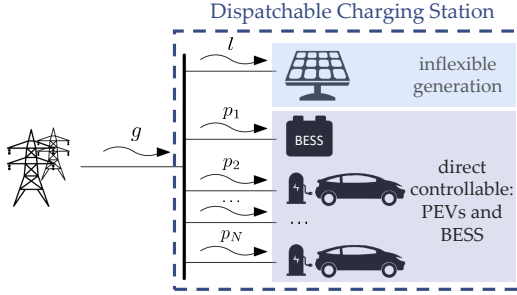


Figure 6.1: Schematic diagram of a DCS.

with a scheme in Figure 6.1. The connections are assumed lossless and such that the system components can exchange power mutually without any technical restriction. Note that the number of connected PEVs might vary over time. As in the previous chapters,  $g(k)$  denotes the power exchange with the main grid,  $l(k)$  the aggregated power output from uncontrollable generation, and  $p_j(k)$  the power output of the  $j$ -th controllable device. The sign convention is the same for all power variables, with positive power flow directed as depicted in Figure 6.1. Following the notation introduced in Chapter 4, we denote the index set of devices connecting to the DCS over  $\mathcal{K}$  with  $\mathcal{N}_{\mathcal{K}}$ , where index 1 corresponds to the BESS and the remaining indexes to the PEVs.

The dynamics and constraints of each device follow (4.37) and (4.2). For the sake of simplicity, we assume that the BESS and all the PEVs are subject to the same efficiency  $\mu_1 = \dots = \mu_N = \mu$ . The capability and capacity limits of the devices are time-invariant, and such to satisfy Assumptions 1 and 2.

Regarding the system parameters, we account for two sources of uncertainty (as in Section 4.8.2): the inflexible power output  $\{l\}_{\mathcal{K}}$ , and the energy state of the  $v$ -th PEV at  $k_v^a$ ,  $e_v(k_v^a)$  for all  $v \in \{\mathcal{N}_{\mathcal{K}} \setminus \{1\}\}$ . We consider

the remaining characteristics of each  $v$ -th PEV— $\bar{p}_v, \underline{p}_v, \bar{e}_v, \underline{e}_v, e_v^{\min}, k_v^a$ , and  $k_v^d$ —as known.<sup>1</sup>

## 6.1.2 Requirements

The scheduling and control scheme tested in the present chapter aims at *dispatch-as-scheduled* of the power exchange  $g(k)$ , with the aid of a coordinated and collaborative control of the system components. Thus, the DCS has the same requirements of the system presented in Chapter 4, with the addition of a further requirement on the energy state of the PEVs.

Regarding the requirement on the power exchange  $g(k)$ , operating revenues (or costs) can be directly associated to the DS through a cost function  $c^{\text{DS}}(\tilde{g}(k), k)$ , see (3.5), while imbalances are penalized in operation and/or limited by regulation, see (3.6) and (3.7).

Additionally, scheduling for the DCS should account for the charging requests of each PEV. We suppose that, upon departure, the energy state of each  $v$ -th PEV ( $v \in \{\mathcal{N}_{\mathcal{K}} \setminus \{1\}\}$ ) should have reached at least a minimum threshold  $e_v^{\min}$ . We model this requirement by modifying the constraints of each  $v$ -th PEV at  $k_v^d$  to

$$e_v^{\min} \leq e_v(k_v^d) \leq \bar{e}_v. \quad (6.1)$$

Note that, as in [Kou *et al.*, 2016], we consider a setting without any operating revenues proportional to the power exchanged with the PEVs. Although possible, charging the battery of the  $v$ -th PEV beyond  $e_v^{\min}$  would not yield any additional revenue, with the only (practically rare) exception of negative

<sup>1</sup> It may seem that this is an unrealistic modeling choice. However, it is reasonable in several cases. A trivial example is given by a setting in which the PEVs declare their intended arrival and departure times on the day before. A second case can be found in parking lots of office buildings, where the variance on  $k_v^a$ , and  $k_v^d$  is generally smaller than an hour [Sarabi *et al.*, 2016]. With respect to the DCS, if the variance on  $k_v^a$  and  $k_v^d$  is of the same order of the duration of the dispatch intervals  $\delta$ , the arrival and departure times of a PEV could be considered as certain. Last, worst case estimates can be used if these considerations do not apply.

costs for acquiring power from the grid. Additionally, we avoid modeling that certain energy states or charging profiles should be preferred over others to avoid deteriorating the battery health. Such phenomena are still under discussion, see [Schwenk *et al.*, 2019]. Therefore, their consideration is left to future works. Summing up, the requirements on the charging of PEVs are such to provide flexibility to balance uncertainty in two different manners: i) flexibility in regulating the charging profile over the parking period, and ii) flexibility in the energy state of a PEV upon departure.

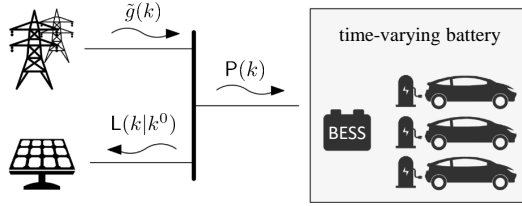
## 6.2 Three-stage Scheduling and Operation

Following the framework presented in Chapters 3 and 4, and similarly to [Vandael *et al.*, 2013], we undertake the scheduling and operation of a DCS in *three* subsequent decision stages. A separate optimization is conducted at each stage depending on a stage-specific model. This three-stage structure extends the hierarchical scheduling and control scheme depicted in Figure 3.2, adding the aggregation and dispersion phases described in Chapter 4.

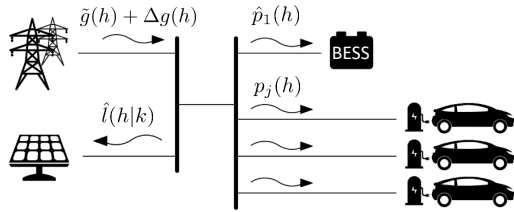
At the first stage, a DS is computed based on an aggregation of the constraints of all controllable devices. At the second stage, a charging plan for the PEVs is computed. This second stage serves two purposes at once: i) it performs the online rescheduling that is necessary to control the imbalances, as described in Section 3.4, and ii) it computes a consistent dispersion of the aggregated energy state, as described in Chapter 4. At the third and last stage, the power output of the BESS is regulated in compliance with the DS. We depict this three-stage scheme in Figure 6.2 and summarize the main aspects of each decision stage in the following.

### Stage 1: Dispatch Schedule

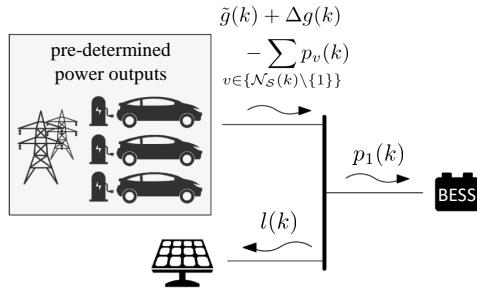
The first decision stage is the calculation of the DS  $\{\tilde{g}\}_{\mathcal{K}}$  at  $k^0$ , by means of optimization. We tackle this task by means of aggregated scheduling, as



(a) Stage 1: dispatch schedule



(b) Stage 2: power outputs of the PEV



(c) Stage 3: power output of the BESS

Figure 6.2: Device aggregation at different stages.

described in Chapter 4. In particular, we utilize the results on aggregations with time-varying connections, as detailed in Section 4.8.

### Stage 2: Power Outputs of the Plug-in Electric Vehicles

The power outputs of the PEVs at  $k$ ,  $p_v(k)$  for  $v \in \{\mathcal{N}_{\mathcal{K}}(k) \setminus \{1\}\}$  are determined at the second stage. This is equivalent to “dispersing” the aggregated energy state among the various devices, as discussed in Chapter 4. Note that we perform the dispersion by means of receding horizon optimization, see Remark 1, and not with direct computation of a consistent dispersion, as described in Theorem 1. One reason guiding this choice is that in the case of a DCS some consistent dispersions are preferable over others, because they reduce the probability of leading to a trajectory that is unfeasible (even if composed by a sequence of feasible states, cf. Section 4.8), especially towards the end of the schedule. As mentioned in Section 4.8, it is preferable to charge the BESS before the PEVs. Another reason is the possibility of planning ahead imbalances that cannot be avoided, eventually re-distributing them over different time-steps, see Section 3.4.

For the sake of simplicity, we set the second-stage receding horizon optimization to be performed at each step of the DS, i.e.  $p_v(k)$  is computed at  $k$ . Similarly to the on-line rescheduling presented in Section 3.4, the second-stage optimization solved at  $k$  spans the interval  $\mathcal{M}(k) = \{k, k + 1, \dots, k + M\}$ . Aggregation is not possible anymore; Figure 6.2b depicts the model of the DCS used at this stage. The optimization aims at determining  $p_v(h)$  and the expected power output of the BESS,  $\hat{e}_1(h)$ ,  $h \in \mathcal{M}$ , for which  $g(h)$  follows the DS.

For the sake of clarity, we report the second-stage optimization problem entirely

$$\min_{\{\mathbf{x}^M(h)\}_{\mathcal{M}(k)}} \sum_{h \in \mathcal{M}(k)} \alpha \Delta g(h) + \sum_{v \in \mathcal{L}(\mathcal{M}(k))} c_v^v (e_v(k_v^d) - e_v^{\min})^2 \quad (6.2a)$$

$$\text{s.t. } \forall h \in \mathcal{M}(k)$$

$$\tilde{g}(h) + \Delta g(h) = \hat{l}(h) + \hat{p}_1(h) + \sum_{v \in \{\mathcal{N}_{\mathcal{M}(k)}(h) \setminus \{1\}\}} p_v(h), \quad (6.2b)$$

$$(4.37), (4.2) \text{ for } j \in \mathcal{N}_{\mathcal{K}}(h), \quad (6.2c)$$

$$p_v(h) = 0 \text{ for } v \notin \{\mathcal{N}_{\mathcal{K}}(k) \setminus \{1\}\}, \quad (6.2d)$$

with decision variables collected in vector

$$\mathbf{x}^M(h) := [\Delta g(h) \hat{p}_0(h) p_1(h) \dots p_N(h)]^\top \in \mathbb{R}^{2(2+V)}.$$

Therein, (6.2b) represents the power balance, (6.2c) and (??) cover the constraints of the connected devices,<sup>2</sup> and (6.2d) sets to zero the power outputs of the not-connected PEVs. The imbalance  $\Delta g(h)$  is introduced to guarantee the feasibility of the power balance, acting as a soft-constraint slack variable. In other words, the controller can schedule deviations from the DS whenever the system is in a state from which such imbalances cannot be avoided. Even if not considered in this test case, requirements on imbalances can be enforced as discussed in Section 3.4. The cost function (6.2a) is designed accordingly to penalize  $\Delta g(h)$  with an appropriate weight  $\alpha$  [Kerrigan and Maciejowski, 2000]. Additionally, over-charging of the  $v$ -th PEV is also penalized with weight  $c_v^v$ , which can differ for distinct PEVs and which can adapt in subsequent iteration of (6.2). As discussed in Section 4.8, it may be useful to delay the “departure” of any eventual energy excess as long as possible. In this manner, any excess of energy stored in

<sup>2</sup> Note a slight simplification of notation: in (6.2c) one should consider the *expected* power output and energy state of the BESS,  $\hat{p}_1$  and  $\hat{e}_1$ , and not their realizations  $p_1$  and  $e_1$ .

the PEVs remains available for compensation of uncertainty as much as possible. This is attained with (6.2) by setting higher values of  $c_v^v$  for the PEVs leaving at first.

Note that the values of the intermittent power output  $l(h)$  over  $\mathcal{M}(k)$  and of the energy state of the not-yet-connected PEVs upon arrival are still uncertain at this stage. However, consistently with the online rescheduling presented in Section 3.4, the second-stage optimization does not involve random variables, making use of a *deterministic* forecast  $\hat{l}(h)$  and deterministic vehicle parameters. The DS itself already accounts for long-term uncertainty and short-term uncertainty is compensated by the BESS (see the description of the next stage). Finally, note that the DS over  $\mathcal{M}(k)$  enters (6.2) as a parameter. Therefore, the horizon  $M$  should satisfy  $M < (k^b - k^0)$ , thus ensuring the availability of a reference for  $\tilde{g}$  over the entire time interval covered by (6.2).

### Stage 3: Power Outputs of the Energy Storage System

The power output of the BESS  $p_1$  is finally computed at the third stage, once the uncontrolled power output is known. Figure 6.2c illustrates the system model used at this stage. At  $k$ , the power outputs of the PEVs follow the references computed at the second stage while the BESS regulates the power exchange with the grid to  $g_{\text{ref}}(k) = \tilde{g}(k) + \Delta g(k)$ , as in Section 3.2. In other words, the actual power output  $p_1$  complies with the realization  $l(k)$  in accordance to the power balance

$$p_1(k) = \tilde{g}(k) + \Delta g(k) - l(k) - \sum_{v \in \{\mathcal{N}_{\mathcal{K}}(k) \setminus \{1\}\}} p_v(k). \quad (6.3)$$

## 6.3 Simulation

Next, the efficacy of the proposed scheduling and control scheme is evaluated by simulating a realistic test case built upon real data of uncontrolled

generation and vehicle traffic. Furthermore, a state-of-the-art two-stage stochastic programming with scenario forecast is implemented as a benchmark for the computation of the DS. As in the previous chapter, PFS denotes the proposed method and SFS refers to the selected benchmark.

### 6.3.1 Description of the Case Study

A small parking lot of an office building, similar to the one examined in [Mouli *et al.*, 2016], provides the case study. The parking lot is equipped with a PV generator, a BESS and five charging spots. All the devices are connected to the distribution grid and operate together as a DCS. A DCS controller is responsible: i) to communicate the DS to the system operator, ii) to regulate the power output of the chargers, and iii) to set the value of  $g_{\text{ref}}(k)$  for the low-level storage controller. The details of the various components are as follows.

#### Photovoltaic Generator

The PV generator has 10 kW of peak power, and it is controlled to track its maximum power point. The PV generation data is taken from the dataset for the solar track of the Global Energy Forecasting Competition of 2014 [Hong *et al.*, 2016]. This dataset consists of time series—with hourly resolution—of measured PV generation and of their corresponding solar irradiation forecasts. The measurements have been taken in an unnamed region of Australia.

#### Energy Storage System

The parameters of the BESS are retrieved from the catalog of a commercial producer.<sup>3</sup> Table 6.1 details the power and energy limits (only the usable capacity is considered), while  $\mu = 0.05$ .

<sup>3</sup> [www.tesla.com/powerwall](http://www.tesla.com/powerwall) [Accessed: 15-Jan-2018]

Table 6.1: Parameters of BESS and PEV

BESS parameters				PEV parameters			
$\underline{p}_1$	-5 kW	$\bar{p}_1$	5 kW	$\underline{p}_v$	0 kW	$\bar{p}_v$	10 kW
$\underline{e}_1$	0 kWh	$\bar{e}_1$	13 kWh	$\underline{e}_v$	7 kWh	$\bar{e}_v$	40 kWh

Table 6.2: Arrival/departure data

$v$	1	2	3	4	5
arrival time	07:00	08:00	09:00	09:00	10:00
departure time	17:00	16:00	17:00	17:00	18:00

### Plug-in Electric Vehicle

For the sake of simplicity, we consider that all the charging stations are used daily, i.e.  $\mathcal{N}_{\mathcal{K}} = [1 \dots 6]$  every day (weekends included), and that all the connecting PEVs have the same characteristics. These values have been selected after a consultation of the catalogs of different producers, as average values among the chosen products.<sup>4</sup> Table 6.1 reports the power and energy limits, while  $\mu = 0.05$  (same as for the BESS, cf. Section 6.1.1). Even if the model considered in designing the scheduling and control scheme is fully general, we suppose in the case study the challenging situation in which the owners of the PEVs do not allow for a vehicle-to-grid service, i.e. the DCS cannot discharge a connected PEV. Thus,  $\underline{p}_v$  is set to 0. The minimum charge required at departure is  $e_v^{\min} = 30\text{kWh} \forall v \in \{\mathcal{N}_{\mathcal{K}}(k) \setminus \{1\}\}$ . A survey on vehicle usage carried out within the Institute for Automation and Applied Informatics at the Karlsruhe Institute of Technology over a time period of three months is the reference for the data on the vehicle mobility

<sup>4</sup> Tesla Model 3, Chevrolet Bolt 2017, Nissan Leaf 2018, BMW i3s

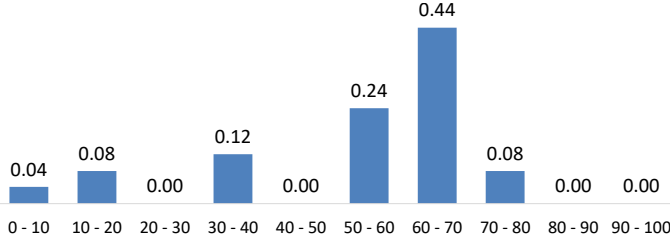


Figure 6.3: Relative frequency of the energy state (in % of the total capacity) of the PEVs upon arrival.

(energy state upon arrival, arrival and departure times).<sup>5</sup> The arrival times of the five PEVs are assigned proportionally to their statistical frequency. The departure times, instead, are chosen as the weighted average of the departure times of the PEVs arriving within the same hour, rounded down. Table 6.2 lists the resulting data. The (statistical) relative frequency of the energy state of the PEVs upon arrival is estimated on the base of the traveling distance, as in [Sarabi *et al.*, 2016]. We consider an autonomy of 280km with full charge and that each  $v$ -th PEV charges only at the DCS, up to  $e_v^{\min}$ . The results are depicted in Figure 6.3. In simulation,  $e_v(k_v^a)$  is randomly extracted in accordance with this frequency.

### Scheduling Requirements

The chosen case study observes the regulation for day-ahead markets: the DS is computed at 12:00 of the previous day and it extends over 24 hours with discrete steps of one hour, i.e.  $\delta = 1\text{h}$ ,  $k^b = 12$ ,  $K = 24$  and  $k^0$  at 12:00. The coefficients of the cost function  $c^{\text{DS}}(\tilde{g}(k), k)$  are time-independent and equal to  $c^{q+} = c^{q-} = 0.05 \frac{\text{€}\cdot\text{h}}{\text{kW}^2}$ ,  $c^{l+} = 0.3 \frac{\text{€}\cdot\text{h}}{\text{kW}}$ ,  $c^{l-} = 0.015 \frac{\text{€}\cdot\text{h}}{\text{kW}}$ ,  $c^c = 0.02 \frac{\text{€}\cdot\text{h}}{\text{kW}^2}$ , and  $c_v^d = 0.03 \frac{\text{€}}{\text{kW}}$ .

<sup>5</sup> We report here only the results of the survey that are relevant for the present work. Please note that the only aim of the survey is to provide a realistic test case for the proposed scheme and does not allow to infer general trends on the vehicle usage. However, our data is aligned with the tendencies described by other works, cf. [Sarabi *et al.*, 2016; Lee *et al.*, 2012].

### 6.3.2 Forecasts

As for the case studies analyzed in Chapter 5, we use the data of PV generation and radiation forecasts to train several quantile regressions based on a method described in [González Ordiano *et al.*, accepted] with the open-source MATLAB toolbox SciXMiner [Mikut *et al.*, 2017]. Thereafter, we derive probabilistic forecasts for both power and energy from those models, using the procedure detailed in 5.1.3. Then, we apply (4.52) approximating  $f_{E_v}(y)$  by the frequency illustrated in Figure 6.3. Finally, we obtain the analytic description of  $F_{\Delta E_c(k)}(\Delta e_c)$  required in the scheduling problem by fitting the quantiles to a logistic function as in Section 5.1.3.

### 6.3.3 Benchmark Scheduling Method

In order to find a benchmark case for the proposed scheduling and control method, we examine existing work from the literature. Among these works, aggregated scheduling of PEVs is well investigated, and does not constitute a novelty. Examples can be found in [Momber *et al.*, 2015; Liu and Etemadi, 2017; Alipour *et al.*, 2017; Zhang *et al.*, 2018; Baringo and Amaro, 2017; Herre *et al.*, 2019]: aggregated scheduling is a common element among these works, which distinguish by the specifics of the investigated problem and by the feedback to the uncertainty realization. For example, Zhang *et al.* [2018] consider a sub-hourly regulation signal with offers of regulation capacity determined by means of optimization; Momber *et al.* [2015]; Liu and Etemadi [2017]; Alipour *et al.* [2017] include the volatility of price signals and of reserve activation directly in the computation of the schedule; Baringo and Amaro [2017] conceive price-dependent bidding functions; Herre *et al.* [2019] consider the case of a risk-adverse aggregator bidding on multiple energy markets. The main difference between the cited works and the proposed method lies in the computation of a DS. In fact, despite their differences, all the cited works cope in the same manner with the long-term uncertainties affecting the scheduling. In particular, they engineer

a stochastic optimization problem with a two-stage structure and they solve the problem using a sampling based method with scenario forecasts [Conejo *et al.*, 2010]. Alternatives to stochastic optimization with scenario forecasting for scheduling the charging of a fleet of PEVs exist, e.g. [Kou *et al.*, 2016], but they have received little attention. For these reasons, stochastic optimization with scenario forecast provides a benchmark for the evaluation of the proposed DS computation, similar to the household case study, cf. Section 5.1.4. The three-stage scheme as well as the aggregation model are instead both maintained in the benchmark case.

For the sake of completeness, we report in the following the computationally tractable optimization problem with scenario forecasts

$$\begin{aligned}
& \min_{\substack{\{\mathbf{x}\}_{\mathcal{K}^s}, \\ \{\mathbf{x}^{\omega'}\}_{\mathcal{K}^s}}} C^{\text{DS}} + C^i \\
& \text{s.t. } \forall k \in \mathcal{K}^s, \quad \forall \omega' \in \mathcal{S}' \\
& \tilde{g}(k) + \Delta g^{\omega'}(k) = p^{\omega'}(k) + l^{\omega'}(k), \\
& e^{\omega'}(k+1) = e^{\omega'}(k) + \sum_{v \in \mathcal{A}_{\mathcal{K}}(k)} e_v^{\omega'}(k_v^a) \\
& \quad + \delta \cdot \left( p^{\omega'}(k) - \mu p^{+, \omega'}(k) + \mu p^{-, \omega'}(k) \right), \\
& e^{\omega'}(k^b) = e^0, \\
& [\tilde{g}^+(k), \tilde{g}^-(k)] \in \mathcal{F}'_d(\tilde{g}(k)), \\
& [p^{+, \omega'}(k), p^{-, \omega'}(k)] \in \mathcal{F}''_d(p^{\omega'}(k)), \\
& p^{\omega'}(k) \in \mathcal{P}(k), \\
& e^{\omega'}(k+1) \in \mathcal{E}(k+1),
\end{aligned}$$

with scenario-independent decision variables collected in vector

$$\mathbf{x}(k) = [\tilde{g}(k) \ \tilde{g}^+(k) \ \tilde{g}^-(k)]^\top \in \mathbb{R}^3,$$

and scenario-dependent decision variables in vector

$$\mathbf{x}^{\omega'}(k) = \left[ e^{\omega'}(k+1) p^{\omega'}(k) p^{+, \omega'}(k) p^{-, \omega'}(k) \Delta g^{\omega'}(k) \right]^T \in \mathbb{R}^5 \quad \forall \omega' \in \mathcal{S}'.$$

### 6.3.4 Simulation Setup

The simulations investigate six different weeks in the time frame between October 2013 and May 2014. Seasonal changes are examined by selecting weeks from separate months. Multiple simulations are conducted for each week, with different values for the security level  $(1 - \varepsilon)$ . Horizon  $M$  is set to 11. The simulations are implemented in MATLAB, using standard open-source optimization tools developed in the systems and control community. Specifically, we use CasaDi [Andersson, 2013] with IPOPT [Wächter and Biegler, 2006]. All the calculations have been performed using a PC with an Intel® Core™ i5-6400 CPU at 2.70 GHz and 8.00 GB RAM.

### 6.3.5 Results

The results of the simulations are summarized in the following. First, we report the results achieved with the application of the proposed method. Then, we compare these results with the ones generated with the SFS.

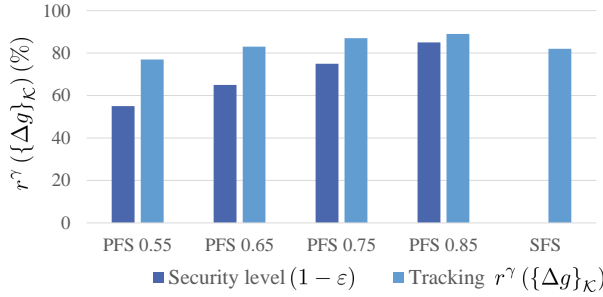
#### Performance of Proposed Method

The average time to compute the DS, reported in Table 6.3, is always a fraction of a second. Hence, the computational load does not restrain the implementation.

The average values of  $r^\gamma(\{\Delta g\}_{\mathcal{K}})$  (defined in (3.8)) measure the tracking performance. Values of  $r^\gamma(\{\Delta g\}_{\mathcal{K}})$  obtained with different choices of  $(1 - \varepsilon)$  are depicted in Figure 6.4 and listed in Table 6.3. The realized  $r^\gamma(\{\Delta g\}_{\mathcal{K}})$  is always higher than  $(1 - \varepsilon)$ , implying that the proposed method fulfills the reliability requirement. The accurate tracking is noticeable also in Figure 6.5, showing various power profiles over simulated sum-

Table 6.3: Simulation of a DCS results.

$(1 - \varepsilon)$	PFS				SFS
	0.55	0.65	0.75	0.85	
$r^\gamma(\{\Delta g\}_{\mathcal{K}})$	0.77	0.83	0.87	0.89	0.82
bal. energy (kWh)	7.67	5.94	4.12	3.51	7.00
comp. time (s)	0.51	0.52	0.52	0.54	12.54
cost $\{\tilde{g}\}_{\mathcal{K}}$ (€)	-0.25	0.37	1.28	2.86	-0.02
cost $\{\Delta g\}_{\mathcal{K}}$ (€)	4.60	3.56	2.47	2.10	4.20
cost total (€)	4.35	3.94	3.76	4.96	4.18

Figure 6.4: Simulation of a DCS: tracking of the DS with different values of  $(1 - \varepsilon)$  / scheduling schemes.

mer days (Figure 6.5a) and autumn days (Figure 6.5b). There, the dotted line represents an eventual baseline presumption  $l'(k)$ ,

$$l'(k) = l(k) + \sum_{v \in \{\mathcal{N}_{\mathcal{K}}(k) \setminus \{1\}\}} \frac{e_v^{\min} - e_v(k_v^a)}{(k_v^d - k_v^a)},$$

corresponding to the case where the power absorbed by each  $v$ -th PEVs cannot be manipulated and remains constant over the interval  $[k_v^a, k_v^d]$ . The

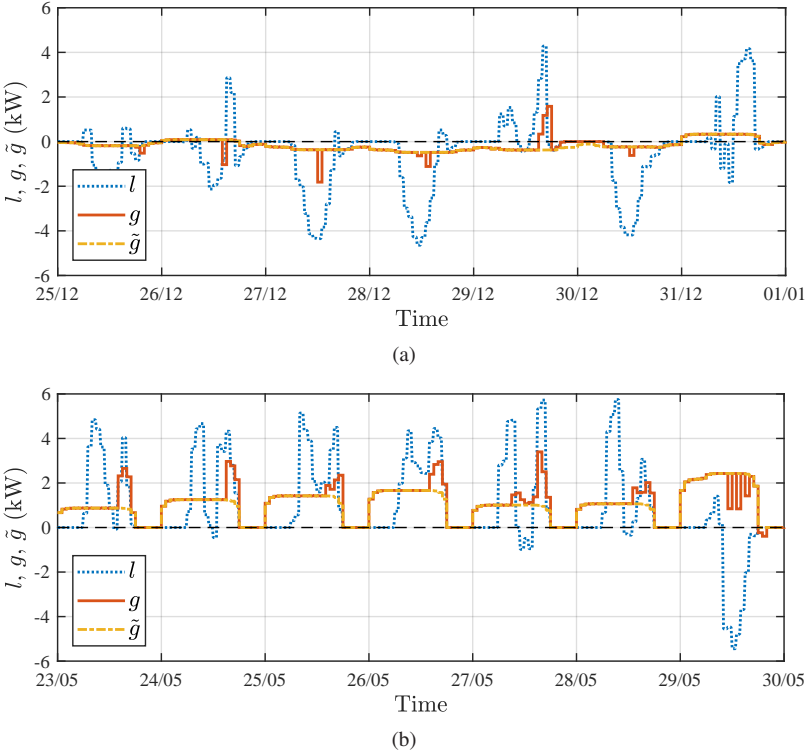


Figure 6.5: Simulation of a DCS: power profiles of the inflexible load  $l$ , of the power exchange with the grid  $g$ , and of the DS  $\tilde{g}$  over two simulated week with  $(1 - \varepsilon) = 0.75$ .

dashed line depicts the DS  $\tilde{g}(k)$  and the full line is the realized power exchange  $g(k)$ . Note that the DS is not trivial and varies daily in accordance with the forecasts and the initial energy state of the BESS. Seasonality has a great impact on the DS, because of its influence on PV generation.

In Figure 6.5 it can be also observed that imbalances are more likely to appear towards the end of the day, where the uncertainty on the aggregated energy state is higher (see Figure 4.7). Note that extended or excessive im-

balances might negatively affect the stability of the overall system. This is an important aspect that should be considered within the operation requirements to consent the implementation of the proposed method on a large scale. Options to deal with this issue at the second decision stage (conceptually similar to the online rescheduling level of the hierarchical scheme in Section 3.1.3) can be found in Section 3.4. Last, Figure 6.5 exhibits that the proposed method highly reduces the ramp power required from the grid. In particular, the average of the daily maximum difference among two subsequent values of  $l'$  is of 2.98 kW, which diminishes to 1.34 kW for  $g$  (55% less).

A quantitative evaluation of the improvements in the power profile is obtained by applying cost functions  $c^{\text{DS}}(\tilde{g}(k), k)$  (see (3.5) and (3.5b)) to  $\{g\}_{\mathcal{K}}$ , considering the linear coefficients in €/kW, and the quadratic ones in €/kW<sup>2</sup>. The average daily cost of the hypothetical baseline load  $l'$ , evaluated according to  $c^{\text{DS}}(\tilde{g}(k), k)$  as if it was dispatched, is of 7.07€. The average daily costs of the DS, reported in Table 6.3, are between  $-0.25\text{€}$  and 2.86€. Table 6.3 also details an hypothetical daily cost of the imbalance profile  $\{\Delta g\}_{\mathcal{K}}$  calculated with respect to cost function  $c^{\text{i}}(\Delta g(k))$  introduced in (3.6), with tariffs that are twice as high as the one of the DS counting both power excess and shortage as purchased power, i.e.  $c^{\Delta \text{q}} = 0.1\text{€/kW}^2$  and  $c^{\Delta \text{l}} = 0.6\text{€/kW}$ . The total costs obtained with different values of  $(1 - \varepsilon)$  are depicted in Figure 6.6, with different colors differentiating the component associated to the schedule from the one associated to the imbalances. As for the test case in Section 5.1, one notices that a higher  $(1 - \varepsilon)$  corresponds to a higher cost of the schedule and to a reduced cost of imbalances. The chosen pricing implies that values in the middle of the selected range achieves the best trade off between reducing the cost of the DS and the one of imbalances.

Figure 6.7 depicts the energy state profile of the BESS and of two of the five PEVs over the same days illustrated in Figure 6.5, with varying values for  $(1 - \varepsilon)$ . First, observe that the proposed scheme meets the requirement

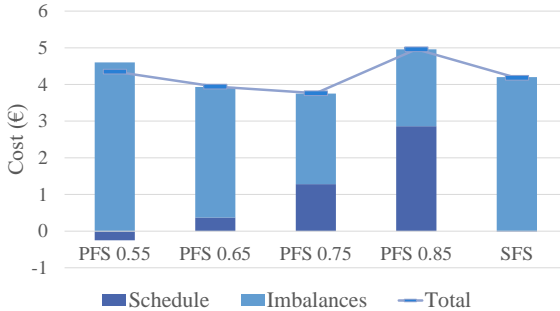


Figure 6.6: Simulation of a DCS: average daily cost with different values of  $(1 - \varepsilon)$  / scheduling schemes.

on the minimum energy state of each PEV upon departure in every case. Then, note how the behavior of the system changes with  $(1 - \varepsilon)$ . This is caused by a different allocation of the energy reserves: increasing  $(1 - \varepsilon)$  reduces the reserves required on the grid side (see Table 6.3 on Page 165) and increases the internal ones.<sup>6</sup> Consequently, with low values of  $(1 - \varepsilon)$ : i) the available capacity of the BESS is used both to provide energy reserves and to optimize the DS, and ii) the final energy state of each PEVs rarely exceeds its respective  $e_v^{\min}$ . In contrast, with high values of  $(1 - \varepsilon)$ : i) the BESS is almost solely used for reserves purposes, and ii) the PEVs are generally charged over their  $e_v^{\min}$ . In this latter case the BESS is maintained charged such that it can inject power in case of underproduction; concurrently, the PEVs have to absorb production excess.

### Benchmark Comparison

The DS calculated with the SFS considers explicitly the expected cost of imbalances and aims at minimization of the total cost. The PFS can target (indirectly) cost minimization with an appropriate choice of  $(1 - \varepsilon)$ ,

<sup>6</sup> As in Table 5.1, “balancing energy” indicates the average amount of energy needed each day to compensate for deviations from the DS, which is considered positive regardless of whether it is absorbed or injected into the grid.

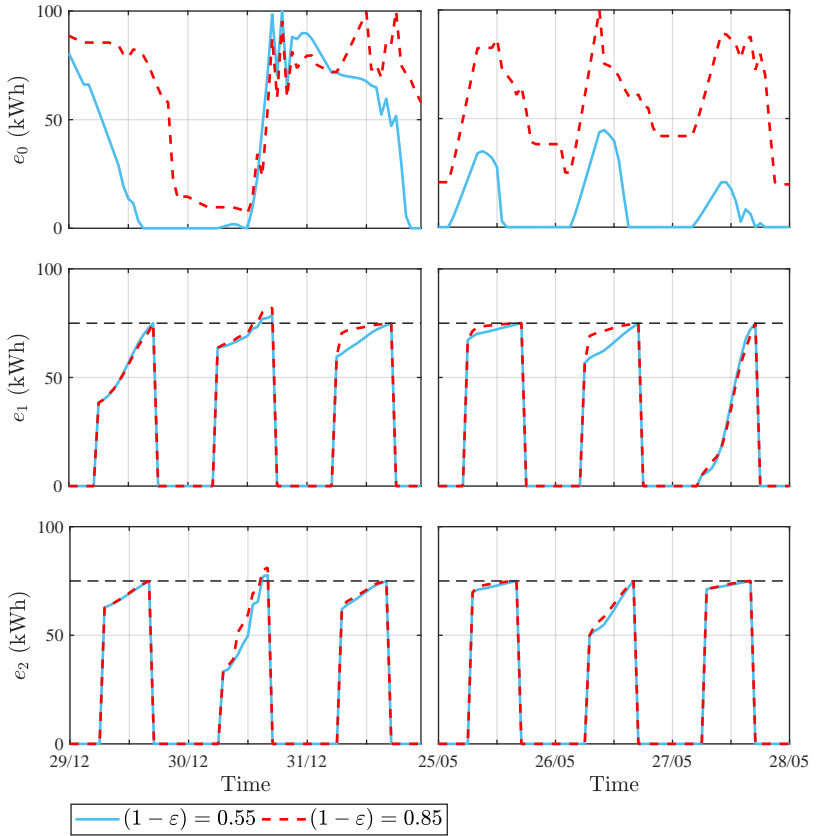


Figure 6.7: Simulation of a DCS: energy profile of the BESS and of two PEVs with different  $(1 - \varepsilon)$ .

as described in the previous chapter. Thus, in a similar way to the household case in Section 5.1, a fair comparison between SFS and PFS should be based on the total cost, accounting for a range of  $(1 - \varepsilon)$ . It can be observed that the total cost in the SFS case is indeed lower than the one of the “dispatched baseline”, which is of 7.07€. However, the PFS attains better results than the SFS for a range of values of  $(1 - \varepsilon)$ : both  $(1 - \varepsilon) = 0.75$  and  $(1 - \varepsilon) = 0.65$  lead to a total cost lower than the one of the SFS.

Additionally, note that the computation time required by the SFS is more than twenty times higher than the one required by the proposed method. Thus, the PFS reduced the computational burden significantly.

## 6.4 Summary

In this chapter we analyze scheduling and operation of a DCS, i.e. an aggregation of flexible and inflexible power devices comprising a BESS, PEV and PV generation. As outlined in Chapter 3, we resort to hierarchical scheduling and operation by distributing the decision making over subsequent stages, each based on a different model of the system. The core of the study is the first decision stage, i.e. the computation of a DS for the entire system, where the application of probabilistic forecasts to a dynamic aggregation of diverse devices leads to a DS with a given probability of being realized in operation. The simulation results show that the requirements on vehicle charging and power dispatch are always met, thus attesting the goodness of the proposed method. In simulations the proposed scheduling scheme also exhibits better performance than two-stage stochastic programming based on scenario forecast, coherently with what has been already observed in Section 5.1.

# 7 Conclusions and Outlook

## 7.1 Conclusions

This thesis deals with scheduling the active power output of an aggregation of distributed energy resources including controllable and uncertain power outputs.

In Chapter 2 we report and analyze existing techniques to deal with such scheduling problems. The literature review indicates that the majority of the works addressing the problem proposes algorithms based on numerical optimization, where the optimization parameters are evaluated via appropriate data processing. In this framework, the state-of-the-art procedure to deal with the uncertainty affecting some parameters of the optimization problem (e.g. future PV generation) is to approximate the uncertain parameters by a finite set of possible realizations—in other words, by sampling. This choice is motivated by the generality of this approach and allows to tackle data processing and numerical optimization *separately*. The data processing outputs a set of realizations of the uncertain parameter; the numerical optimization receives a set of realization of the uncertain parameters in input. In other words, these two elements work in a “plug-and-play manner”: modifying one does not require the other to change. However, in Chapter 2 we also observe that approximating the uncertain parameters with a finite set of realizations might compromise the performance of the computed schedule. Thus, it is worth investigating different scheduling algorithms that do not rely on sampling.

Extending the state-of-the-art methods, this thesis proposes to design scheduling algorithms that avoid sampling by joint consideration of data processing and numerical optimization. Chapter 3 describes a novel scheduling algorithm for an EC-DER coupled with uncertain generation/load that does not resort to samples of the uncertain parameters. Key idea is that the mathematical model describing the system is such that no equality includes uncertain parameters and each inequality contains no more than one uncertain parameter. This way, computational tractability is achieved by describing the constraints containing an uncertain parameter as chance constraints and then reformulating them as deterministic inequalities by exploiting the CDF of their uncertain parameter, received from data processing. Obtaining such a model requires the use of uncertain parameters described as functions of the directly measurable quantities. For example, the algorithm in Chapter 3 leverages on forecasts of the uncertain generation/consumption in terms of both power (directly measurable) and energy (constructed integrating power measurements). One of the main advantages of this technique is that the correlation among subsequent uncertain power outputs does not have to be explicitly estimated and dealt with in the numerical optimization, but it is indirectly considered in the forecasting model. From a high level perspective, we design the scheduling algorithm with a holistic approach that shifts parts of the computation from the numerical optimization to the data processing by requiring the estimation of parameters that indirectly embed some calculation that would have otherwise be undertaken by the numerical optimization. However, if on the one hand the considered mathematical description of the system does not approximate the uncertainties (no sampling is required), on the other hand it approximates the physical characteristics of the devices and of their operating requirements.

Chapter 4 examines the possibility of applying the ideas presented in Chapter 3 to systems comprising multiple EC-DERs. To this end, we formulate an optimization problem for scheduling that contains not only aggregated *parameters*, but also aggregated *decision variables*. This approach,

common in the literature, poses the questions of whether the solution of the aggregated problem attains the same cost of the original problem and whether there exists a feasible combination of the original decision variables that corresponds to the optimal aggregated decision variable. The investigation in Chapter 4 proves that both these questions have a positive answer whenever the models of the single-device constraints respect some assumptions. Our findings justify the application of an aggregated model in scheduling, provide a technique to check the consistency of an aggregated model, and propose a way to disperse the aggregated energy state which is free from any time dependence.

We validate the proposed scheduling method against realistic test cases in Chapters 5 and 6. In Chapter 5, we analyze via simulation different cases involving a single BESS. We conclude that the proposed algorithm attains the desired outcome and that it attains better results (with an appropriate tuning of the tracking requirement) than state-of-the-art scheduling algorithms based on deterministic or scenario forecasting. Furthermore, we notice that the algorithm can be applied to a household as much as to an industrial setting, and that it could be regulated towards different scheduling objectives (e.g. peak-shaving, price-dependent energy arbitrage...). Finally, we report experimental results indicating that the simulation results are inline with what is practically obtainable in real-life.

Last, in Chapter 6, we address scheduling of a population of EC-DERs. To this end, we analyze the case of a DCS, clustering a charging station for PEVs with a BESS and uncertain renewable generation. The chosen test case requires to further extend the scheduling algorithm described in Chapters 5 and 6 to include multiple sources of uncertainty and time-varying connections. Even in this case, the result supports the proposed algorithm with respect to state-of-the-art approaches based on scenario forecasts.

## 7.2 Suggestions for Future Work

The promising performance showed in the analyzed case studies motivate to further investigate the scheduling algorithm proposed in this thesis. In fact, while answering to the research questions presented in Chapter 1, the work outlined here raises new research questions that can initiate novel research lines along three main directions.

### Extension of the Proposed Framework

The first direction consists in extending the scheduling algorithm proposed in Chapters 3 and 4. Aspects that have yet to be analyzed comprise:

- aggregated scheduling with consideration of network constraints
- dispersing the aggregate states with respect of location and network constraints
- distributed computation of a feasible dispersion.

Additional simulations and real-life experiments are also required to further validate the proposed scheduling algorithm and its eventual extensions.

### Proposed Framework at a System Level

Another research direction involves analyzing the results of the proposed scheduling algorithm from a system perspective, similarly to the study presented in Bozorg *et al.* [2018]. In particular, it is of interest to examine the interaction among clusters of resources that are dispatching their aggregated power output in accordance to a schedule computed with the proposed algorithm. Possible research studies include:

- sizing of the aggregations in view of an economically viable allocation of reserves

- designing tracking constraints and policies to penalize the imbalances that enforce network requirements (e.g. stability of the overall system, minimization of allocated reserves, ...)
- sizing of the energy reserves for the entire system by means of probabilistic energy forecasts.

### **Holistic Approach to Scheduling**

The last research direction indicated by this thesis is to investigate the application of a holistic approach to the design of scheduling algorithms (similar to the one presented in this thesis) to different settings. In particular, it would be of interest to explore the idea of shifting part of the computation from the numerical optimization to the data processing by creating synthetic random processes that incorporate multiple uncertain parameters and constraints. To this end, an appealing problem in the energy sector is the participation of aggregated distributed resources, including storage, on real time energy markets—as the Australian one. In this context, examples of synthetic stochastic processes that are worth examining are:

- time-integration of wholesale prices
- time-integration of prices spanning multiple energy markets
- time-integration of curtailed generation from uncertain renewable resources.



# Personal Remarks

Ideas, though, are not singular.

---

*E. Catmull, Creativity.Inc*

An old professor once asked his students what mankind hungers for. The students gave in return the more diverse answers: power, money, love... However, none of their answers seemed to satisfy the professor. "Nothing of that", he replied, "mankind hungers for only two things: energy and information".

The professor's answer may seem disappointing, an answer that only an engineer could have given, but it is actually a wise one. While it is questionable whether energy and information suffice, humans need both to tackle the challenges they face, to bring their visions to reality, to thrive: energy provides the power, and information yields the knowledge. It was only a matter of time before mankind discovered that energy and information would have been even more powerful together. The massive, global communication infrastructure that we use on a daily base to exchange information hinges on energy consumption. And soon enough, the infrastructures we use to produce, transport and consume energy will pivot on collecting, processing and exchanging a large amount of information. Different terms are in use to denote this phenomenon: "smart grid", "internet of things", "energy informatics".

Energy empowering information, and information empowering energy. Nowadays, this is a potent, diffuse, even unquestionable vision. One may wonder why this powerful idea, which claims to touch humanity's cravings at their core, is not yet reality. What else is still required when numerous

minds agree on this vision and most of the technology is already there? Working at this thesis, I found an answer.

This vision requires connecting existing technologies from different fields. However, visions alone will not suffice to connect the pieces. Imagining a bridge in the right spot is one thing, building the bridge is a different one: it requires both parts reaching towards the other while remaining each on their side. Connections, likewise a bridge, cannot be imposed from above by an omniscient mind overlooking both shores. Instead, they need to be built from the ground by one-sided experts; which is difficult, especially in science. Sometimes, pride grows with knowledge. Sometimes, explaining is tiring and understanding is an even greater effort. Sometimes, pushed by a need for belonging, we hold so much on the comfort of an identity that we become reluctant towards whatever does not comply with it.

Because of all these reasons, it seems to me that we keep on forgetting an obvious truth: whenever the completion of a process depends on multiple sub-tasks, the way in which the various tasks connect is more influential on the final outcome than the means in which the isolated tasks are completed. Even the greatest tool (being it a powerful forecasting model or an advanced numerical solver) is useless if it is unable to link with the other pieces. For this reason, it is pivotal to find the courage to face the uncomfortable difficulties of joining expertise and knowledge. Staying curious, seeing value in the works of others, entering worlds in which we have to humbly leave the chair of the expert and sit trustfully in the pupil's spot.

In the years required to write this thesis, I have encountered the struggle of connecting: I have seen it in others, and felt it myself. Nonetheless, I have also experienced the price for going beyond these obstacles. Creativity awaits those who can peace the mindset-clash and embrace unfamiliar ideas, who can venture in the chaos and find a new order. So grew this thesis, on a ground fertilized by different scientific fields.

Going through this manuscript has probably overwhelmed you, dear reader, with concepts, equations and diagrams. I hope that you could find some-

thing interesting in here, something capable of whetting your curiosity and fostering bright ideas in your mind. If that was not the case, you should take away from this long flow of words and equations at least this final—non-scientific—message: dare to connect, challenge and contaminate your world with the surrounding ones. It will be rewarding.



# List of Figures

2.1	Discrete-time scheduling horizon . . . . .	15
2.2	Phases of an automated decision process and aspects of problem formulation . . . . .	16
2.3	Schematic representation of the computationally tractable reformulation of chance constraint (2.9). . . . .	30
3.1	Schematic representation of a dispatchable feeder. . . . .	36
3.2	Three-level hierarchical scheduling and control scheme. . . . .	41
3.3	Example of inflexible power and energy sequences. . . . .	50
3.4	Example of probabilistic forecasts for $l$ and $e_l$ . . . . .	51
3.5	Representation of chance constraint on energy state. . . . .	57
4.1	Schematic representation of an aggregated energy system. . . . .	68
4.2	Illustration of Example 1. . . . .	76
4.3	Illustration of the feasible and reachable energy states in Example 1. . . . .	81
4.4	Illustration of Example 2. . . . .	84
4.5	Graphical representation of a consistent dispersion of $e(k)$ . . . . .	85
4.6	Example of aggregated energy state and of its bounds (time-varying battery). . . . .	103
4.7	Scheduling for a DCS: graphical representation of the stochastic energy state $E(k)$ and of its corresponding constraint with $(1 - \varepsilon) = 0.75$ . . . . .	108

5.1 Simulation of a household: tracking of the DS, sorted by scheduling scheme. . . . . 121

5.2 Simulation of a household: comparison of imbalances profiles over a simulated week. . . . . 122

5.3 Simulation of a household: average daily cost under different imbalance pricing policies, sorted by scheduling scheme. . . . . 124

5.4 Simulation of a household: comparison of energy state profiles over a simulated week. . . . . 125

5.5 Simulation of a household: power profiles. . . . . 126

5.6 Trend of energy prices for a day in different time periods of 2018 at the EPEX day-ahead market (German market). . . . . 129

5.7 Comparison of probabilistic forecasts for a campus load (consumption + PV generation) with and without weather input. . . . 131

5.8 Simulation of an industrial campus: tracking of the DS with different values of  $(1 - \varepsilon)$ . . . . . 133

5.9 Simulation of an industrial campus: power and energy profiles over a simulated week in September 2018 with  $(1 - \varepsilon) = 0.70$ . 135

5.10 Simulation of an industrial campus: power and energy profiles over a simulated week in November 2018 with  $(1 - \varepsilon) = 0.70$ . 136

5.11 Simulation of an industrial campus: power and energy profiles over a simulated week in September 2018 with  $(1 - \varepsilon) = 0.40$ . 137

5.12 Conversion efficiency of the AC/DC conversion for battery charging; adapted from [Barry and Thomas, 2017]. . . . . 140

5.13 Experimental dispatching: power profiles. . . . . 144

5.14 Experimental dispatching: imbalances profiles, comparison of simulation and experimental results. . . . . 146

5.15 Experimental dispatching: stored energy profiles, comparison of simulation and experimental results. . . . . 147

5.16 Experimental dispatching: power profiles, minute resolution. . . 148

5.17 Experimental dispatching: state of charge profile, sampling period of 1 minute . . . . . 149

---

6.1	Schematic diagram of a DCS. . . . .	152
6.2	Device aggregation at different stages. . . . .	155
6.3	Relative frequency of the energy state (in % of the total capacity) of the PEVs upon arrival. . . . .	161
6.4	Simulation of a DCS: tracking of the DS with different values of $(1 - \varepsilon)$ / scheduling schemes. . . . .	165
6.5	Simulation of a DCS: power profiles. . . . .	166
6.6	Simulation of a DCS: average daily cost with different values of $(1 - \varepsilon)$ / scheduling schemes. . . . .	168
6.7	Simulation of a DCS: energy profiles. . . . .	169



# Bibliography

- H. Abdi and L. J. Williams. Principal component analysis. *Wiley interdisciplinary reviews: computational statistics*, 2(4):433–459, 2010.
- M. Alipour, B. Mohammadi-Ivatloo, M. Moradi-Dalvand, and K. Zare. Stochastic scheduling of aggregators of plug-in electric vehicles for participation in energy and ancillary service markets. *Energy*, 118:1168–1179, 2017.
- J. Andersson. *A general-Purpose Software Framework for Dynamic Optimization*. PhD thesis, Arenberg Doctoral School, KU Leuven, October 2013.
- J. Antonanzas, N. Osorio, R. Escobar, R. Urraca, F. Martinez-de Pison, and F. Antonanzas-Torres. Review of photovoltaic power forecasting. *Solar Energy*, 136:78–111, 2016.
- R. R. Appino, J. Á. González Ordiano, R. Mikut, T. Faulwasser, and V. Hagenmeyer. On the use of probabilistic forecasts in scheduling of renewable energy sources coupled to storages. *Appl. Energy*, 210(Supplement C):1207 – 1218, 2018.
- R. R. Appino, J. Á. González Ordiano, R. Mikut, V. Hagenmeyer, and T. Faulwasser. Storage scheduling with stochastic uncertainties: Feasibility and cost of imbalances. In *2018 Power Systems Computation Conference (PSCC)*. IEEE, 2018.
- R. R. Appino, M. Munoz-Ortiz, J. A. G. Ordiano, R. Mikut, V. Hagenmeyer, and T. Faulwasser. Reliable dispatch of renewable generation via charging of time-varying PEV populations. *IEEE Trans. Power Syst.*, 34(2):1558–1568, 2018.
- R. R. Appino, J. Á. González Ordiano, N. Munzke, R. Mikut, T. Faulwasser, and V. Hagenmeyer. Assessment of a scheduling strategy for dispatching prosumption of an industrial campus. In *Proc., Internationaler ETG-Kongress 2019, 08. - 09.05.2019, Esslingen am Neckar*, pages 289–294. VDE-Verlag, 2019.

- R. R. Appino, V. Hagenmeyer, and T. Faulwasser. Towards optimality preserving aggregation for scheduling distributed energy resources. *arXiv preprint arXiv:1906.09183*, 2019. Submitted to “IEEE Transactions on Control of Network Systems”.
- K. J. Aström and R. M. Murray. *Feedback systems: an introduction for scientists and engineers*. Princeton university press, 2010.
- L. Baringo and R. S. Amaro. A stochastic robust optimization approach for the bidding strategy of an electric vehicle aggregator. *Electric Power Systems Research*, 146:362–370, 2017.
- J. Barry and J. Thomas. Online and offline PV power forecasts for optimal control of storage systems. In *33rd European Photovoltaic Solar Energy Conference and Exhibition*, 2017.
- H. Beltran, E. Perez, N. Aparicio, and P. Rodriguez. Daily solar energy estimation for minimizing energy storage requirements in PV power plants. *IEEE Trans. Sustain. Energy*, 4(2):474–481, 2013.
- A. Bernstein, L. Reyes-Chamorro, J.-Y. Le Boudec, and M. Paolone. A composable method for real-time control of active distribution networks with explicit power setpoints. part i: Framework. *Electric Power Systems Research*, 125:254–264, 2015.
- D. Bertsimas, D. B. Brown, and C. Caramanis. Theory and applications of robust optimization. *SIAM review*, 53(3):464–501, 2011.
- R. Bessa, C. Möhrle, V. Fundel, M. Siefert, J. Browell, S. Haglund El Gaidi, B.-M. Hodge, U. Cali, and G. Kariniotakis. Towards improved understanding of the applicability of uncertainty forecasts in the electric power industry. *Energies*, 10(9):1402, 2017.
- A. Bitlislioglu, T. T. Gorecki, and C. N. Jones. Robust tracking commitment. *IEEE Trans. Autom. Control*, 2017.

- 
- P. Bonami, L. T. Biegler, A. R. Conn, G. Cornuéjols, I. E. Grossmann, C. D. Laird, J. Lee, A. Lodi, F. Margot, N. Sawaya, et al. An algorithmic framework for convex mixed integer nonlinear programs. *Discrete Optimization*, 5(2):186–204, 2008.
- M. Bozorg, F. Sossan, J.-Y. Le Boudec, and M. Paolone. Influencing the bulk power system reserve by dispatching power distribution networks using local energy storage. *Electric Power Systems Research*, 163:270–279, 2018.
- P. Braun, T. Faulwasser, L. Grüne, C. M. Kellett, S. Weller, and K. Worthmann. Maximum grid disconnection time of a small scale neighbourhood electricity network. In *Proc. of 22nd Int. Symposium on Mathematical Theory of Networks and Systems (MTNS), Minneapolis, USA*, 2016.
- S. Burger, J. P. Chaves-Ávila, C. Batlle, and I. J. Pérez-Arriaga. A review of the value of aggregators in electricity systems. *Renewable and Sustainable Energy Reviews*, 77:395–405, 2017.
- G. C. Calafiore and L. El Ghaoui. On distributionally robust chance-constrained linear programs. *Journal of Optimization Theory and Applications*, 130(1):1–22, 2006.
- M. C. Campi, S. Garatti, and M. Prandini. The scenario approach for systems and control design. *Annual Reviews in Control*, 33(2):149–157, 2009.
- M. A. Carlton, J. L. Devore, et al. *Probability with Applications in Engineering, Science, and Technology*. Springer, 2014.
- M. A. Carlton, J. L. Devore, et al. *Probability with Applications in Engineering, Science, and Technology*. Springer, 2017.
- A. Charnes and W. W. Cooper. Chance-constrained programming. *Management science*, 6(1):73–79, 1959.
- A. Charnes, W. W. Cooper, and G. H. Symonds. Cost horizons and certainty equivalents: an approach to stochastic programming of heating oil. *Management Science*, 4(3):235–263, 1958.

- C. Citro, A. Luna, J. Rocabert, R. S. Muñoz-Aguilar, I. Candela, and P. Rodriguez. Overview of power processing structures for embedding energy storage in pv power converters. In *37th Society IECON*, pages 2492–2498. IEEE, 2011.
- A. J. Conejo, M. Carrión, and J. M. Morales. *Decision Making Under Uncertainty in Electricity Markets*, volume 1. Springer, 2010.
- H. Ding, Z. Hu, and Y. Song. Stochastic optimization of the daily operation of wind farm and pumped-hydro-storage plant. *Renewable Energy*, 48:571–578, 2012.
- S. Engell and I. Harjunkoski. Optimal operation: Scheduling, advanced control and their integration. *Computers & Chemical Engineering*, 47:121–133, 2012.
- E.-E. ENTSOG. TYNDP2018 scenario report. Technical report, 2018. <https://tyndp.entsoe.eu/tyndp2018/scenario-report/>, accessed August, 2018.
- EPEX SPOT. EPEX SPOT operational rules. Technical report, EPEX SPOT, 2018. Retrieved from <http://www.epexspot.com/en/extras/download-center>.
- M. P. Evans, D. Angeli, and S. H. Tindemans. Robustly maximal utilisation of energy-constrained distributed resources. In *2018 Power Systems Computation Conference (PSCC)*, pages 1–7. IEEE, 2018.
- L. Fabietti, T. Gorecki, F. Qureshi, A. Bitlislioglu, I. Lympelopoulous, and C. Jones. Experimental implementation of frequency regulation services using commercial buildings. *IEEE Trans. Smart Grid*, 2016.
- L. Fabietti, T. T. Gorecki, E. Namor, F. Sossan, M. Paolone, and C. N. Jones. Enhancing the dispatchability of distribution networks through utility-scale batteries and flexible demand. *Energy and Buildings*, 172:125–138, 2018.
- B. A. Francis and W. M. Wonham. The internal model principle of control theory. *Automatica*, 12(5):457–465, 1976.
- J. Garcia-Gonzalez, R. M. R. de la Muela, L. M. Santos, and A. M. Gonzalez. Stochastic joint optimization of wind generation and pumped-storage units in an electricity market. *IEEE Trans. Power Syst.*, 23(2):460–468, 2008.

- J. Á. González Ordiano, W. Doneit, S. Waczowicz, L. Gröll, R. Mikut, and V. Hagenmeyer. Nearest-neighbor based non-parametric probabilistic forecasting with applications in photovoltaic systems. In *Proc., 26. Workshop Computational Intelligence, Dortmund*, pages 9–30, 2016.
- J. Á. González Ordiano, S. Waczowicz, V. Hagenmeyer, and R. Mikut. Energy forecasting tools and services. *Wiley Interdisciplinary Reviews: Data Mining and Knowledge Discovery*, 8(2):e1235, 2018.
- J. Á. González Ordiano, R. R. Appino, T. Faulwasser, V. Hagenmeyer, and R. Mikut. On the creation of quantile regression based scenario and parametric probabilistic forecasts in the context of energy forecasting. In *38th International Symposium on Forecasting*, 2018.
- J. Á. González Ordiano, L. Gröll, R. Mikut, and V. Hagenmeyer. Probabilistic energy forecasting using the nearest neighbors quantile filter and quantile regression. *International Journal of Forecasting*, accepted.
- J. Á. González Ordiano. *New Data-Driven Probabilistic Forecasting Methods with Applications in Energy Systems*. PhD thesis, Karlsruhe Institute of Technology, 2019.
- N. Good and P. Mancarella. Flexibility in multi-energy communities with electrical and thermal storage: A stochastic, robust approach for multi-service demand response. *IEEE Trans. Smart Grid*, 2017.
- L. Grüne, J. Pannek, M. Seehafer, and K. Worthmann. Analysis of unconstrained nonlinear MPC schemes with time varying control horizon. *SIAM Journal on Control and Optimization*, 48(8):4938–4962, 2010.
- V. Hagenmeyer, H. Kemal Çakmak, C. Döpmeier, T. Faulwasser, J. Isele, H. B. Keller, P. Kohlhepp, U. Kühnapfel, U. Stucky, S. Waczowicz, et al. Information and communication technology in Energy Lab 2.0: Smart energies system simulation and control center with an open-street-map-based power flow simulation example. *Energy Technology*, 4(1):145–162, 2016.

- H. Hao, B. M. Sanandaji, K. Poolla, and T. L. Vincent. Aggregate flexibility of thermostatically controlled loads. *IEEE Trans. on Power Systems*, 30(1):189–198, 2015.
- L. Herre, J. Dalton, and L. Söder. Optimal day-ahead energy and reserve bidding strategy of a risk-averse electric vehicle aggregator in the nordic market. In *2019 IEEE Milano PowerTech*, pages 1–6. IEEE, 2019.
- J. P. Hespanha and A. Singh. Stochastic models for chemically reacting systems using polynomial stochastic hybrid systems. *International Journal of Robust and Nonlinear Control: IFAC-Affiliated Journal*, 15(15):669–689, 2005.
- J. Hoffmann-Jørgensen. *Probability with a view toward statistics*, volume 1. New York: Chapman and Hall, 1994.
- T. Hong, P. Pinson, S. Fan, H. Zareipour, A. Troccoli, and R. J. Hyndman. Probabilistic energy forecasting: Global energy forecasting competition 2014 and beyond. *International Journal of Forecasting*, 32(3):896 – 913, 2016.
- IEEE PES Task Force on Microgrid Stability Analysis and Modeling. Microgrid stability definitions, analysis, and modeling. Technical report, IEEE PES, 2018. [Online; accessed 14-December-2018].
- L. Jaulin, M. Kieffer, O. Didrit, and E. Walter. *Applied interval analysis: with examples in parameter and state estimation, robust control and robotics*, volume 1. Springer Science & Business Media, 2001.
- P. Kall, S. W. Wallace, and P. Kall. *Stochastic programming*. Springer, 1994.
- P. Keil, S. F. Schuster, J. Wilhelm, J. Travi, A. Hauser, R. C. Karl, and A. Jossen. Calendar aging of lithium-ion batteries i. impact of the graphite anode on capacity fade. *Journal of The Electrochemical Society*, 163(9):A1872–A1880, 2016.
- W. Kempton and J. Tomić. Vehicle-to-grid power implementation: From stabilizing the grid to supporting large-scale renewable energy. *Journal of Power Sources*, 144(1):280–294, 2005.

- E. C. Kerrigan and J. M. Maciejowski. Soft constraints and exact penalty functions in model predictive control. In *Control 2000 Conference, Cambridge*, 2000.
- K.-K. K. Kim, D. E. Shen, Z. K. Nagy, and R. D. Braatz. Wiener’s polynomial chaos for the analysis and control of nonlinear dynamical systems with probabilistic uncertainties [historical perspectives]. *IEEE Control Systems*, 33(5):58–67, 2013.
- A. J. King and S. W. Wallace. *Modeling with stochastic programming*. Springer Science & Business Media, 2012.
- B. P. Koirala, E. Koliou, J. Friege, R. A. Hakvoort, and P. M. Herder. Energetic communities for community energy: A review of key issues and trends shaping integrated community energy systems. *Renewable and Sustainable Energy Reviews*, 56:722–744, 2016.
- M. Korpaas, A. T. Holen, and R. Hildrum. Operation and sizing of energy storage for wind power plants in a market system. *International Journal of Electrical Power & Energy Systems*, 25(8):599–606, 2003.
- P. Kou, F. Gao, and X. Guan. Stochastic predictive control of battery energy storage for wind farm dispatching: Using probabilistic wind power forecasts. *Renewable Energy*, 80:286–300, 2015.
- P. Kou, D. Liang, L. Gao, and J. Lou. Probabilistic electricity price forecasting with variational heteroscedastic gaussian process and active learning. *Energy Conversion and Management*, 89:298–308, 2015.
- P. Kou, D. Liang, L. Gao, and F. Gao. Stochastic coordination of plug-in electric vehicles and wind turbines in microgrid: A model predictive control approach. *IEEE Trans. Smart Grid*, 7(3):1537–1551, 2016.
- C. M. Lagoa, X. Li, and M. Sznaier. Application of probabilistically constrained linear programs to risk-adjusted controller design. In *American Control Conference, 2001. Proceedings of the 2001*, volume 2, pages 738–743. IEEE, 2001.
- I. Lampropoulos, P. Garoufalis, P. P. van den Bosch, and W. L. Kling. Hierarchical predictive control scheme for distributed energy storage integrated with

- residential demand and photovoltaic generation. *IET Gener. Transm. Distrib.*, 9(15):2319–2327, 2015.
- C. H. Lee, K.-H. Kim, and P. Kim. A moment closure method for stochastic reaction networks. *The Journal of chemical physics*, 130(13):134107, 2009.
- T.-K. Lee, Z. Bareket, T. Gordon, and Z. S. Filipi. Stochastic modeling for studies of real-world phev usage: Driving schedule and daily temporal distributions. *IEEE Trans. Veh. Technol.*, 61(4):1493–1502, 2012.
- K. Li, F. Wei, K. J. Tseng, and B.-H. Soong. A practical lithium-ion battery model for state of energy and voltage responses prediction incorporating temperature and ageing effects. *IEEE Transactions on Industrial Electronics*, 65(8):6696–6708, 2017.
- K. Li, F. Wei, K. J. Tseng, and B.-H. Soong. A practical lithium-ion battery model for state of energy and voltage responses prediction incorporating temperature and ageing effects. *IEEE Trans. Ind. Electron.*, 65(8):6696–6708, 2018.
- S. Liu and A. H. Etemadi. A dynamic stochastic optimization for recharging plug-in electric vehicles. *IEEE Trans. Smart Grid*, 2017.
- K. Margellos, P. Goulart, and J. Lygeros. On the road between robust optimization and the scenario approach for chance constrained optimization problems. *IEEE Trans. Autom. Control*, 59(8):2258–2263, 2014.
- J. L. Mathieu, M. Kamgarpour, J. Lygeros, G. Andersson, and D. S. Callaway. Arbitraging intraday wholesale energy market prices with aggregations of thermostatic loads. *IEEE Trans. Power Syst.*, 30(2):763–772, 2014.
- R. Mikut, A. Bartschat, W. Doneit, J. Ángel González Ordiano, B. Schott, J. Stegmaier, S. Waczowicz, and M. Reischl. The MATLAB toolbox SciXMiner: User’s manual and programmer’s guide. Technical report, arXiv:1704.03298, 2017.
- B. L. Miller and H. M. Wagner. Chance constrained programming with joint constraints. *Oper. Res.*, 13(6):930–945, 1965.

- I. Momber, A. Siddiqui, T. G. San Román, and L. Söder. Risk averse scheduling by a PEV aggregator under uncertainty. *IEEE Trans. Power Syst.*, 30(2):882–891, 2015.
- J. M. Morales, A. J. Conejo, H. Madsen, P. Pinson, and M. Zugno. *Integrating renewables in electricity markets: Operational problems*, volume 205. Springer Science & Business Media, 2013.
- G. C. Mouli, P. Bauer, and M. Zeman. System design for a solar powered electric vehicle charging station for workplaces. *Appl. Energy*, 168:434–443, 2016.
- J. C. Mukherjee and A. Gupta. A review of charge scheduling of electric vehicles in smart grid. *IEEE Systems Journal*, 9(4):1541–1553, 2015.
- K. P. Murphy. *Machine learning: a probabilistic perspective*. MIT press, 2012.
- A. Murray, T. Faulwasser, and V. Hagenmeyer. Mixed-integer vs. real-valued formulations of battery scheduling problems. *IFAC-PapersOnLine*, 51(28):350–355, 2018.
- Z. K. Nagy and R. D. Braatz. Robust nonlinear model predictive control of batch processes. *AIChE Journal*, 49(7):1776–1786, 2003.
- E. Namor, F. Sossan, R. Cherkaoui, and M. Paolone. Load leveling and dispatchability of a medium voltage active feeder through battery energy storage systems: Formulation of the control problem and experimental validation. In *PES Innovative Smart Grid Technologies Conference Europe (ISGT-Europe), 2016 IEEE*, pages 1–6. IEEE, 2016.
- E. Namor, F. Sossan, R. Cherkaoui, and M. Paolone. Control of battery storage systems for the simultaneous provision of multiple services. *IEEE Trans. Smart Grid*, 10(3):2799–2808, 2018.
- A. Nemirovski and A. Shapiro. Convex approximations of chance constrained programs. *SIAM Journal on Optimization*, 17(4):969–996, 2006.
- NERC. Reliability standards for the bulk electric systems of North America, 2018. [https://www.nerc.com/pa/stand/reliability\\_standards\\_complete\\_set/rscompleteset.pdf](https://www.nerc.com/pa/stand/reliability_standards_complete_set/rscompleteset.pdf) Accessed July, 2018.

- J. Nocedal and S. J. Wright. Sequential quadratic programming. *Numerical optimization*, pages 529–562, 2006.
- S. M. Nosratabadi, R.-A. Hooshmand, and E. Gholipour. A comprehensive review on microgrid and virtual power plant concepts employed for distributed energy resources scheduling in power systems. *Renewable and Sustainable Energy Reviews*, 67:341–363, 2017.
- D. E. Olivares, J. D. Lara, C. A. Cañizares, and M. Kazerani. Stochastic-predictive energy management system for isolated microgrids. *IEEE Trans. Smart Grid*, 6(6):2681–2693, 2015.
- N. P. Padhy. Unit commitment—a bibliographical survey. *IEEE Trans. Power Syst.*, 19(2):1196–1205, 2004.
- Y. Parag and B. K. Sovacool. Electricity market design for the prosumer era. *Nature Energy*, 1(4):16032, 2016.
- Parameter. Parameter — Wikipedia, the free encyclopedia, 2019. [Online; accessed 02-August-2019].
- E. Perez, H. Beltran, N. Aparicio, and P. Rodriguez. Predictive power control for PV plants with energy storage. *IEEE Trans. Sustain. Energy*, 4(2):482–490, 2013.
- P. Pinson, H. Madsen, H. A. Nielsen, G. Papaefthymiou, and B. Klöckl. From probabilistic forecasts to statistical scenarios of short-term wind power production. *Wind Energy*, 12(1):51–62, 2009.
- E. N. Pistikopoulos, M. C. Georgiadis, and V. Dua. *Multi-parametric programming*, volume 1. Wiley-vch, 2007.
- J. Priebe, H. K. Cakmak, N. Wehbring, H. Chang, U. Kühnapfel, V. Hagenmeyer, and A. Moser. Exploiting unused capacity in the grid. In *IEEE Innovative Smart Grid Technologies - Asia 2019 (ISGT Asia 2019)*, 2019.
- E. L. Ratnam, S. R. Weller, C. M. Kellett, and A. T. Murray. Residential load and rooftop PV generation: an Australian distribution network dataset. *International Journal of Sustainable Energy*, pages 1–20, 2015.

- 
- J. B. Rawlings, D. Q. Mayne, and M. Diehl. *Model predictive control: theory, computation, and design*, volume 2. Nob Hill Publishing Madison, WI, 2017.
- L. A. Roald. *Optimization methods to manage uncertainty and risk in power systems operation*. PhD thesis, ETH Zurich, 2016.
- S. M. Ross. *Introduction to probability and statistics for engineers and scientists*. Academic Press, 2014.
- A. Saez-de Ibarra, V. I. Herrera, A. Milo, H. Gaztañaga, I. Etxeberria-Otadui, S. Bacha, and A. Padrós. Management strategy for market participation of photovoltaic power plants including storage systems. *IEEE Trans. Ind. Appl.*, 52(5):4292–4303, 2016.
- A. Saint-Pierre and P. Mancarella. Active distribution system management: a dual-horizon scheduling framework for dso/tso interface under uncertainty. *IEEE Trans. Smart Grid*, 8(5):2186–2197, 2016.
- S. Sarabi, A. Davigny, V. Courtecuisse, Y. Riffonneau, and B. Robyns. Potential of vehicle-to-grid ancillary services considering the uncertainties in plug-in electric vehicle availability and service/localization limitations in distribution grids. *Appl. Energy*, 171:523–540, 2016.
- K. Schwenk, M. Faix, R. Mikut, V. Hagenmeyer, and R. R. Appino. On calendar-based scheduling for user-friendly charging of plug-in electric vehicles. In *2019 IEEE 2nd Connected and Automated Vehicles Symposium (CAVS)*, pages 1–5. IEEE, 2019.
- A. Shapiro, D. Dentcheva, and A. Ruszczyński. *Lectures on stochastic programming: modeling and theory*. SIAM, 2009.
- F. Sossan, E. Namor, R. Cherkaoui, and M. Paolone. Achieving the dispatchability of distribution feeders through prosumers data driven forecasting and model predictive control of electrochemical storage. *IEEE Trans. Sustain. Energy*, 7(4):1762–1777, 2016.

- E. Stai, L. Reyes-Chamorro, F. Sossan, J.-Y. Le Boudec, and M. Paolone. Dispatching stochastic heterogeneous resources accounting for grid and battery losses. *IEEE Trans. Smart Grid*, 9(6):6522–6539, 2018.
- W. Su, J. Wang, and J. Roh. Stochastic energy scheduling in microgrids with intermittent renewable energy resources. *IEEE Trans. Smart grid*, 5(4):1876–1883, 2013.
- A. Subramanian, M. J. Garcia, D. S. Callaway, K. Poolla, and P. Varaiya. Real-time scheduling of distributed resources. *IEEE Trans. Smart Grid*, 4(4):2122–2130, 2013.
- Swissgrid. Contributions to the market design for the swiss energy strategy 2050. Technical report, Swissgrid, 2016. Retrieved from <https://www.swissgrid.ch>.
- F. Trespalacios and I. E. Grossmann. Review of mixed-integer nonlinear and generalized disjunctive programming methods. *Chemie Ingenieur Technik*, 86(7):991–1012, 2014.
- B. P. Van Parys, D. Kuhn, P. J. Goulart, and M. Morari. Distributionally robust control of constrained stochastic systems. *IEEE Trans. on Autom. Control*, 61(2):430–442, 2016.
- S. Vandael, B. Claessens, M. Hommelberg, T. Holvoet, and G. Deconinck. A scalable three-step approach for demand side management of plug-in hybrid vehicles. *IEEE Trans. Smart Grid*, 4(2):720–728, 2013.
- M. Vrakopoulou, K. Margellos, J. Lygeros, and G. Andersson. A probabilistic framework for reserve scheduling and n-1 security assessment of systems with high wind power penetration. *IEEE Trans. Power Syst.*, 28(4):3885–3896, 2013.
- A. Wächter and L. T. Biegler. On the implementation of an interior-point filter line-search algorithm for large-scale nonlinear programming. *Mathematical Programming*, 106(1):25–57, 2006.
- Q. Wang, C. Zhang, Y. Ding, G. Xydis, J. Wang, and J. Østergaard. Review of real-time electricity markets for integrating distributed energy resources and demand response. *Appl. Energy*, 138:695–706, 2015.

- J. Warrington, P. Goulart, S. Mariétoz, and M. Morari. Policy-based reserves for power systems. *IEEE Trans. Power Syst.*, 28(4):4427–4437, 2013.
- G. Wenzel, M. Negrete-Pincetic, D. E. Olivares, J. MacDonald, and D. S. Callaway. Real-time charging strategies for an electric vehicle aggregator to provide ancillary services. *IEEE Trans. Smart Grid*, PP(99), 2017.
- D. Xiu. *Numerical Methods for Stochastic Computations*. Princeton University Press, Princeton, New Jersey, 2010.
- Z. Xu, D. S. Callaway, Z. Hu, and Y. Song. Hierarchical coordination of heterogeneous flexible loads. *IEEE Trans. Power Syst.*, 31(6):4206–4216, 2016.
- Z. Yang, K. Li, and A. Foley. Computational scheduling methods for integrating plug-in electric vehicles with power systems: A review. *Renewable and Sustainable Energy Reviews*, 51:396–416, 2015.
- J. H. Yi, R. Cherkaoui, and M. Paolone. Optimal siting and sizing of energy storage systems in active distribution networks to achieve their dispatchability. *arXiv preprint arXiv:1909.12667*, 2019.
- Y. Zhang, J. Wang, and X. Wang. Review on probabilistic forecasting of wind power generation. *Renewable and Sustainable Energy Reviews*, 32:255–270, 2014.
- H. Zhang, Z. Hu, Y. Song, and S. Moura. Coordination of V2G and distributed wind power using the storage-like aggregate PEV model. In *Innovative Smart Grid Technologies Conference (ISGT), 2016 IEEE Power & Energy Society*, pages 1–5. IEEE, 2016.
- H. Zhang, Z. Hu, E. Munsing, S. J. Moura, and Y. Song. Data-driven chance-constrained regulation capacity offering for distributed energy resources. *IEEE Trans. Smart Grid*, 2018.
- H. Zhao, Q. Wu, S. Hu, H. Xu, and C. N. Rasmussen. Review of energy storage system for wind power integration support. *Appl. Energy*, 137:545–553, 2015.
- J. Zwartscholten, D. M. Gonzalez, C. Rehtanz, and J. Myrzik. Hierarchical distribution network control scheme for power flow regulation at the interconnection

points between several voltage levels. In *2018 IEEE 7th International Conference on Power and Energy (PECon)*, pages 221–226. IEEE, 2018.